Synthesis of dendritic gadolinium complexes with enhanced relaxivities

O'Halloran, Mark

Synthesis of Dendritic Gadolinium Complexes with Enhanced Relaxivities

Mark O'Halloran

Department Of Chemistry
University of Durham

A Thesis Submitted for the Degree of Doctor of Philosophy

2002

Abstract

This thesis deals with the synthesis of dendritic gadolinium complexes based on DOTA, with a view to obtaining enhanced relaxivities. In addition to the inherently long electronic relaxation time and high paramagnetic moment of the gadolinium (III) ion, the speed of rotation of its complexes in solution is a decisive parameter in the determination of the relaxivity. This parameter is dependent on the molecular mass of the complex.

Initially, the enantioselective synthesis of novel α-substituted analogues of DOTA was attempted but was not successful due to difficulties encountered in attaining the tetraalkylation of cyclen and the purification of the products obtained. Therefore, further studies were carried out based on the known $[Gd(gDOTA)]^-$ system.

The synthesis of three medium M_w dendrons, each with a focal primary amino group was carried out. Their structures may be described as dendrimeric analogues of poly(ethylene glycol). Two of these structures were successfully coupled to the gadolinium (III) chelate, $[Gd.gDOTA]^-$. The acid-catalysed epimerisation of the statistical distribution of stereoisomers yielded solely the (RRRR)/(SSSS) isomeric pair. This system had previously been shown to undergo fast water exchange. The coupling and deprotection procedure yielded paramagnetic dendritic complexes with molecular weights of 2013 and 3535.

Relaxivity measurements were carried out on these systems and the results showed significantly higher relaxivities of 18 and 21 $mM^{-1}\ s^{-1}$ respectively, compared with a value of 7.8 $mM^{-1}\ s^{-1}$ for the parent compound. Examination of NMRD profiles for the larger system showed a decrease in the rotational correlation time to 310 ps at 298 K, as expected. However, this was accompanied by an increase in the inner-sphere water exchange lifetime to 570 ns at 298 K.

Therefore, although an improvement in relaxivity was obtained through a coupling to the slower rotation of the system in solution, this enhancement was limited by the accompanying decrease in the rate of water exchange. The best fitting procedure of the NMRD profiling procedure revealed the presence of 8 second-sphere water molecules at an average distance of 4Å. The second sphere contribution was shown to be the dominant contributor to the overall relaxivity. This accounted for >50% of the increased relaxivity.

Declaration

The work described herein was carried out in the Department of Chemistry at the University of Durham, UK between October 1998 and December 2001. All work is my own, unless otherwise stated, and no part of it has been submitted for a degree at this or any other university.

Statement of Copyright

Acknowledgements

I would like to express my gratitude to the following people;

Mum, Dad and Kerrie for all they have done to make this possible.

Prof. David Parker for all his help and support, and for sharing his ideas and skill.

Dr. Mark Woods for his previous work in the area and indispensible thesis.
Dr. Kanthi Senanayake for her help with some challenging synthetic work.
Phil Woodward for all those columns and jokes at my expense.

Dr. Justin Perry, Dr. James Bruce, Dr. Ofer Reany, Dr. Linda Govenlock, Dr. Rachel Dickins, Dr. Mark Lowe, Dr. Juan-Carlos Frias, Dr. Yann Bretonnière and Dr. Suzy Keen for their knowledge, experience and friendship.

Céline Mathieu, Dimitri Messeri, Gabriella Bobba, Alessandra Badari, Nicola Thompson, Simon Welsh, Aileen Congreve, Dr. Ian Clarkson and Dr. Phil Skinner for making CG27 the friendliest, most fun lab. in Durham.

All my friends in Durham, particularly Dr. Ollie Sutcliffe, Cath Poulton, Dave Bryant, Dr. Stephanie Blair, Kelly Flook, Dr. Andy Johnson, Jacqui Burke, Debbie McMillan and Maya Mei-Tal for making my time at Durham the best in my life.

Dr. Mauro Botta for carrying out NMRD profiling.

Dr. Alan Kenwright, Ian McKeag and Catherine Heffernan for an excellent NMR service.

Dr. Mike Jones and Lara Turner for all their help with the electrospray MS measurements.

The Department of Chemistry and the University of Durham for funding this work.

"One's mind, once stretched by a new idea, never regains its original dimensions."

- Oliver Wendell Holmes

Abbreviations

12N4	1,4,7,10-tetraazacyclododecane
Ac	Acetyl
AIBN	Azo-*iso*-bis(butyronitrile)
9-BBN	9-Borabicyclo[3.3.1]nonane
Bn	Benzyl
Boc	*tert*-Butoxycarbonyl
Boc-ON	2-(*tert*-Butoxycarbonyloxyimino)-2-phenylacetonitrile
BSA	Bovine Serum Albumin
Bu	Butyl
^{t}Bu	*tert*-Butyl
Cbz	Benzyloxycarbonyl
COSY	Correlation Spectroscopy
DBU	1,5-Diazabicyclo[5.4.0]undec-5-ene
DCC	Dicyclohexylcarbodiimide
DCM	Dichloromethane
DIP-Cl	(+)-*B*-Chlorodiisopinocampheylborane
DMAP	4-(Dimethylamino)pyridine
DMF	Dimethylformamide
DMSO	Dimethylsulphoxide
DO3A	1,4,7,10-Tetraazacyclododecane-1,4,7-triacetate
DOTA	1,4,7,10-Tetraazacyclododecane-1,4,7,10-tetraacetate
DOTMA	1,4,7,10-Tetraazacyclododecane-1,4,7,10-tetra(α-methyl acetate)
DTPA	Diethylenetriamine-*N,N,N',N'',N''*-pentaacetate
DTPA-BMA	*N,N''*-bis(Methylcarboxamidomethyl)-diethylenetriamine- *N,N',N''*-triacetate
EDC	1-(3-Dimethylaminopropane)-3-carbodiimide Hydrochloride
EDTA	Ethylenediamine-*N,N,N',N'*-tetraacetate
ESMS	Electrospray Mass Spectrometry
Et	Ethyl

EXSY	Exchange Spectroscopy
gDOTA	1,4,7,10-tetraazacyclododecane-1,4,7,10- tetra(2-glutaric acid)
HOBt	1-Hydroxybenzotriazole
HPDO3A	10-(2-Hydroxy)propyl-1,4,7,10-tetraazacyclododecane-1,4,7-triacetate
HSA	Human Serum Albumin
IgG	Immunoglobulin G
IR	Infra Red
Ln	Lanthanide
LD_{50}	Lethal Dose for 50% of Subjects
Me	Methyl
Mp	Melting Point
MRI	Magnetic Resonance Imaging
Ms	Mesyl
NBS	*N*-Bromosuccinimide
NHS	*N*-Hydroxysuccinimide
NMR	Nuclear Magnetic Resonance
NMRD	Nuclear Magnetic Resonance Dispersion
Ns	Nosyl
PAMAM	Poly(amidoamine)
PEG	Poly(ethylene glycol)
^{i}Pr	*iso*-Propyl
PTSA	*para*-Toluenesulphonic Acid
R_f	Retention Factor
Tf	Triflyl
TFA	Trifluoroacetic Acid
THF	Tetrahydrofuran
TLC	Thin Layer Chromatography
TRIS	*tris*-(Hydroxymethyl)aminomethane
UV	Ultraviolet
VT NMR	Variable Temperature Nuclear Magnetic Resonance

Chapter 3 - Gadolinium Chelates

Chapter 4 - High Molecular Weight Contrast Agents

Chapter 5 - Results and Discussion

Chapter 6 - Experimental

Chapter 1

Introduction

This chapter is a general introduction to nuclear magnetic resonance, magnetic resonance imaging (MRI) and relaxation theory.

1.1 Overview

1.1a Principle of NMR

Chemists have used the magnetic properties of atomic nuclei to gain information about molecular structures and behaviour for several decades.[1] The technique's early development led to the award of two Nobel Prizes for Physics, to Rabi (1944)[2,3] and jointly to Bloch and Purcell (1952).[4-6] Nuclear magnetic resonance uses the fact that the behaviour of the magnetic moments of suitable nuclei is very dependent on their surroundings.

When a nucleus possessing a magnetic moment is placed in a magnetic field, this moment may adopt only a limited number of orientations with respect to the applied magnetic field. These orientations each have a different energy. The difference in energy depends primarily on the identity of the nucleus, the strength of the applied magnetic field, the magnitude of the nuclear magnetic moment itself and crucially on the magnetic microenvironment of the nucleus under observation.

The magnitude of the energy difference may be determined by irradiating the system with electromagnetic radiation at a frequency, which causes resonance between the two levels. This resonance frequency gives valuable information about the magnetic environment of the nucleus, which depends on the electronic environment of the nucleus, which in turn depends on its chemical environment.

1.1b Medical Applications

This technique has also been developed for application to medicine. It has proven to be an extremely powerful, though expensive tool for the detection of a range of diseases. A variety of human conditions, in particular cancer, can be detected in a non-invasive manner by the medical variant of NMR, magnetic resonance imaging, or MRI. Water hydrogen atoms are NMR sensitive and ^{1}H NMR is by far the most frequently used

technique. Water is abundant throughout the body, but different types of biological tissue have different water concentrations and environments. MRI observes the three-dimensional distribution and environment of water protons in the body (i.e. it uses a 3D representation of NMR parameters for clinical diagnosis).[7,8] The parameters used are T_1 (the spin-spin relaxation parameter), T_2 (the spin-lattice relaxation parameter) and the spin density. The relaxation times T_1 and T_2 are dependent on the local environment of the water molecule and the spin density is dependent on the concentration of water in the tissue, which is a function of tissue type (**figure 1.1**).

Tissue	Water Content
Kidney	81%
Liver	71%
Teeth/Bones	10%

Figure 1.1 – Water content of some tissue types.[9]

1.1c Three Dimensional Representation

In standard NMR spectroscopy, the spatial relationship between different molecules is not relevant. However a three dimensional representation of the body is required for MRI. This is achieved by applying a magnetic field gradient across the patient. Because the Larmor precessional frequency is dependent on the strength of the field, the value of this frequency yields information about the position of any nucleus with respect to the field gradient. The repetition and reconstruction of many of these spatially encoded scans leads to the computational generation of a three dimensional image.

The projection-reconstruction techniques needed to use NMR for three-dimensional imaging purposes were detailed by Lauterbur,[10] and the relationship between spin density (i.e. water concentration) and signal intensity was discovered by Mansfield and Grannell,[11] both in 1973.

1.1d MRI and Cancerous Tissue

The discovery that certain cancerous tissues have unusually long values of the NMR parameter T_1, (**figure 1.2**)[12] allowing detection and early treatment, made clear the

applicability of NMR to medicine. Brain tumour blood supplies have defective blood-brain barriers, through which blood pool contrast agents diffuse, allowing diagnosis. However, it is not solely cancer which may be detected by MRI – many lesions exhibit abnormal extracellular:intracellular water ratios which may be detected.[13] It was not until 1978 that the world's first medical NMR imager went into clinical trials at the Hammersmith Hospital, London. However, public relations demanded the word nuclear be dropped from the technique's name – magnetic resonance imaging was born.

Tissue	T_1 (Cancerous)/s	T_1 (Healthy)/s
Breast	1.080	0.367
Liver	0.832	0.570
Skin	1.047	0.616

Figure 1.2 – Variation in T_1 between cancerous and healthy tissue.[14]

1.2 NMR Theory

In an MRI scan the equilibrium bulk magnetisation, $\boldsymbol{M}$, is perturbed by the magnetic component of a radiofrequency pulse, and the response of the system is monitored to yield a spectrum. An MRI machine carries out three basic functions. It maintains a strong uniform magnetic field around the patient. It irradiates the patient using the desired radiofrequency pulse sequence and then detects and processes the MRI signal.

The static magnetic field, $\boldsymbol{B}_0$, is provided by a superconducting solenoid. The radiofrequency pulses must be coherent and monochromatic. They are generated by passing a sinusoidally oscillating current through a coil which surrounds the patient. The circulating electrons in the coil generate an oscillating electromagnetic field whose magnetic component excites the sample nuclei, provided that it has a component at the correct resonance frequency.

The radiofrequency-generating coil in the MRI machine is positioned in the xy-plane causing the bulk magnetisation to experience a sinusoidal, linearly oscillating magnetic field along the x-axis.

Because of the coherent nature of the radiofrequency excitation, it induces a component of the magnetisation in the xy-plane. After removal of the radiofrequency, the coil detects the coherent precession of the sample nuclei from the electrical current they

induce in the coil. Because different nuclei have slightly different Larmor precessional frequencies, these may be processed by a Fourier transform to yield an MRI spectrum.

1.3 Relaxation Theory

1.3a Spin-Lattice Relaxation

After radiofrequency excitation, the system is in a higher energy, non-equilibrium state. The coherent MRI signal in the xy-plane will therefore decay over time, as equilibrium is re-established.

Any change in the relative populations of the ground and excited states in a system under MRI conditions involves an energy change. During radiofrequency excitation, this energy input is electromagnetic in origin. After excitation however, the system must return to its ground state Boltzmann distribution before any further scans can be carried out. This process of dissipation of energy to the surroundings or lattice is called spin-lattice relaxation or longitudinal relaxation.

Because the difference in spin state energy levels is so small, spontaneous relaxation does not occur. There has to be a means of passing the energy to the lattice as thermal energy. However, thermal collisional motion is not effective in these systems because nuclear spins interact so weakly with the motion of their molecules.

Therefore, the only significant mechanisms of relaxation are magnetic in origin. The most important of these is dipolar coupling. The magnetic field experienced by any magnetic nucleus in the system is dependent on the position, motion, spin state and concentration of other magnetic nuclei in its vicinity, in both the intermolecular and intramolecular sense (i.e. nuclei generate magnetic fields as well as being effected by them). Consider two magnetic dipoles in solution. Although their rapid thermal motion does not affect the direction of their magnetic dipole, which is always parallel or antiparallel to the applied field, it does mean that their relative positions in space change rapidly as they translate (**figure 1.3**). Each dipole generates a magnetic field with lines of force similar to that of a bar magnet. The strength of the dipolar magnetic field is a function of $1/r^3$. Its direction depends on Θ, the angle between the nucleus undergoing relaxation and the z-axis in a polar coordinate system.

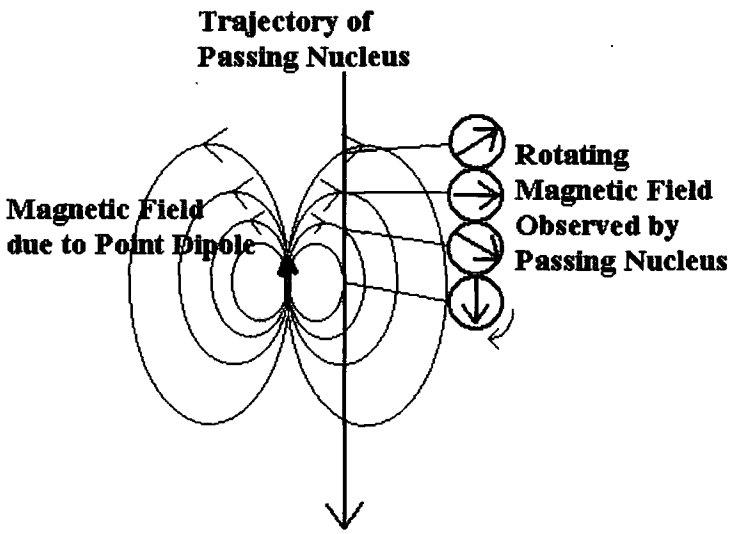

Figure 1.3 - Magnetic Field due to Point Dipole

Therefore as any dipole undergoes translation in solution, the magnetic field due to its neighbours is rapidly varying in direction and strength in a complex and unpredictable manner. In this way, dipolar coupling in conjunction with molecular motion causes nuclei to experience time-dependent local magnetic fields.

If the change in magnetic field has a component which has a frequency equal to the transition frequency, then interaction with an excited state nucleus can occur leading to radiationless transfer of thermal energy to this lattice component, allowing the nucleus to relax back to its ground state. When this process is repeated throughout the sample, the system eventually reaches equilibrium.

1.3b Molecular Tumbling

Because of their proximity to each other, molecules in liquids undergo constant acceleration/deceleration and directional changes to their rotational and translational motions. Translational motion is not a very effective modulator of dipolar interactions because intermolecular distances are generally too large. Vibrational interactions, although intramolecular and short-range in nature, are too fast to have a significant component at relatively low MRI frequencies.

However, molecules also undergo constantly changing rotational motion, which is referred to as tumbling. Rotational motion is more important for spin relaxation processes because it has a much lower frequency than vibrational motion. The definition of the characteristic time for this motion, the rotational correlation time, τ_R, is approximately the time taken for the root mean squared deflection of the molecules to be 1 rad. τ_R depends on the viscosity and temperature of the solution as well as the mass of the molecule. Since τ_R is the average time taken to tumble through an angle of 1 rad, this means that τ_R^{-1} is the root mean squared rotational angular frequency. Because this is a root mean square averaged frequency, frequencies below this value will be quite probable, while higher frequencies are much less likely. The value of the rotational correlation time for a spherical molecule is a function of the radius of the molecule, *r*, the intrinsic viscosity, η, and the temperature, *T*, as follows.

$$\tau_R \approx \frac{4\pi r^3 \eta}{3kT} \qquad \textbf{Eq. 1}$$

The frequency spectrum of an intramolecular magnetic interaction, modulated by molecular tumbling, is defined by a spectral density function, $J(\omega)$, (**figure 1.4**).

$$J(\omega) = \frac{2\tau_R}{1+\omega^2\tau_R^2} \qquad \textbf{Eq. 2}$$

This function is approximately proportional to the probability of finding a component of the random motion at a particular frequency. The frequency dependence of $J(\omega)$ is governed by τ_R. Therefore, less viscous solvents, smaller molecules and higher temperatures will result in shorter correlation times, and therefore a spectral density which extends towards higher frequencies. The value corresponding to $J(\omega_0)$ has its maximum value (i.e. the greatest number of frequency components at the chosen transition frequency, and therefore the maximum relaxation rate), when $\tau_R = \frac{1}{\omega_0}$, or $\tau_R\omega_0 = 1$, where ω_0 is the applied radiofrequency. Because most molecules tumble rapidly (i.e. $\tau_R\omega_0 << 1$), the relaxation rate gets slower as the temperature is increased.

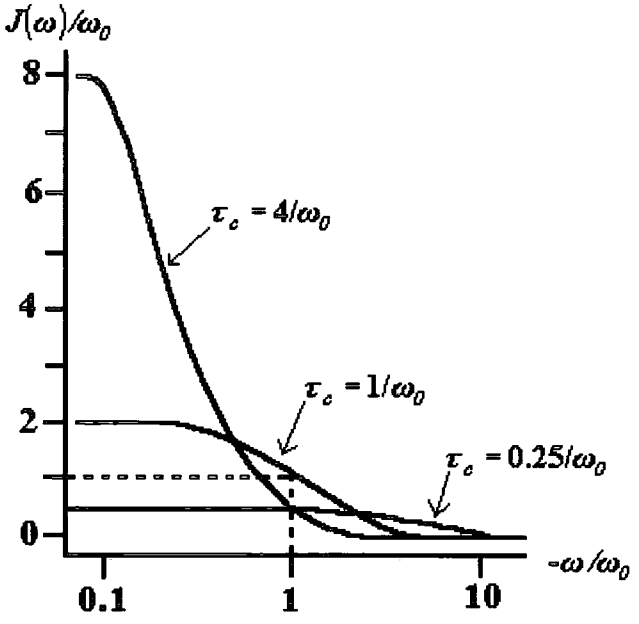

Figure 1.4 – Spectral Density Function, $J(\omega)$.

1.3c Spin-Lattice Relaxation Time Constant

The characteristic time for the process of exponential relaxation for a sample of nuclei is the spin-lattice relaxation time constant, T_1. The rate constant of this relaxation process, R_1 where $R_1=T_1^{-1}$, is proportional to the spectral density, $J(\omega)$, the spectral density being a function of τ_R.

1.3d Relaxation and the Rotating Frame of Reference

Many of the problems associated with attempting to visualise the dynamic MRI system are avoided by adopting a rotating frame of reference. A schematic representation of this concept is shown in **figures 1.5** and **1.6**. The sinusoidally oscillating magnetic field from the radiofrequency pulse may be resolved into two constituent magnetic fields, which rotate in opposite directions. One of these fields rotates in the opposite direction to the Larmor precessional frequency and therefore never resonates with the magnetic nuclei in the sample. The second rotating field however will do so when the applied radiofrequency is equal to the Larmor precessional frequency of the nucleus under investigation.

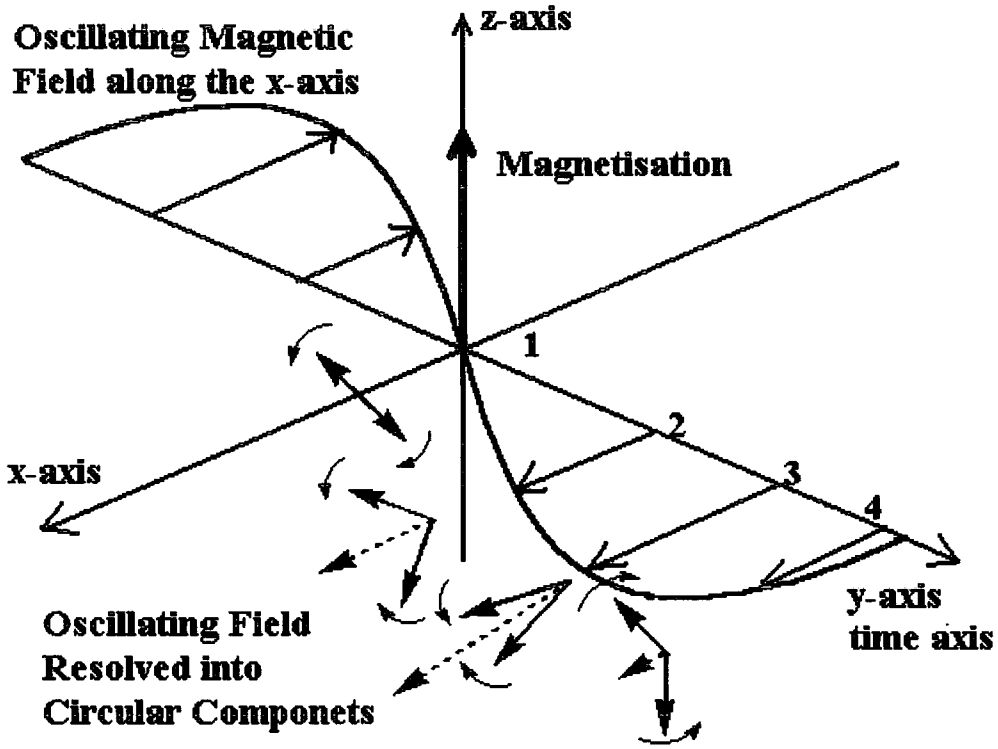

Figure 1.5 – Representation of the Rotational Effect of an Oscillating Magnetic Field on Nuclear Magnetisation.

The magnetic component of the applied field will deflect the magnetisation, ***M***, away from the z-axis by an amount proportional to the length of the radio pulse. This then has an important secondary effect – it allows the magnetisation to precess around the z-axis, a process which is obviously impossible while the magnetisation and the z-axis are coincident. The Larmor frequency for this precession in the static frame of reference, is at or near the radio frequency, depending on the exact identity of the nucleus.

The adoption of a rotating frame of reference means that the point of observation of the system is a point rotating around the z-axis with the radiofrequency, ω_{rf}. In the rotating frame, the magnetic component of the radiofrequency field appears to be static, and is arbitrarily assigned to be along the x' axis. This also means that any Larmor precession at the radiofrequency is also invisible. This discussion will now be based in the rotating frame of reference, unless stated otherwise.

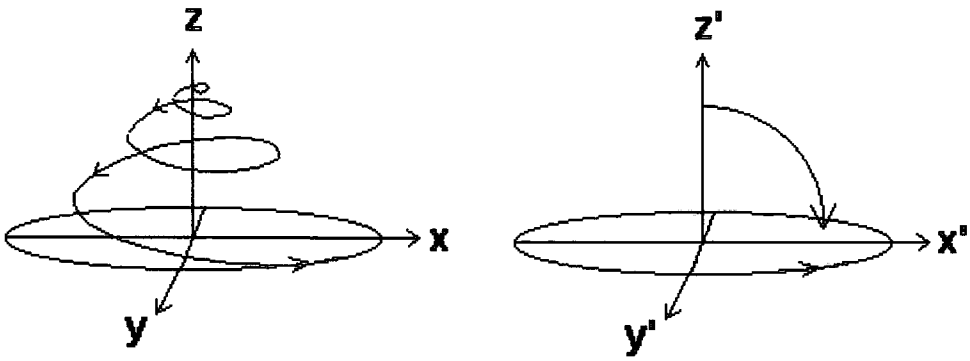

Static frame of reference – combination of Larmor precession in xy-plane and flipping of magnetisation in xz-plane.

Rotating frame of reference – effect of precession no longer visible.

Figure 1.6 – Static Frame of Reference vs. Rotating Frame of Reference

Upon application of a radiofrequency in the laboratory frame of reference, the bulk magnetisation, $\boldsymbol{M}$, is disturbed from its equilibrium and precesses around $\boldsymbol{B}_0$ at a frequency $\omega_0 = \gamma B_0$. However if $\omega_0 = \omega_{rf}$, then the precession of $\boldsymbol{M}$ around $\boldsymbol{B}_0$ appears to be static in the rotating frame (but not the precession of $\boldsymbol{M}$ as a result of the magnetic field due to the radiofrequency, $\boldsymbol{B}_1$). Therefore any deviation from this condition will cause $\boldsymbol{M}$ to rotate around $\boldsymbol{B}_0$ in the rotating frame of reference. This frequency of rotation within the rotating frame, Ω, is therefore equal to the difference between the precession frequency and the radiofrequency.

$$\Omega = \omega_0 - \omega_{rf} \qquad \textbf{Eq. 3}$$

The effective field or offset field, ΔB, is defined as that portion of the applied field, $\boldsymbol{B}_0$, which causes precession at frequency Ω in the rotating frame of reference. The effective field along the z-axis in the rotating frame is therefore,

$$\Delta B = \frac{\Omega}{\gamma} = \left(\omega_0 - \omega_{rf}\right) = B_0 - \frac{\omega_{rf}}{\gamma} \qquad \textbf{Eq. 4}$$

In the rotating frame $\boldsymbol{M}$ precesses around the resultant field from ΔB and $\boldsymbol{B}_1$.

1.3e Radiofrequency Excitation

When a resonant electromagnetic pulse where $\omega_0 \approx \omega_{rf}$ is applied to an MRI system at thermal equilibrium, the offset field ΔB is negligible in comparison to the radiofrequency field, $\boldsymbol{B}_1$. Under these conditions $\boldsymbol{M}$ precesses in the y'z' plane with a frequency γB_1. The angle through which the magnetisation precesses is called the flip angle, β, and is determined by the duration of the applied pulse, t_p.

$$\beta = \gamma B_1 t_p \qquad \textbf{Eq. 5}$$

A 90° pulse rotates $\boldsymbol{M}$ onto the y' axis, causing equalisation of the two population states and conversion of the entire equilibrium magnetisation into z-magnetisation. In this way, coherent electromagnetic radiation causes coherent magnetisation in the laboratory frame in the xy-plane. An 180° pulse inverts the population difference and rotates $\boldsymbol{M}$ onto the negative z' axis.

Although an MRI pulse is monochromatic, the extremely short duration of the pulse has the effect of causing a small spread of frequencies around the desired frequency, where the bandwidth is inversely proportional to the pulse duration. This property is quantum mechanical in origin. It has the effect of exciting uniformly and simultaneously all the nuclei in the sample, despite the small differences in their resonance frequencies.

1.3f Free Precession and Relaxation

After the completion of a 90° pulse, $B_1 = 0$ and the only remaining magnetic field in the rotating frame is ΔB along the z' axis. $\boldsymbol{M}$ therefore precesses in the xy-plane at frequency Ω.

$$\Omega = \gamma \Delta B = \gamma B_0 - \omega_{rf} \qquad \textbf{Eq. 6}$$

However all nuclei actually experience slightly different applied magnetic fields, $B_0 - \sigma B_0$ or $B_0(1-\sigma)$, and therefore they precess at slightly different frequencies, which are characteristic of their chemical shifts.

1.3g Spin-Spin Relaxation

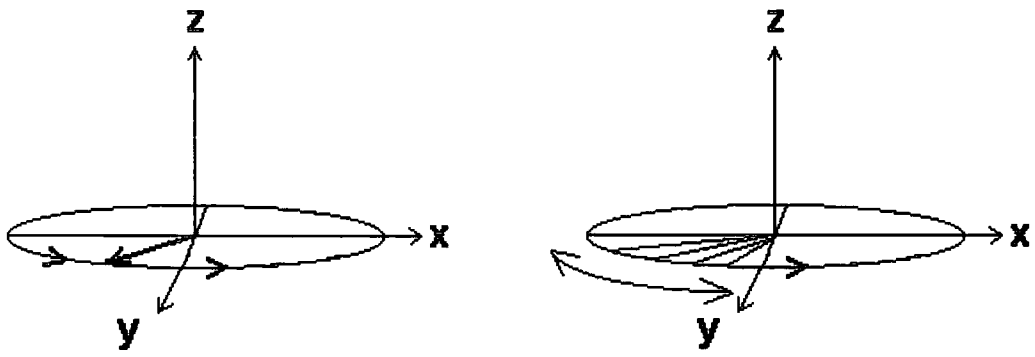

Immediately after 90° flip – all nuclei precessing coherently

At time τ after 90° flip, coherence is being lost and the transverse magnetisation is dephasing out around the xy-plane

Figure 1.7 – Spin-Spin Relaxation

After the removal of a 90° pulse, the system has a magnetisation in the xy plane and this value will return to its equilibrium value of zero by relaxation. This is a second relaxation process called spin-spin relaxation or transverse relaxation, and operates separately to spin-lattice relaxation (see **figure 1.7**).

In this process the coherence of the magnetisation in the xy-plane is lost by randomisation. This occurs because the precession frequency is proportional to $B_0(1-\sigma)$, the actual time-dependent magnetic microenvironment experienced by the nucleus. These differences cause the individual components of the xy magnetisation to fan out and dephase. There is no energy change involved in this process. The rate constant of transverse relaxation must necessarily be equal to or less than that of longitudinal relaxation. The transverse relaxation time constant is T_2.

The MRI receiver coil detects the time dependence of $\boldsymbol{M}$, or transverse decay, following a 90° pulse. This is called the free induction decay and is composed of all the oscillating voltages in the sample, each with its own characteristic frequency, T_2 and amplitude. These data are processed by computer using a Fourier transform to produce an MRI spectrum.

1.3h Measuring T_1 by Inversion Recovery

Spin lattice relaxation times can be measured by inverting ***M*** with a 180° pulse onto the negative z-axis (**figure 1.8**). A delay time τ is then allowed to pass, during which ***M*** undergoes partial spin-lattice relaxation to give a magnetisation $M_z(\tau)$. A 90° pulse is then applied which rotates this magnetisation onto the y-axis. The free induction decay is then recorded which gives a spectrum in which the peak intensity $I_z(\tau)$ is proportional to $M_z(\tau)$.

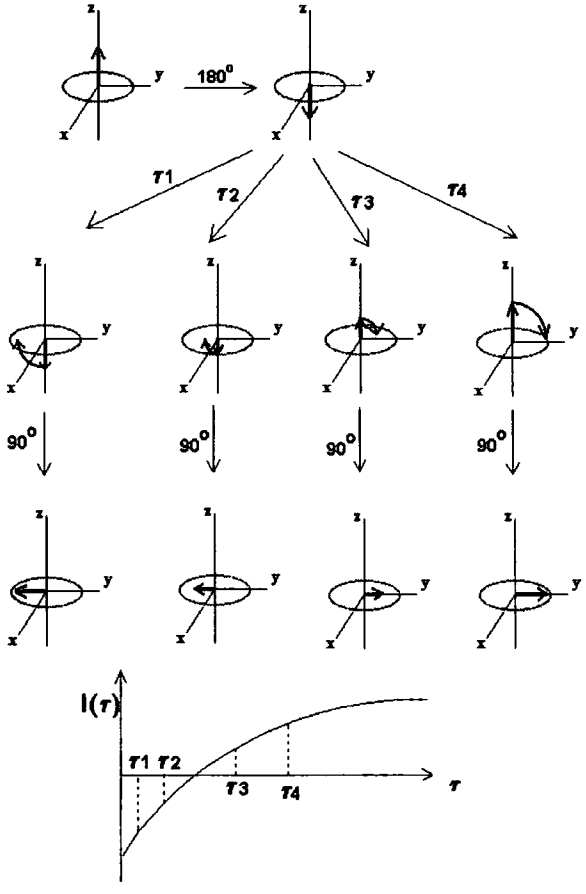

Figure 1.8 – Inversion Recovery Method of Measuring T_1

If this is repeated for a range of values of τ the recovery of the inverted relaxation may be followed. Relaxation is assumed to be exponential and the value T_1 is calculated as follows.

$$M_z(\tau) = M_0[1 - 2\exp(-\tau/T_1)] \qquad \textbf{Eq. 7}$$

The spin-lattice relaxation time (or longitudinal relaxation time) may be determined by plotting $\ln[I(\infty)-I(\tau)]$ against τ, where $I(\infty)$ is the fully relaxed MRI intensity (i.e. when $\tau \gg T_1$.

Chapter 2

Contrast Agents

This chapter introduces contrast agents and describes the structure-function relationships, which are relevant to contrast agent design. These relationships are initially introduced and explained in general terms. Subsequently, a more precise mathematical treatment of their interdependent behaviour with respect to MRI variables is presented (i.e. Solomon-Bloembergen-Morgan theory).

2.1 Gadolinium as a Contrast Agent

2.1a Introduction

It has long been known that paramagnetic metal ions in solution catalytically enhance the proton relaxation rate during NMR experiments.[4,5,15-17] Contrast agents are paramagnetic substances, which accelerate the relaxation of water molecules during an MRI scan. During an NMR experiment, high-energy proton spin states are created by radio frequency irradiation in a strong magnetic field. After the radio frequency has been removed, the system is relaxed back to its equilibrium spin state distribution by interacting with the fluctuating magnetic moment of the paramagnetic metal complex (**figure 1.3**). This allows rapid removal of excess energy from the protons and a return to the equilibrium spin distribution.

Water molecules directly bound to highly paramagnetic metal ion typically experience a relaxation rate enhancement of a factor of 10^6.[18] This catalytic effect takes place through dipole-dipole interactions between the unpaired spins of the electrons on the metal ion and the spin of the proton. The bound water molecules are then exchanged with the bulk solvent, transferring the effect throughout the solution. In addition to this, rapid proton exchange between water molecules transmits the effect throughout the solution.

Initially during the development of this area of research, metal ions such as Fe(III)[19] and Mn(II)[15] were used as paramagnetic cations, but modern contrast agents use Gd(III) almost exclusively. This is because it has seven unpaired electrons making it highly paramagnetic (S=7/2). It also has a symmetric S-state making its electronic

relaxation time long (*ca.* 10^{-9} s, *cf.* 10^{-13} s for Eu^{3+}, Yb^{3+} and Dy^{3+}). Both these attributes increase its ability to relax water protons.[7,20]

In most cases, in the absence of a paramagnetic solvent, the values of the longitudinal relaxation time constant (T_1) and the transverse relaxation time constant (T_2) are similar. However, in the presence of Gd(III) for example, after enhancement of the rate of relaxation, T_1/T_2=2.5. The effect of a contrast agent is to reduce both T_1 and T_2 of protons, but not necessarily by the same amount. A reduction in T_1 will lead to an increase in signal intensity, whereas a reduction in T_2 leads to a decrease in signal intensity. As a result of this, MRI pulse sequences are weighted towards T_1 and therefore it is the longitudinal relaxation rate constant (R_1) which is more important, and that which should be optimised. Therefore this research deals mainly with the longitudinal relaxation process, and the transverse process will not be discussed.

2.1b Clinical Use

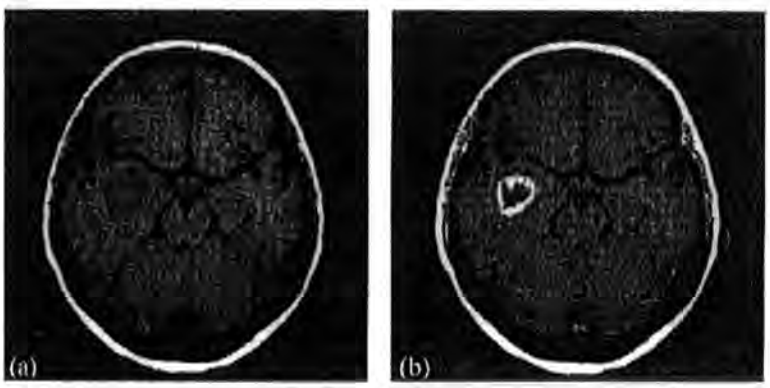

Figure 2.1
a) MRI scan of the head without a contrast agent.
b) MRI scan of the head with a contrast agent highlighting the tumour (outlined in white)

As previously noted, the use of paramagnetic substances to enhance the rate of relaxation of water protons has found wide application in the medical sphere.[15,21] The efficacy of a complex with regard to the process of re-equilibrating proton spin states is called its relaxivity. (Or more accurately, the relaxivity of a complex is defined as the increase in the rate of water relaxation per unit concentration of the complex.) This enhanced rate of relaxation allows NMR experiments to be completed in less time. Before any scan in a series of scans can commence, the system must have returned to its

equilibrium spin distribution. The more scans which can be carried out per minute, the less the effect of noise and the better the resolution.

This increased physiological resolution yields far more biological information (**figure 2.1**). As well as static information, a series of scans at suitable intervals may be used to track for example the clearance pattern of the contrast agent from the body as it is excreted by the kidneys, or the distribution of the agent across the blood-brain barrier to show any abnormalities. Much research is underway to find more specific ways to target certain types of tissue, especially cancerous tissue.

Figure 2.2 MRI Scanner

Gadolinium (III) has the electronic configuration [Xe] $4f^7$ (i.e. it has 7 unpaired electrons and the highest spin quantum number of any stable element.) It also has a long spin relaxation time (~ 10^{-9}s) under normal MRI conditions. This is due to the inherent symmetry, and therefore stability, of the Gd(III) electronic configuration. The lower electronic transition frequencies displayed by Gd(III) are nearer to the water proton Larmor frequencies in MRI (e.g. 4×10^8 rad s^{-1} at 60 MHz), allowing efficient dipole-dipole energy transfer between Gd(III) electrons and water protons. Both a high spin quantum number and a long electron spin relaxation time are necessary for efficient internuclear spin relaxation.

Gadolinium is toxic however (LD_{50} = 0.14 mmol kg^{-1}).[21] This is because it has a similar size to Ca^{2+}, but a much higher charge density. This impedes the vital functions of Ca^{2+} in the body by replacing it in biological processes, especially in light of the fact that quite high dosages of contrast agent must be used for medical purposes, typically 0.1 - 0.2 mmol $kg^{-1}$of body mass.

2.2 Gadolinium Chelates as MRI Contrast Agents[22,23]

2.2a Features of Gadolinium Chelates

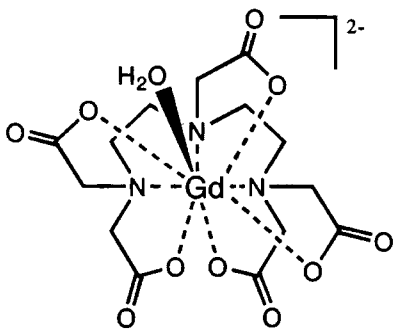

Magnevist; $[Gd.DTPA]^{2-}$
DTPA = Diethylenetriamine-N,N,N',N",N"-pentaacetate

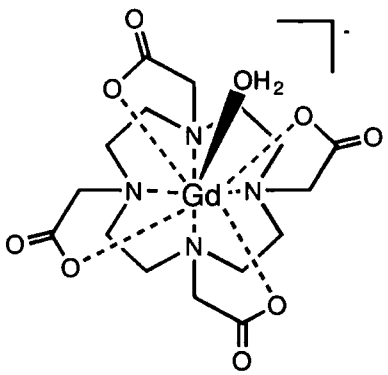

Dotarem; $[Gd.DOTA]^{-}$
DOTA = 1,4,7,10-Tetraazacyclododecane-1,4,7,10-tetraacetate

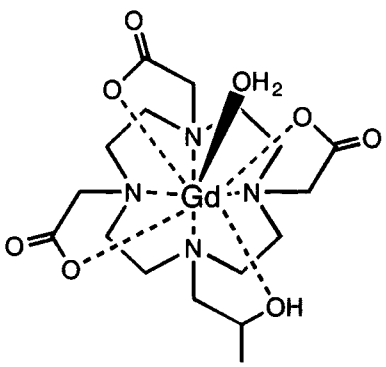

Prohance; GdHPDO3A
HPDO3A = 10-(2-Hydroxy)propyl-1,4,7,10-tetraazacyclododecane-1,4,7-triacetate

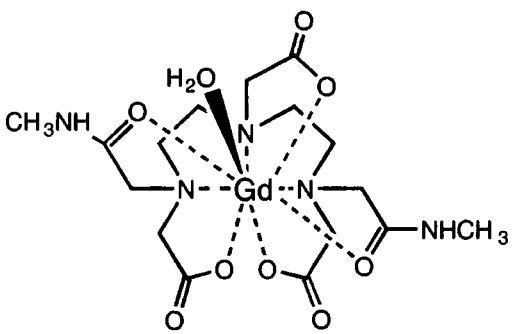

Omniscan; GdDTPA-BMA
DTPA-BMA = N,N"-bis(methylcarboxamidomethyl)-diethylenetriamine-N,N',N"-triacetate

Figure 2.3 - Main extracellular contrast agents currently in use.[21,22]

Due to its toxicity, Gd(III) must be encapsulated by a multidentate chelate to yield a complex which is very stable under biological conditions. This chelation reduces the potency of the Gd(III) by reducing the number of coordinated water molecules which can interact with the metal.

The following are the features of chelates favoured by Gd(III). The lanthanide ions are classified as hard acids, and therefore prefer hard σ-donor atoms such as nitrogen

and oxygen. Because the nature of the lanthanide co-ordination is highly polar in nature, hard anionic donors such as carboxylate are also favoured. Stability is enhanced by the chelate effect.[24] For the relatively large lanthanide ions, five-membered chelate rings are favoured over six-membered.[25] Extra stability may be attained by incorporating some of the donor atoms into a macrocyclic ring.[26] This macrocyclic effect, like the chelate effect, is due to favourable enthalpic and entropic factors. Suitable complexes therefore will contain oxygen and nitrogen donors, they will be based on a macrocyclic core and they will form five-membered chelate rings. Octadentate ligands derived from the tetra-N-substitution of 1,4,7,10-tetraazacyclododecane (cyclen or $12N_4$) comprise a very important structural motif, which satisfies these requirements.[27]

Much work has been carried out on the thermodynamic stabilities of a range of Gd(III) chelates. Equilibrium stability constants for the formation of the complexes have been used to assess stability *in vivo*, but it is the kinetic stability with respect to acid or base-catalysed dissociation, which is more important in a biological system.[28-32] Following the work of Desreux,[33-35] the anionic gadolinium complex of DOTA[36] has become the most widely used extracellular contrast agent in MRI, (**figure 2.3**). $Gd(DOTA)^-$ and analogues thereof are resistant to protonation and subsequent dissociation. Biodistribution studies of the $^{153}Gd(DOTA)$ chelate have shown their excellent stability *in vivo*. Note that the DTPA and HPDO3A ligand systems are significantly less stable than DOTA (**figure 2.4**).[28]

Complex	k_{obs}/s^{-1}	Zn^{2+} Transcomplexation
Gd(DOTA)	0.84	<1%
Gd(HPDO3A)	31	<1%
Gd(DTPA)	1.1	21%

Figure 2.4 – Acid Catalysed Dissociation Rate Constants (pH 1.0, 298 K)[37] and Percentage Zn^{2+} Transcomplexation ($[Zn^{2+}]$ = 25 mmol, 10 min, 298 K).[30]

However, as well as acid catalysed dissociation, the endogenously available cations Ca^{2+} and Zn^{2+} can act as catalysts. Again, the DOTA system performed well, as did macrocyclic systems in general.

As well as being stable, these complexes must be very water-soluble, they must be excreted rapidly by the body after administration and they should have a low osmotic potential. The osmotic potential of a complex increases with its charge density. Blood has an osmolality of 0.2 mol kg^{-1} whereas the contrast agents Magnevist, Dotarem and Prohance (**figure 2.3**) have osmolalities of 2.0, 1.1 and 0.5 mol kg^{-1} respectively.[38] A highly charged complex disrupts the ionic balance of the tissue through which it passes, causing severe pain upon injection in many cases. On the other hand, significantly hydrophobic contrast agent molecules must also be avoided, especially in the case of blood-pool agents, as they tend to associate in a detrimental manner with lipophilic biological structures such as cell membranes and proteins. More polar systems are therefore preferable.

2.2b Water Coordination

As well as these requirements, the complex must have at least one vacant site in its inner co-ordination sphere to allow the binding of water molecules. The more water molecules there are in the inner co-ordination sphere, the greater the relaxivity of the complex. However, due to the nature of the outer complex-forming orbitals of Gd(III), the metal usually forms quite labile complexes. This in practice means that an eight co-ordinate ligand is needed for stability, and because gadolinium (III) complexes are usually nine co-ordinate, in most cases only one water molecule is directly bound to the gadolinium ion.

This is a result of a trade-off between having the maximum number of water co-ordination sites and having a stable complex. Any ligand which was less than octacoordinate may be more rapidly displaced in aqueous solution by water, which is an excellent ligand for lanthanide ions, or would have its guest displaced by dissolved biological ions such as zinc or calcium. In addition, the presence of two adjacent vacant binding sites on the metal ion would encourage the competitive binding of bidentate ligands, such as carbonate or lactate which are present *in vivo*.[39] This may reduce the advantage of having two vacant binding sites. Because of this limitation on the number of co-ordinated water molecules, relatively large dosages of contrast agent are necessary for good resolution. For the reasons discussed above, macrocyclic ligands containing

coordinative pendant arms based on the 1,4,7,10-tetraazacyclododecane macrocycle are ideally suited for use.

2.2c Commercial Contrast Agents

Four extra-cellular (i.e. non-targeted) contrast agents are currently in widespread use- Magnevist, Dotarem, ProHance and Omniscan (**figure 2.4**). Dotarem was the first macrocyclic agent to become commercially available. It is based on the DOTA ligand and is still generally considered the best contrast agent in clinical use. It was first synthesised from $12N_4$ and chloroacetic acid.[40]

Omniscan and ProHance have the advantage that they are charge neutral and thus cause less osmotic shock in patients. Also, neutral and cationic complexes are more stable than anionic complexes with respect to dissociation *in vivo*. This is probably because the dissociation process is promoted by proton or cation interaction/displacement.[31] Neutral and cationic complexes are less likely to interact with these cations as there is no electrostatic attraction.

The charge of a complex is also important in determining the biodistribution of the complex. If penetration of the blood-brain barrier or of the cell wall is desired, it is necessary to use a charge-neutral complex. This is because charged complexes cannot penetrate the cell's hydrophobic phospholipid bilayer.

2.2d Choice of Complexes for this Work

The complexes dealt with in this work are based on a tetrasubstituted 1,4,7,10-tetraazacyclododecane ($12N_4$) core. In complexes already studied, which are based on $12N_4$, the stability of the macrocycle is increased to an acceptable level by the participation of one oxygen donor group on each of four nitrogen-bound pendant arms. The identity of the oxygen donor has included carboxylate, hydroxyl, amide and phosphinate. This work will deal with carboxylate groups.

2.3 Stereoisomerism

2.3a Overview

The structure of chelates such as Gd[DOTA]$^-$ has been investigated by X-ray solid state studies,[36] exchange spectroscopy (EXSY)[41,42], 2D NMR[43] and variable temperature (VT) NMR.[44,45] In the solid state it was revealed that the macrocyclic chelate was in an eight coordinate regular square antiprismatic arrangement, capped on the oxygen face by an inner sphere water molecule, making the overall co-ordination number nine. However in solution, a twisted square antiprismatic structure was also observed. These types of complex display two types of helical chirality.[46,47]

2.3b Helical Chirality of Pendant Arms

The first aspect of chirality deals with the orientation of the pendant arms. If one imagines looking at the molecule along the C_4 axis of symmetry (*i.e.* perpendicular to the plane of the page), from the side with the pendant arms (*i.e.* the O_4 face), the arms have a helical arrangement (see **figure 2.5**). Note that the single water-binding site is located on this O_4 face equidistant from each of the carboxylates. The plane containing the four coordinative oxygen atoms is at an angle of either 40° (square antiprism) or 29° (twisted square antiprism) with respect to the plane containing the four macrocyclic nitrogen atoms. This means that the pendant arms, which link the nitrogen and oxygen atoms must twist through the appropriate angle (40° or 29°) in a helical fashion. However the plane of the oxygen atoms may be twisted in either a clockwise or anti-clockwise direction, Δ or Λ respectively. This is illustrated in **figure 2.5** where the slope and twist angle of the pendant arms are indicated with simplified wedged bonds. These stereochemical arrangements are interchangeable via the conversion processes shown in the diagram. Arm rotation is a concerted reversal of the helicity of the pendant arms. Ring inversion involves the reversal of the helicity of puckering associated with the $12N_4$ ring.

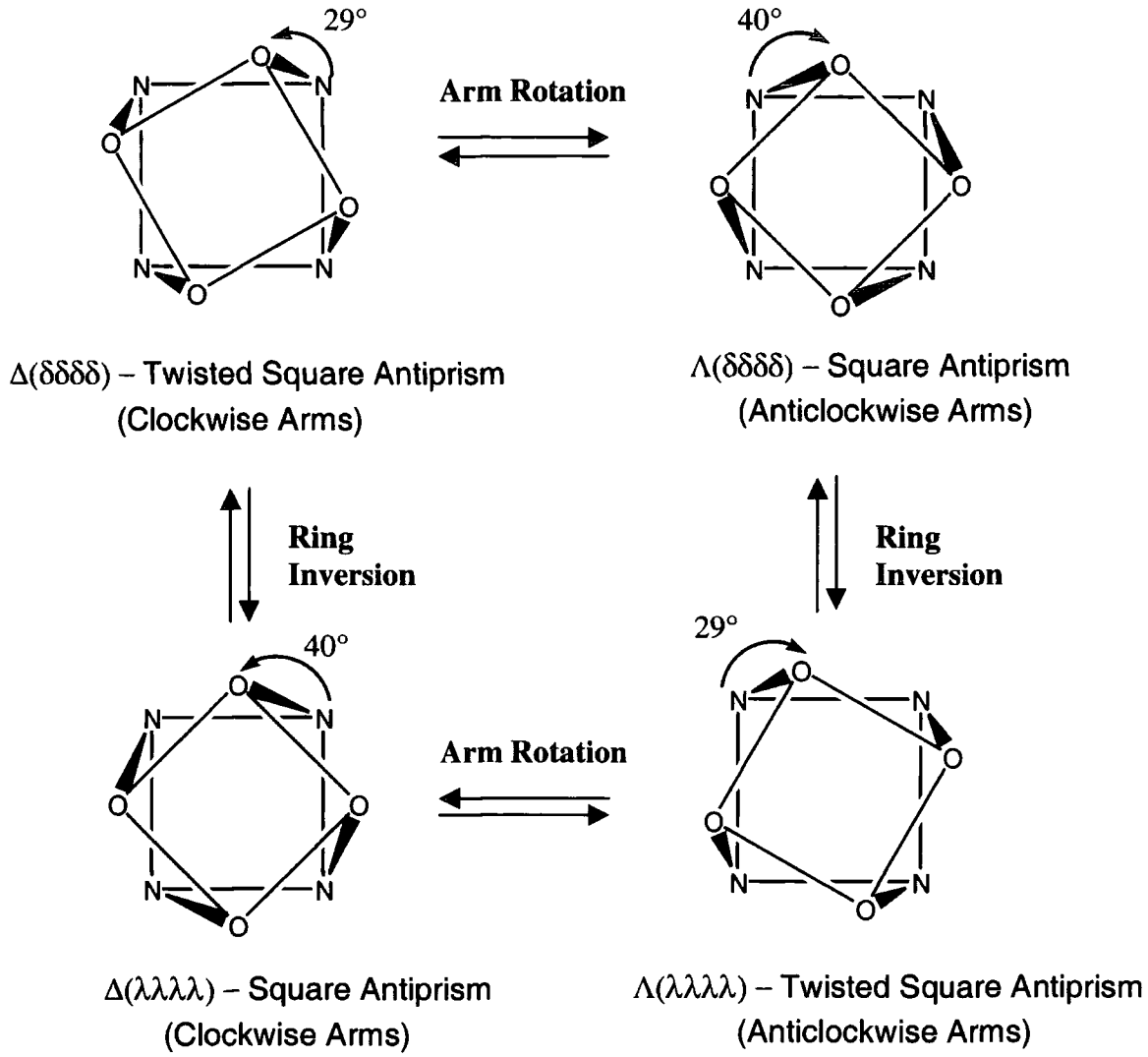

Figure 2.5 – Square Antiprism and Twisted Square Antiprism

2.3c Helical Chirality of Cyclen

The second type of helical chirality deals with the $12N_4$ ring itself.[48] If one again imagines looking along the C_4 axis of the molecule onto the face containing the pendant arms, there are three relevant planes of atoms at right angles to the C_4 axis. The uppermost plane contains the four nitrogen atoms (black in **figure 2.6**). Behind this and parallel to it is the upper plane of CH_2 groups (blue). Behind this plane is another one parallel to it containing the second type of CH_2 group (red). Each ethylene bridge therefore contains two types of CH_2 group, in different planes. Because of the non-coplanarity of the two types of CH_2 groups, the bonds connecting them slope with respect

to the three atomic planes. The slopes of the ethylene bridges can therefore be clockwise or anticlockwise, (δδδδ) or (λλλλ) respectively.

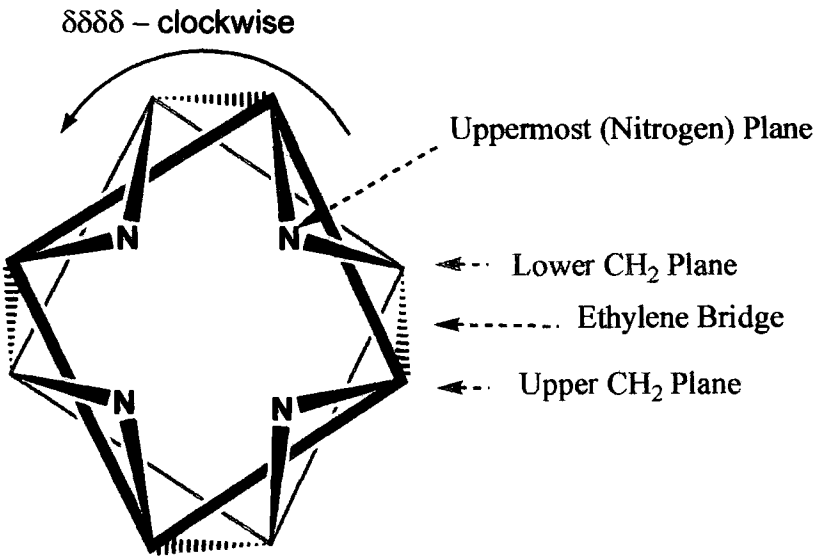

Figure 2.6 – Ring Stereochemistry – δδδδ

The combination of these two independent aspects of helical chirality gives rise to four possible stereoisomers. The Λ(δδδδ) and Δ(λλλλ) isomers, which constitute an enantiomeric pair, correspond to the (regular) square antiprismatic co-ordination geometry. The twist angle of this geometry around the four fold axis is ca. 40°. The Δ(δδδδ) and Λ(λλλλ) enantiomeric pair corresponds to the twisted square antiprismatic geometry. The twist angle here is ca. 29°.

2.3d Interconversion of Stereoisomers

Exchange spectroscopy (EXSY)[41,42] and variable temperature NMR[44,45] studies have shown each of the four isomers to be in dynamic exchange in solution. In solution the (δδδδ) to (λλλλ) interconversion occurs through cooperative ring inversion and the Δ to Λ interconversion via concerted arm rotation (**figure 2.7**). All these isomers are represented in simplified fashion in **figure 2.8**.

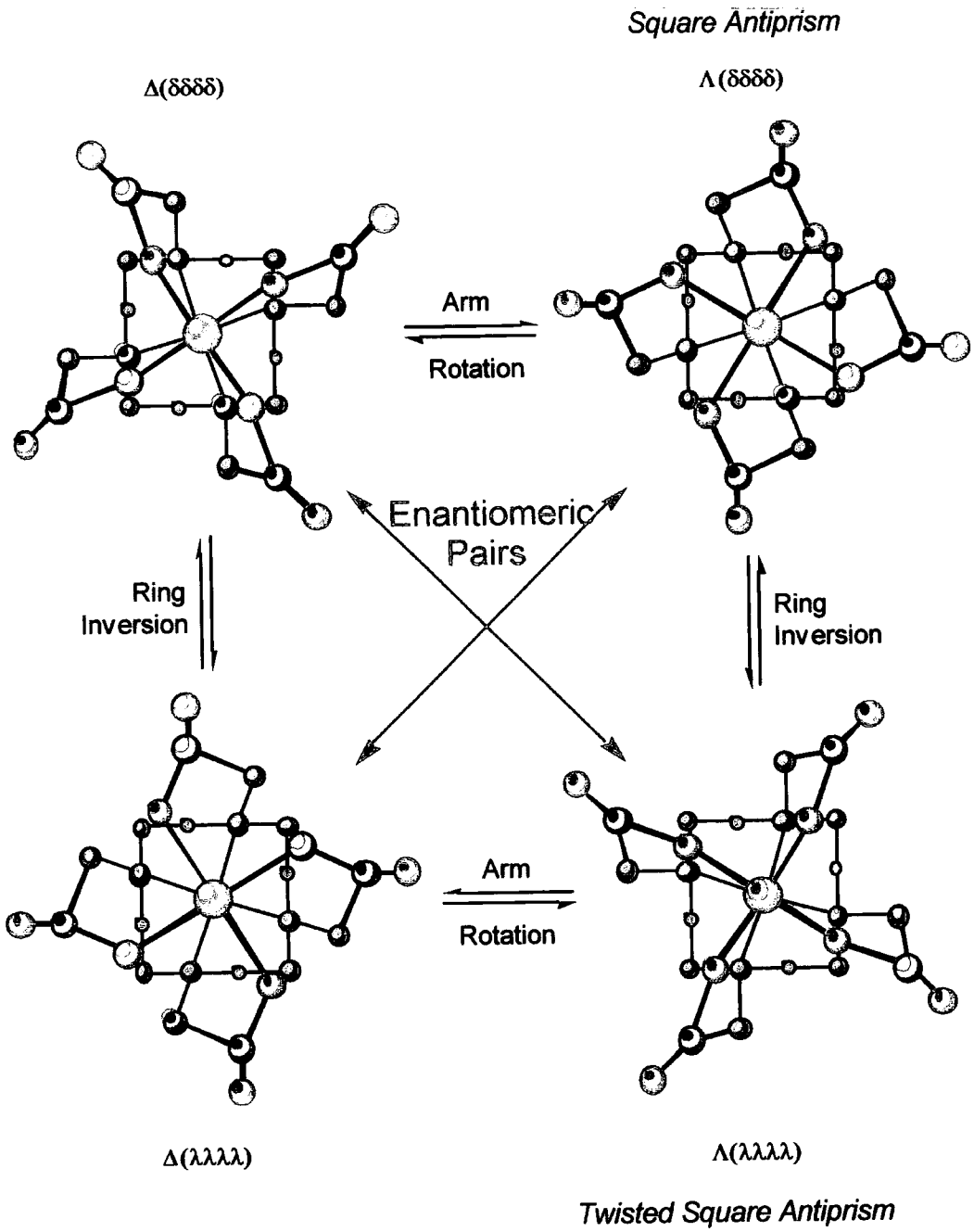

Figure 2.7 – Isomeric Interconversion (nitrogen = blue, oxygen = red)[49]

(δδδδ)

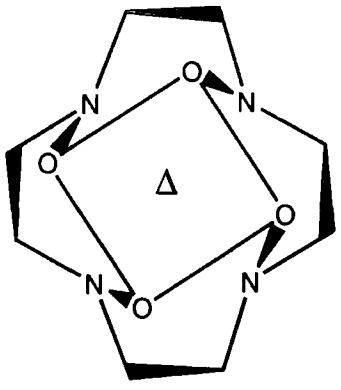

(δδδδ) Arrangement of Ethylene Bridges
(Clockwise)
Δ Arrangement of Pendant Arms

(δδδδ)

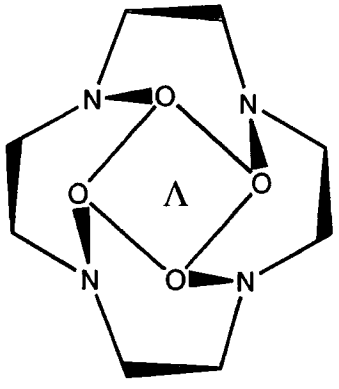

(δδδδ) Arrangement of Ethylene Bridges
(Clockwise)
Λ Arrangement of Pendant Arms

(λλλλ)

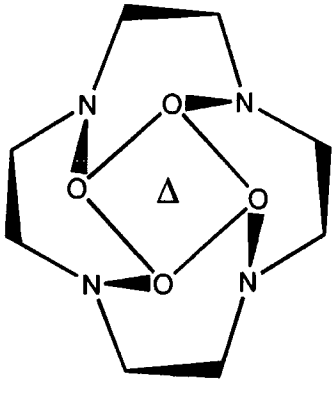

(λλλλ) Arrangement of Ethylene Bridges
(Anticlockwise)
Δ Arrangement of Pendant Arms

(λλλλ)

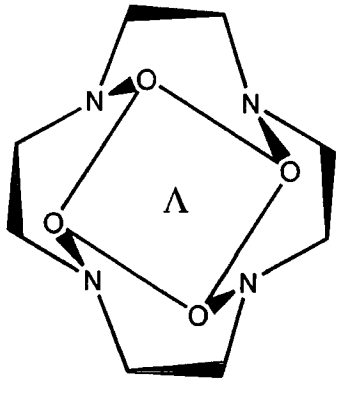

(λλλλ) Arrangement of Ethylene Bridges
(Anticlockwise)
Λ Arrangement of Pendant Arms

Figure 2.8 – Simplified Stereochemistry

2.3e Chirality of Substituted Pendant Arms

As well as these 2 basic levels of stereochemistry which pertain to Gd[DOTA]$^-$ the addition of a chiral substituent to the pendant arm, α to the carboxylate introduces a whole new set of stereochemical possibilities. Now each pendant arm may have either an

R or *S* conformation. This leads to the following possibilities; (*RRRR*)/(*SSSS*), (*RRRS*)/ (*SSSR*), (*RRSS*) and (*RSRS*), the first two pairs of which are enantiomers. The introduction of a substituent α to the ring nitrogen imparts considerable rigidity to the complex, inhibiting arm rotation (see **section 2.4**).[43]

2.4 Effect of Stereochemistry on Relaxivity

2.4a Dependence of Stereochemistry on Pendant Arms

As discussed above, [Ln.DOTA]$^-$ complexes and analogues thereof have two forms, which have also been termed M and m. The M isomer has square antiprismatic geometry, while the m isomer has twisted square antiprismatic geometry.[44]

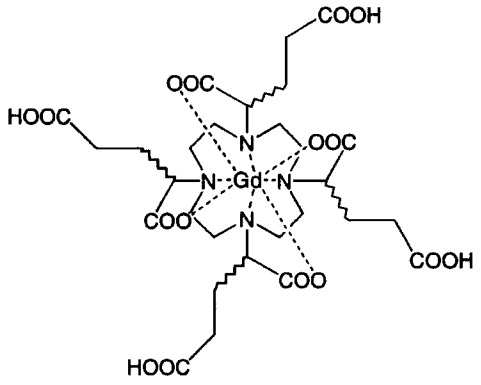

Figure 2.9 – [Gd.gDOTA]$^-$

Work carried out on the exchange characteristics of the metal-bound water in gadolinium complexes of the tetra(carboxyethyl) derivative of DOTA ([Gd.gDOTA]$^-$, **figure 2.9**) revealed an important dependency of the overall stereochemistry on the chirality of the pendant arms.[49] It was found by ^{1}H NMR that the ratio of the twisted to regular mono-capped square anti-prismatic isomers for the Eu(III) and Tb(III) complexes was in the order (*RRRR*)/(*SSSS*)>(*RRRS*)/(*SSSR*)>(*RSRS*)>(*RRSS*). It was found that the predominant isomer for [Eu (*RRRR*)] in solution was the twisted square antiprismatic configuration with a ratio of 4:1. This is opposite to the most favoured configuration in the solid state, and is probably due to favourable solvation characteristics. In the case of Tb(III) however the ratio was only 1.5:1. This is due to the smaller size of Tb(III). Because Gd(III) lies between these two isomers, it is expected that the corresponding ratio for the Gd(III) analogue lies between 4:1 and 1.5:1.

In the case of the *(RRRR)/(SSSS)* EXSY studies showed that ring inversion was occurring, but showed no sign of pendant arm rotation at room temperature. Arm rotation also appeared to be frozen out for the pair *(RRRS)/(SSSR)*. This was in contrast to the other isomers where both ring inversion and arm rotation were evident. Because of this rigidity, the *(RRRR)/(SSSS)* and *(RRRS)/(SSSR)* isomers are slow to attain complete stereochemical interconversion on the NMR timescale.

2.4b Dependence of Water Exchange Rate on Stereochemistry

The dipolar interaction of the coordinated water with the paramagnetic gadolinium cation is modulated by the molecular reorientation time, τ_R, the electron spin relaxation time, τ_S, and the water exchange lifetime, τ_M. The latter phenomenon is usually sufficiently fast to transmit the relaxation effect throughout the bulk water, but it also needs to be fast enough (fast exchange condition), not to be the limiting factor in the complex interdependent determination of the relaxation rate R_1 by these parameters (See Solomon-Bloembergen-Morgan theory).[50-52] The mean residence lifetime of $[Gd(DOTA)]^-$, τ_M, has been determined as 244 ns at 298 K.[22] It has been estimated that the optimal value of this parameter in a slowly tumbling system is in the region 10-30 ns.[22]

In the case of the tetra(carboxyethyl) derivative of DOTA, water exchange rates, determined by ^{17}O NMR, were fastest for the *(RRRR)/(SSSS)* isomer (τ_M = 16 ns, 312 K), which is significantly shorter than the parent compound. The rates were also found to correlate well with the percentage of the twisted square antiprismatic isomer, m. This is quite close to the estimated optimal value of 30 ns, for a slowly tumbling system.[22] The m isomer is responsible for 90% of the exchange events because the water exchange rate on the m-isomer is around 50 times faster than the M-isomer.[49,53,54] Indeed, it has been shown by Merbach and Pubanz[55] that the twisted square antiprismatic isomer of $[Gd.DOTA]^-$ may be the only one, which undergoes water exchange in the region of 20-40 °C.

The interconversion of the M- and m-isomers, which occurs by a concerted arm-rotation mechanism, has been suggested to be related to the water exchange process via a common non-hydrated intermediate. It may therefore be expected that the rate of water exchange will be greater for systems in which the twisted square anti-prismatic isomer

predominates. This property is ascribed to the steric crowding around the water-binding site in the twisted square antiprism isomer. The rate of water exchange is determined by the energy difference between the nine-coordinate ground state and the eight-coordinate activated state. The ground state is destabilised by steric crowding, decreasing the activation energy, thus making water exchange more favourable. Another more obvious explanation is that steric crowding lengthens slightly the Gd-OH_2 bond, making it weaker.

It was additionally shown that the *(RRRR)/(SSSS)* isomer does not undergo rapid arm rotation at room temperature. This enhanced rigidity may also be associated with an increase in the stability of the complex with respect to metal ion dissociation.[49]

2.4c Effect of Coordination Environment on Electronic Relaxation Time

In summary, the stereochemical characteristics of Gd(III) complexes have a significant effect on their relaxivity. It is the parameters τ_S and τ_M, the zero field electron spin relaxation time and the residence lifetime of a bound water molecule respectively, which are sensitive to stereochemistry, as τ_R, the rotational correlation time, is primarily dependent on the molecular mass of the complex. The electronic relaxation time, τ_S, is dependent on stereochemistry because the degree of symmetry in the coordination environment of the Gd(III) ion is one of the factors thought to determine this parameter.[22]

A very symmetric system such as the *(RRRR)/(SSSS)* isomer promotes the longer electronic relaxation times desirable for improved relaxivities. Electron relaxation on the paramagnetic metal cation causes significant fluctuations in the magnetic dipole, however this process is sufficiently slow to be near the resonant frequency range required to relax protons only in symmetrical systems.

Additionally, it is thought that the freezing out of the pendant arm rotation in solution at ambient temperature also stabilises the coordination environment symmetry, allowing even longer electron relaxation times. It has also been found that the identity of the coordinating group has an effect on τ_S.[56-58] For example, amide carbonyl co-ordination causes lower values for τ_S, (and therefore for relaxivity) compared to carboxylate groups.[22]

2.5 Relaxivity Theory

2.5a Introduction

For the purposes of modern MRI contrast agents, longitudinal relaxation rates are much more important than transverse rates. This discussion is limited to the longitudinal mechanism.

In the case of an aqueous solution of a paramagnetic species such as a Gd(III) complex, an increase in the longitudinal relaxation rate constant of the solution, R_1, where $R_1 = 1/T_1$, is observed in comparison with pure water. The observed relaxation rate, $1/T_{1,obs}$, is the sum of two components. Firstly the diamagnetic relaxation rate, $1/T_{1,d}$, which is the relaxation rate in the absence of contrast agent, and secondly the paramagnetic relaxation rate, $1/T_{1,p}$, which is the overall enhancement in relaxation rate due to the presence of the Gd(III) complex. The equation governing the longitudinal inner sphere relaxation rate is as follows.[59]

$$\frac{1}{T_{1,obs}} = \frac{1}{T_{1,d}} + \frac{1}{T_{1,p}} \qquad \textbf{Eq. 8}$$

$1/T_{1,p}$ is proportional to the concentration of the paramagnetic species, [Gd]. Note that at the concentrations normally encountered millimolarity is used, but at unusually high concentrations millimolality must be used. Therefore the mathematical definition of relaxivity, r_1, a measure of the potency of a contrast agent is as follows.

$$\frac{1}{T_{1,obs}} = \frac{1}{T_{1,d}} + r_1[\mathrm{Gd}] \qquad \textbf{Eq. 9}$$

The unit of relaxivity is therefore $mM^{-1}\ s^{-1}$, the same as that of a second order rate constant.

2.5b Gd-H Distance

As previously discussed, relaxation processes are caused by fluctuating magnetic dipole-dipole interactions. Although gadolinium has a very large paramagnetic moment, dipole-dipole relaxation is inversely proportional to the sixth power of the gadolinium-proton distance. This means that very small changes in this parameter can have a large effect on relaxivity. There are two possible ways to shorten the gadolinium-proton distance. Firstly

any increase in the tilt angle between the Gd-O bond and the plane of the water molecule will decrease r_{GdH}. This could be achieved through preferential hydrogen bonding by the water molecule to an electronegative atom on one side of the chelate only, which is unlikely in a C_4 symmetric complex like Gd[DOTA]$^-$.

Secondly, any electronic anisotropy, which causes electron localisation nearer to the water molecule, will decrease the effective Gd-H distance. However, this is not probable in the case of the stable, highly symmetric electronic state of Gd(III). Although it is very difficult to measure directly the Gd-H distance, it may be estimated from X-ray crystallographic measurements of the Gd-O distance, which has been shown to be 2.46 Å in the case of $[Gd(DOTA)H_2O]^-$ and 2.47 Å in the case of $[Gd(DTPA)H_2O]^{2-}$.[60] The Gd-H distance has been estimated to be around 3.0 Å.

Therefore, due to this dependence on the Gd-H distance, the directly coordinated sphere of water molecules is the most effectively relaxed. Directly bound water rapidly exchanges with bulk water and propagates the effect into the bulk solution. This process is referred to as the inner sphere contribution to the overall proton relaxivity.

Bulk water protons undergoing translational motion near the paramagnetic complex also experience the magnetic dipolar effect of the paramagnetic complex to a lesser degree. This separate longer-range phenomenon is called outer sphere relaxation. The total paramagnetic relaxation rate enhancement is therefore the sum of the inner sphere (IS) rate and outer sphere (OS) rate as follows.

$$\frac{1}{T_{1,p}} = \left(\frac{1}{T_{1,p}}\right)^{IS} + \left(\frac{1}{T_{1,p}}\right)^{OS} \qquad \textbf{Eq. 10}$$

$$R_1 = R_1^{IS} + R_1^{OS} \qquad \textbf{Eq. 11}$$

In addition to this rather simplified inner sphere – outer sphere model, a third category of water association may be identified. Hydrogen bonding and similar interactions with the ligand and with the inner sphere water molecules may result in a loosely coordinated layer of water molecules intermediate between the inner and outer spheres (**figure 2.10**). The contribution to relaxivity due to this interaction is called second sphere relaxivity.

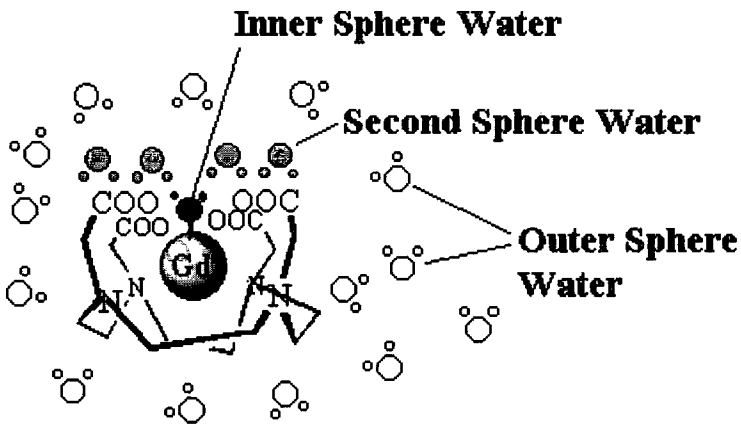

Figure 2.10 – Water Molecules around a Gd(III) DOTA Complex.

2.5c Outer Sphere/Second Sphere Proton Relaxivity

The outer sphere contribution to the overall relaxivity depends on two features of the paramagnetic cation, its spin state and its electronic relaxation time, τ_S.[21] In low molecular weight complexes with a long electronic relaxation time, the outer sphere contribution has been estimated to be equivalent to one bound water molecule.[61] It has also been shown that inner sphere water is not necessary to achieve significant relaxivities.

As shown in **figure 2.10**, there are two types of outer sphere water molecule. The random translational motion of outer sphere water molecules near the Gd(III) chelate causes modulation of the dipole-dipole interaction between the electron spin, *S*, and the proton spin, *I*. When components of the frequency of this modulation are in the right region, they cause relaxation of these protons. However, a region of more strongly associated water molecules also exists nearer to the coordinating groups, more particularly for phosphonate groups, but also in the case of poly(aminocarboxylate) complexes.[62] This type of water coordination environment is referred to as the second sphere. These molecules are less free to undergo translational motion but are nearer to the electronic spin centre. In addition, their association with the chelate system causes them to be more likely to rotate with the molecule, exposing them to rotationally modulated magnetic field fluctuations, which under the correct conditions, can cause significantly enhanced relaxivities. Another aspect of their position relative to the Gd(III) centre is that

they orientate their protons towards the metal, in contrast to inner sphere water. This is due to dipolar and hydrogen bonding to the chelating arms.

2.5d Inner Sphere Proton Relaxivity

Because of the more intimate chemical nature of the bonding between the metal centre and the water molecules in the inner sphere case, this contributor to the overall relaxivity is the most significant and most amenable to optimisation by the chemist. This relaxation process involves exchange of the water molecule, which is bound to Gd(III), with the bulk water, which is relaxed at a rate proportional to the rate of water exchange. Two models of this inner sphere process have been developed, the first for estimating the number of inner sphere water molecules or hydration number, and the second to estimate the inner sphere contribution to the total relaxivity of the complex (Solomon-Bloembergen-Morgan Theory).

2.5e Water Exchange Rate

The proton residence lifetime, τ_m, is important for two reasons. Firstly, it controls the speed and therefore the efficiency of exchange between the inner sphere and bulk water. Secondly, it contributes to the overall correlation time, τ_c, which governs the dipole-dipole interaction between the nuclear spin and the electron (see Solomon-Bloembergen-Morgan Theory). Water exchange lifetimes are optimal at *ca.* 30 ns (310 K).[22]

Proton exchange can occur either with or without the water molecule in its entirety, however at biologically relevant pH values around neutral, the acid-base catalysed exchange mechanism is of negligible importance.

τ_M may be assessed from variable temperature measurements of the O^{17} NMR transverse relaxation rate.[22] As a result of coordination to Gd(III), the relaxation of ^{17}O is enhanced. This effect broadens the linewidth of the resonance of the coordinated water molecule and the effect may be transferred to the bulk solution if the water exchange rate is sufficiently rapid.

Measuring the linewidth in the bulk solution as a function of temperature and correcting for natural linewidth, builds up a profile of the paramagnetic transverse

relaxation rate. Because the linewidth is dependent on the rate of water exchange, $1/\tau_M$, the value of τ_M may be calculated.

Values of 244 ns and 303 ns for τ_M were found for $[Gd(DOTA)H_2O]^-$ and $[Gd(DTPA)H_2O]^{2-}$ at 298 K respectively.[22] These values, which are two orders of magnitude larger than that for $[Gd(H_2O)_8]^{3+}$ (τ_M = 1.2 ns, 298 K), mean that they are within the range which can limit relaxivity values for contrast agents.

One of the factors effecting the rate of exchange on the Gd(III) centre of a octadentate complex is the mechanism of the exchange process. The bare aqua ion, $[Gd(H_2O)_8]^{3+}$, has rapid water exchange ($k_{ex}^{298} = 8 \times 10^8\ s^{-1}$)[63] because it undergoes an associative exchange process with a 9-coordinate transition state. However in systems with an 8-coordinate chelate such as DOTA, there is only one site for the binding of water, making an associative process impossible.[52] A slower dissociative process is therefore followed and the rate of this process is dependent on the stability of the 8-coordinate intermediate.

The identity of the coordinating group also appears to have an empirical effect on the exchange rate. Carboxylate group coordination increases the exchange rate, whereas amide and alcohol groups tend to decrease it. The reasoning behind this is that dissociative exchange processes rely on steric crowding to encourage the initial departure of a water molecule. However, because uncharged amide and alcohol donors have longer bonding distances and are less strongly coordinated to the Gd(III) ion, the inner sphere of the complex is reputed to be less crowded and less willing to undergo water dissociation. Studies carried out using ^{17}O NMR spectroscopy on Ln[DTPA-BMA] complexes showed that as the ionic radius of the cation decreased across the lanthanide series from Eu to Ho, the exchange rate increased greatly.[55] It has also been shown that the more negatively charged the complex, the greater the exchange rate.[64,65]

Although steric crowding around the water binding site has a significant effect on the water exchange rate, the addition of sterically demanding groups which are not in reasonably close proximity to the water binding site has very little effect on the exchange rate.[51,52,63,65-69] The design of sterically more crowded $Gd[DTPA]^{2-}$ systems is an example of how close to the water binding site a bulky group must be to have a significant effect on the water exchange rate.[70] These complexes, which are illustrated in

figure 2.11 show graphically the effect of varying degrees of steric hindrance on the water exchange lifetime, τ_M. An increase in the number of substituents on the DTPA skeleton causes a reduction in the exchange lifetime.

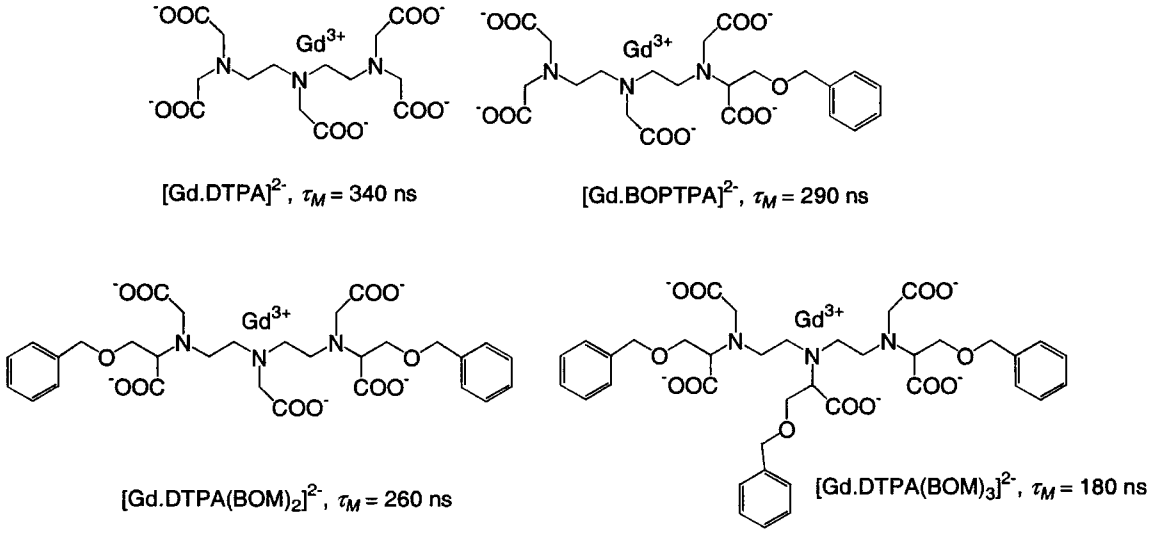

Figure 2.11 – Effect of Steric Hindrance on Exchange Lifetime (298 K)

In addition, the water exchange lifetimes of [Gd.DOTA]$^-$ and the α-methyl substituted derivative, [Gd.DOTMA]$^-$, are 244 and 68 ns respectively,[52,22] illustrating the same phenomenon in the case of DOTA-based complexes. High-resolution NMR work on the analogous Eu complexes indicated a 4:1 ratio of the square antiprismatic isomer in the case of [Gd.DOTA]$^-$, and a 1:4 isomer ratio in the case of [Gd.DOTMA]$^-$. Therefore, on the likely assumption that the same isomeric patterns are maintained for the Gd(III) complexes, it was presumed that the differences in water exchange lifetimes were due to the structural differences between the two isomers.[71]

It has been shown experimentally that the addition of polymers or dendrons to a Gd(III) macrocyclic unit has no significant effect on the water exchange kinetics at the macrocyclic centre. Exchange kinetics were assessed by ^{17}O NMR. Studies have included dendritic amides,[72] poly(ethylene glycol)[67,68] systems and polyalkyl systems.[73]

2.5f Hydration Number

Inner sphere relaxivity is linearly proportional to the number of coordinated water molecules. In aqueous solution, the aqua ion of Gd^{3+} is 8-coordinate,[74,75] and has a correspondingly high relaxivity (11.7 mM^{-1} s^{-1}, 65 MHz, 293 K).

Although the number of inner sphere water molecules may be estimated from crystallographic data, there are examples where the solid-state situation differs from that in solution.[76] This is especially true in cases where coordination equilibria exist in solution. Several techniques have been used to estimate the number of directly bound water molecules, or the q-value of Gd(III) complexes. None of these techniques is suitable for Gd(III) systems themselves, so an isostructural analogue with another lanthanide must be used.

^{17}O NMR spectroscopy may be used to study lanthanide complex systems. The contact contribution to the lanthanide-induced shift of a directly bound ^{17}O atom is independent of the ligand system involved, but depends on the q-value.[77] The slope of a plot of the dysprosium-induced shift of ^{17}O in a Dy(III) chelate system versus the complex concentration is proportional to the hydration number. By comparing known (usually $Dy(H_2O)_8^{3+}$) and unknown systems the hydration number may be calculated. Note that dysprosium is used because the interaction is primarily contact in nature.

Luminescence may also be used to estimate the hydration number.[27,78] The q-value must however be estimated from studies on the corresponding Eu(III) and Tb(III) complexes as Gd(III) is unsuitable. Eu(III) and Tb(III) complexes are the most widely used as they are adjacent to Gd(III) in the periodic table. These lanthanide ions emit relatively strongly in the visible region of the spectrum when excited at 397 nm and 355 nm respectively. However, in the presence of a co-ordinated water molecule these radiative pathways become less favoured.[79-81] This is because the water molecule provides an alternative non-radiative deactivation pathway for the excited state of the lanthanide, via energy transfer to the O-H vibrational manifold. The greater the number of O-H oscillators, the more effective the quenching.

However, this phenomenon does not occur for Gd(III) because the energy gap between the highest J level of the ground state manifold and that of the emissive state is too large (ΔE = 32,000 cm^{-1}). At these higher emissive levels the overlap between the

high-energy state and the correspondingly high vibrational quenching state becomes inefficient.

Similarly, the phenomenon of inefficient energy transfer involving high vibrational levels has an important effect on the quenching ability of D_2O. Because O-D oscillators have smaller stretching frequencies (smaller energies) than O-H oscillators, far more energy levels are needed in the vibrational 'ladder' connecting the emissive state of Ln(III) to the ground state during a non-radiative deactivation. Again, however, at these high vibrational energy levels energy transfer is very inefficient, resulting in D_2O being about 200 times less effective at quenching than H_2O.[27] This becomes important when measuring the q-value of a complex.

The deactivating effect of a co-ordinated water molecule may be assessed as follows.

$$k_{obs}^{H_2O} = k_{nat} + \Sigma k_{nr} + k_{OH} \qquad \textbf{Eq. 12}$$

Where $k_{obs}^{H_2O}$ is the observed luminescence decay constant in water, k_{nat} is the natural radiative rate constant, Σk_{nr} is the sum of the rate constants for the non-radiative processes and k_{OH} is the rate constant for non-radiative energy transfer to the O-H oscillators in water. Because this vibrational quenching is practically absent in D_2O, it may be ignored in the corresponding equation for D_2O.

$$k_{obs}^{D_2O} = k_{nat} + \Sigma k_{nr} \qquad \textbf{Eq. 13}$$

$$\Delta k_{obs} = k_{obs}^{H_2O} - k_{obs}^{D_2O} = k_{OH} \qquad \textbf{Eq. 14}$$

This relationship has been related to the number of coordinated water molecules, q.[78]

$$q_{corr} = A' \Delta k_{corr} \qquad \textbf{Eq. 15}$$

Where A' = 5 ms (Tb); 1.2 ms (Eu);1.0 μs (Yb).[82] Correction factors used for Δk, for outer sphere water molecules and amide quenching, are listed in the reference.

However, neither of these two methods has an accuracy greater than 10-20%, partly because of the difficulty of obtaining pure D_2O. This is a problem because it is not possible to tell whether a non-integral value is due to error or due to coordination equilibria. However UV-visible spectroscopic measurements on Eu(III) analogues can provide an answer. The Eu(III) absorption band in the visible range (578-582 nm, $^7F_0 \rightarrow$

$^5D_0$) is hypersensitive to its coordination environment. Hydration equilibria may be characterised in solution using this method because two species will each have a separate band.[73,83-87] The lower wavelength transition corresponds to the species with the lower hydration number.[88] Combining these data with those from other methods allows a better description of the coordination system. However, recent work has shown that the m and M isomers of [Gd(DOTA)]$^-$ have significantly different UV-visible spectra due to differences in the symmetry environment of the metal centre. This is problematic in the case of any system with coordination equilibria which are not due to different hydration states.

2.5g Solomon-Bloembergen Theory[89]

The basic equation governing the longitudinal inner sphere relaxation rate is as follows.[59]

$$R_1^{IS} = \frac{cq}{55.6}\left(\frac{1}{T_{1M} + \tau_M}\right) = P_M\left(\frac{1}{T_{1M} + \tau_M}\right) \qquad \textbf{Eq. 16}$$

Note that c is the molal concentration of contrast agent, q is the number of inner sphere water molecules per Gd(III), (P_m is therefore the mole fraction of bound water molecules), τ_M is the inner sphere lifetime of the water molecule, and T_{1M} is the longitudinal relaxation time for an inner sphere water proton. In cases where the fast exchange condition is satisfied (*i.e.* where $T_1 \gg \tau_M$), the relaxivity of Gd(III) complexes at high field is a function of q and T_{1M}. It is therefore important to optimise T_{1M}. It should also be noted that T_{1M} and τ_M exhibit opposite temperature dependencies; i.e. on lowering the temperature T_{1M} decreases while τ_M increases

The longitudinal relaxation time of inner sphere bound water molecules can further be broken down into contributions due to dipole-dipole and scalar (contact) mechanisms. However, the scalar contribution to the overall relaxation process is negligible for three reasons. Firstly, bonds to Gd(III) are highly ionic in nature. Ionic bonds do not allow effective scalar transmission. Secondly, the water proton is relatively distant from the cationic centre

The dipole-dipole mechanism is dependent on the magnetic field, the reorientation of the nuclear spin – electron spin vector, the electron spin relaxation and on water exchange. This relationship is shown below, where T_{1M} is the longitudinal

relaxation time for the dipole-dipole mechanism, γ_I is the nuclear gyromagnetic ratio, g is the electron g-factor, r is the electron spin – proton distance, ω_I and ω_S are the nuclear and electron Larmor frequencies respectively, and $A/\hbar$ is the hyperfine or scalar coupling constant between the electron of the paramagnetic centre and the proton of the coordinated water.

$$T_{1M} = \frac{2}{15}\frac{S(S+1)g^2h^2\gamma_I^2\gamma_s^2}{r^6}\left[\frac{7\tau_c}{\left(1+\omega_s^2\tau_c^2\right)}+\frac{3\tau_c}{\left(1+\omega_I^2\tau_c^2\right)}\right]+\frac{2}{3}\frac{A^2}{\hbar^2}S(S+1)\left[\frac{\tau_s}{1+\omega_s^2\tau_s^2}\right] \quad \textbf{Eq. 17}$$

The characteristic correlation time, τ_c, may be simplistically viewed as a measure of the average time interval during which the magnetic field at the nucleus is constant.[7] It is subdivided as follows.

$$\frac{1}{\tau_C} = \frac{1}{\tau_R} + \frac{1}{\tau_S} + \frac{1}{\tau_M} \quad \textbf{Eq. 18}$$

where τ_R is the reorientational correlation time of the metal – proton vector (i.e. the rotational correlation time), τ_S is the electron spin relaxation time and τ_M is the water residence lifetime on the metal.

2.5h Bloembergen-Morgan Theory[90]

This is a modification of the Solomon-Bloembergen equations. This simplified model has several assumptions associated with it:

- it is only valid if the frequency of the lattice motions is far higher than the frequency of the motions within the spin system. This is called the Redfield limit.
- the chemical exchange has no correlation with lattice motion.
- the electron Zeeman interaction dominates the electron spin system, and all other interactions result only in electron spin relaxation.
- the electron spin relaxation is assumed to be uncorrelated with molecular reorientation.
- the reorientation of the nuclear-electron spin vector is isotropic and may be characterised by a single correlation time, τ_R.
- the electron spin can be considered a point dipole at the metal centre.
- the electron g-factor is isotropic.

The rate of relaxation of the electron depends on the magnetic field strength.[90,91] For Gd(III) the rates are interpreted in terms of zero-field splitting (ZFS) interaction. The equation corresponding to the longitudinal electron spin relaxation time, T_{1e}, is as follows.

$$\left(\frac{1}{T_{1e}}\right)^{ZFS} = 2C\left(\frac{1}{1+\omega_S^2\tau_v^2} + \frac{4}{1+4\omega_S^2\tau_v^2}\right) \qquad \textbf{Eq. 19}$$

$$C = \frac{1}{50}\Delta^2\tau_v[4S(S+1)-3] \qquad \textbf{Eq. 20}$$

Where Δ^2 is the mean-square zero field splitting energy and τ_v is the correlation time for the modulation of the zero field splitting interaction. This modulation is a result of the fluctuating, transient distortions of the complex.

2.6 Nuclear Magnetic Resonance Dispersion (NMRD) Profiles

2.6a Introduction

Because the proton relaxation rate is strongly dependent on magnetic field strength, it is necessary to study the behaviour of contrast agents over a range of field strengths of several orders of magnitude, 0.01-50 MHz.[92] Modified NMR machines called field cycling relaxometers[56,93] are used for this purpose, and the plot of relaxivity versus field strength they yield is called a nuclear magnetic dispersion profile.

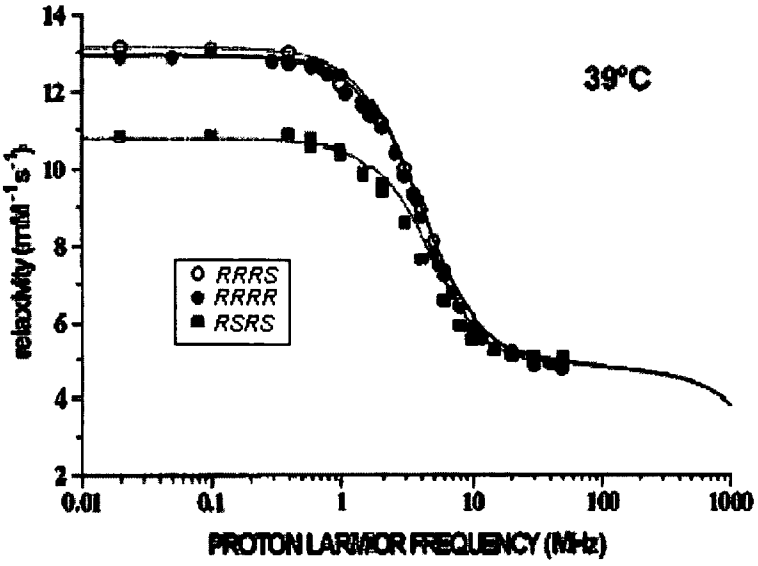

Figure 2.12 – Typical Low M_w NMRD Profiles – the (*RRRR*), (*RRRS*) and (*RSRS*) isomers of [GdgDOTA]$^-$ at 39°C.

The NMRD profile of Gd[gDOTA]$^-$ shown in **figure 2.12** is typical of low molecular weight contrast agents. It is divided into two regions. High relaxivities are obtained at low field strengths, but the relaxivity is reduced at medium to high fields. The reason for this division is that at lower field strengths, the decisive factor determining relaxivity is the electron spin relaxation time, τ_S. The value of this parameter is field dependent and is optimal at field strengths below 5 MHz, when it has values in the nanosecond range. At higher field strengths, it is the reorientational correlation time, τ_R, which is decisive. However the mass of Gd[gDOTA]$^-$ is too low for optimisation of this parameter. Note that the complex exhibits fast water exchange, meaning that the water exchange lifetime, τ_M, is not the limiting factor. The inter-relationship of these parameters has been discussed.

2.6b NMRD Results of [Gd.gDOTA]$^-$

Work carried out using NMRD profiles of Gd[tetra(carboxyethyl)DOTA], ([Gd.gDOTA]$^-$) found that the (*RRRR*)/(*SSSS*) and (*RRRS*)/(*RSSS*) isomers had longer, more favourable electronic relaxation times than the (*RSRS*) isomer (τ_s = 368 ps and 349 ps vs. 137 ps respectively).[49] This suggests some structural aspect of the (*RRRR*)/(*SSSS*)

and *(RRRS)/(RSSS)* isomers which stabilise the excited electronic state. Although the factors which affect this phenomenon are not well understood, the single obvious property shared by both the *(RRRR)/(SSSS)* and *(RRRS)/(RSSS)* isomers is the freezing out of their pendant arm rotation at room temperature. As discussed previously, this extra rigidity may stabilise the excited electronic state of the complex, because of the less perturbed environment of the Gd(III) ion at its centre.

2.6c Effect of Rotation on Relaxivity

The rapid rotation of low molecular mass Gd(III) chelates in solution limits severely their relaxivity because it is mainly τ_R which is the limiting variable at the magnetic field strengths used in MRI.

Nuclear magnetic resonance dispersion (NMRD) profiling is one method which can be used to determine a value for τ_R. Note that two factors can reduce the expected increase in relaxivity due to reduced tumbling speeds. Firstly, fast rotation of the chelate, independent of the slow rotation associated with the macromolecular moiety will reduce the effective τ_R. Secondly, it may be possible that the water molecule itself has a degree of independent rotation around the Gd-O axis within the complex itself. This has yet to be demonstrated however.

2.7 Macromolecular Contrast Agents

2.7a Background

In the case of Gd[DOTA]$^-$ where water exchange rates are favourably high and electronic relaxation times are favourably long, it is the rotational correlation time, τ_R, which limits τ_C and hence the observed relaxivity at higher, clinically relevant field strengths (20 to 60 MHz).[94] Therefore the most substantial gains in relaxivity are to be made by increasing the mass and rotational correlation time, τ_R, of the molecule,[21] up to the point where one of the other parameters, τ_M or τ_S, again becomes limiting.

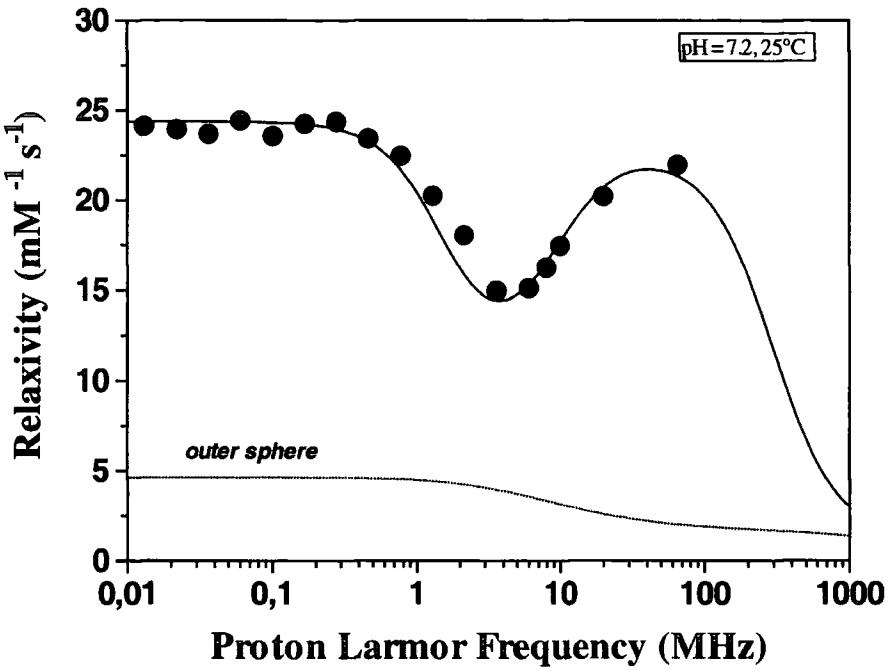

Figure 2.13 – Typical High Molecular Weight Contrast Agent NMRD Profile

The first examples of macromolecular contrast agents were based on the octadentate chelates DTPA (diethylenetriamine-pentaacetate) (**figure 2.3**) and EDTA (ethylenediaminetetraacetic acid) of Gd(III), covalently attached to the proteins bovine serum albumin (BSA) or immunoglobulin G (IgG) to provide the desired high molecular masses. [95] NMRD profiles obtained for these conjugates exhibited significant increases in relaxivity. For example, the [Gd.DTPA]-protein conjugates displayed a five-fold increase in relaxivity in the imaging range (0.15-0.5 T). One advantage of this approach is that if human proteins are used, immune system tolerance issues are avoided. This approach also prolongs the vascular retention time of the paramagnetic agent.

However, a disadvantage is that the complexes are either bound to the macromolecule only in one place, and are free to rotate rapidly about this one bond. Alternatively, they may be bound to a single domain of the protein, which has some conformational flexibility.

In the case of synthetic linear polymers, the rapid segmental motion of the chain precludes any concerted macromolecular tumbling.[96] These rapid rotations, while not as

fast as in the low molecular mass complex alone, may still limit the relaxivity. For this reason it is preferable to bind a macromolecule to several places on the core, thereby reducing the rotational degrees of freedom available to the molecule and more effectively coupling the motion of the core Gd(III) complex to that of the macromolecule.

The highest relaxivity observed to date (ca. 56 mM^{-1} s^{-1} at 312 K, 20 MHz) was exhibited by a host-guest hydrophobic interaction between a $[Gd(DOTA)]^-$ system bearing three β-benzyloxy-α-propionic substituents and human serum albumin (HSA).[45] It is thought that a substantial increase in relaxivity is due to interaction with nearby water molecules from the macromolecular hydration sphere, and from exchangeable protein protons.

An alternative way to restrict rotational degrees of freedom is to make the linker between the low molecular mass chelate and the macromolecule as rigid as possible. The compound MS 325 is an example of this approach.[97] Developed by Epix Medical (USA), the substance bears two phenyl groups for non-covalent bonding to the human serum albumin (HSA) protein. These are linked to a cyclohexyl ring and then via a phosphate ester group to the DTPA chelate of Gd(III). The rotational rigidity imparted by this arrangement leads to enhanced relaxivities of 24 $mM^{-1}s^{-1}$ (312K, 64 MHz).

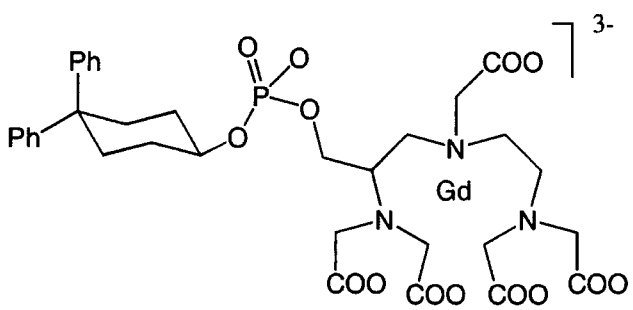

Figure 2.14 – MS 325 (Epix Medical)

It has been shown that tetracarboxymethyl DOTA, tetrasubstituted with β-cyclodextrin exhibited a marked increase in relaxivity in the 5-50 MHz region of the NMRD profile.[98] This is the region where τ_R is the dominant factor in determining relaxivity. However the complex used consisted of a mixture of isomers, and it is presumed that the relaxation rate may be further enhanced by using solely the *(RRRR)/(SSSS)* isomer, which exhibits the greatest water exchange rate. Larger

macromolecules were also expected to have an enhancing effect. It has also been observed that an increase in τ_R enhances the relaxivity of outer sphere water molecules. This has been ascribed to second sphere interactions.

2.7b Principle Behind Strategy of Thesis

An alternative method for effectively coupling slow macromolecular rotational motion to a Gd(III) chelate is to synthesise a system where the metal cation is at the centre of the macromolecule (barycentre). This arrangement ensures that the metal lies on the axis of any reorientational motion. Anchoring the chelate at the centre of the macromolecule greatly restricts any alternative degrees of rotational freedom available. However, polymeric systems are not particularly effective at increasing τ_R because they have considerable internal flexibility.

2.8 Dendrimers

2.8a Synthesis

Dendrimers are monodisperse macromolecules with a regular, highly branched three-dimensional structure (see **figure 2.15**). In contrast to linear polymers, dendrimers[99] are made up of a central core bound to several dendrons. These have a more rigid, wedge-like branched structure and are more likely to form a globular shape when bound to the core, as they are far less flexible due to steric crowding.

Dendrimers are produced by an iterative reaction sequence, which leads to ever higher generations of dendrimer. The first example of such a cascade synthesis was reported by Vögtle.[100] The poly(amido-amine) (PAMAM) dendrimers by Tomalia[101,102] and Newkome's arborol systems[103] were the first dendritic systems to be studied and characterised in more detail. Both systems were synthesised in a divergent fashion, *i.e.* a multifunctional core was iteratively functionalised and extended to form the various generations. The opposite convergent approach to synthesis was introduced by Fréchet in 1990.[104,105] Here the synthesis is commenced at the periphery and elaborated to the core (see **figure 4.8**).

Both the convergent and divergent approaches to dendrimer synthesis involve the repetition of reaction steps, but they have different characteristics, especially regarding

the purity and perfection of the product. Because the divergent synthesis requires that numerous reactions be carried out on the same molecule as it is built up, even reactions with very high selectivities will eventually lead to defects and imperfections. This is because each new generation produces many more functional groups at the periphery which must all be converted successfully in the subsequent steps to the next generation in order for there to be no defects. Because each new generation of dendrimer cannot be purified due to the small differences between defective and defect-free molecules, the presence of a number of statistical defects cannot be avoided.

In the convergent approach, these difficulties have been avoided by starting the synthetic procedure at the periphery and ending at the core. Each 'generation' of dendritic wedge or dendron has only one reaction site for coupling to the monomer to produce the next generation. Defective partially substituted monomers are often chromatographically separable from the pure product, especially in the case of smaller systems.

2.8b Structure

Schematically, dendrimers are generally represented as symmetricallly arranged structures with all dendritic arms radiating outwards from the core having all end groups located at the surface. However, this is not always so. Studies on the localisation of end groups have shown that a considerable degree of backfolding occurs,[99,106,107] which causes a distribution of terminal functionalities throughout the volume of the dendrimer. One such study on poly(arylether) dendrimers with a paramagnetic core measured the spin-lattice relaxation time, T_1.[108] The data revealed that some of the end groups were close to the core of the dendrimer. The degree to which terminal functional groups lie on the surface of a dendrimer molecule is dependent on the polarity of the solvent and on the solvation characteristics of the terminal groups.[109] The better the solvent, the more open the structure of the dendrimer. Poor solvents cause extensive backfolding to minimise energetically unfavourable interactions.

An idealised bifurcated (or bifunctional) dendritic system is represented schematically in a two-dimensional manner in **figure 2.15**. Layers of repeat units are built up iteratively, each time increasing the degree of branching. Each layer of repeat units is called a generation. Note the large number of terminal functional groups. At the

opposite end of the dendron (or dendrimer 'wedge') is the functionality by which it is attached to the core. This is called the focal point group.

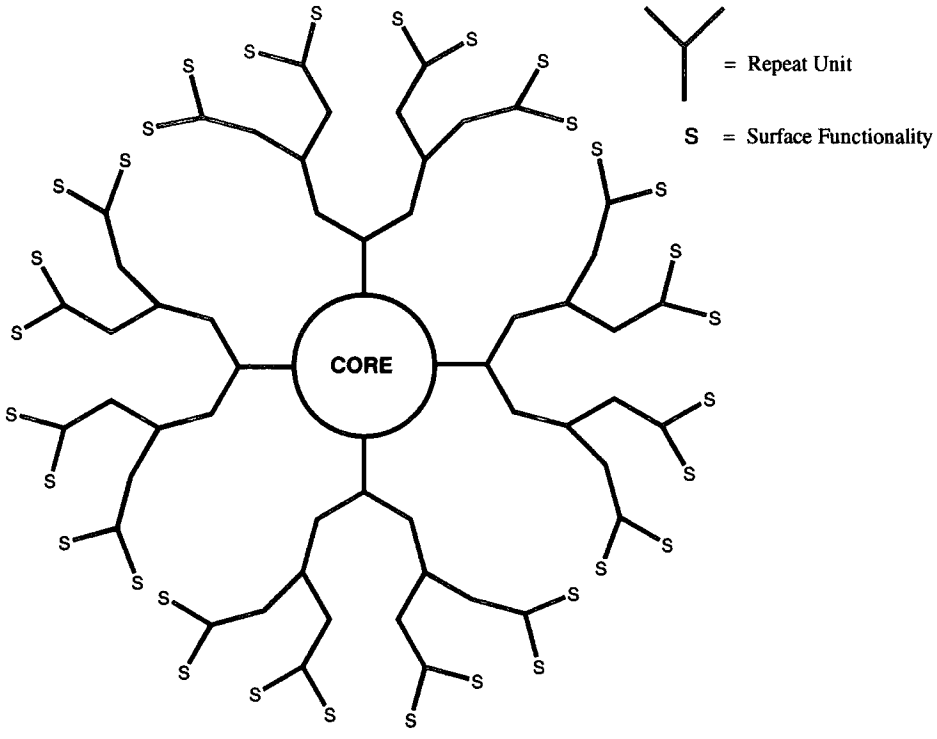

Figure 2.15 – Schematic Representation of a Bifurcated Dendrimer

2.8c Dendritic Contrast Agents

Extra steric crowding ensures that there are fewer degrees of rotational freedom available to the central chelate in a dendrimer. Studies carried out on Starburst® polyamidoamine (PAMAM) dendrimers with multiple terminal Gd(DTPA) moieties showed that the relaxation rates of the carbon atoms in the dendrimer chains, as measured by ^{13}C NMR, multiplied by several orders of magnitude for generations 1-10, and doubled for carbons on the surface.[110,111]

Moreover, similar studies using EPR on vanadyl chelate systems bound to polyamidoamine (PAMAM) dendrons have shown that even though the rotational motion of the molecule as a whole may be slow, the rotation around the bond between the chelate and the dendron may be rapid.[110,112] Unlike polyamides and polysaccharides which exhibit polymer segmental motion which is independent of increases in molecular weight above ca. 10,000 Da,[113,114] and is therefore limiting with respect to relaxivity, the

sterically crowded Starburst® dendrimers have rotational correlation times which continue to increase with molecular weight.[115] This finding has been strengthened by the fact that poly(lysine) and dextran Gd(III) conjugates have been found to exhibit lower molecular relaxivities than dendrimer conjugates of similar molecular weight.[116,117]

Complex	Mw	No. Gd(III)	T/K	Molecular $R_1/mM^{-1}s^{-1}$	Ionic $R_1/mM^{-1}s^{-1}$
Gd(DTPA)-dendrimer	139k	170	293	5800	34
Gd(DTPA)-dendrimer	8.5k	11	293	234	21
Gd(DTPAAM)-albumin	90k	30	298	420	14
Gd(DTPAAM)-poly(lysine)	71k	90	310	990	11
Gd(DTPAAM)-dextran	75k	15	298	158	10.5
Gd(DTPA)	545	1	293	6.4	6.4

Note 1: In these DTPA-based systems, slow water exchange limits any relaxivity gain associated with variation of τ_R.
Note 2: DTPAAM is the monoamide of DTPA resulting from the reaction of DTPA anhydride with the macromolecule.

Figure 2.16 – Relaxivities of Macromolecular Contrast Agents[111]

Enhanced proton relaxivities (r_1 = 14.6, 15.9 and 18.7 mM^{-1} s^{-1} respectively) were also obtained by attaching generation 3, 4 and 5 amide dendrons to Gd(DO3A) (M_w = 22.1 kDa, 37.4 kDa, 61.8 kDa respectively).[72] The absence of a steeper increase in relaxivity was ascribed to some flexibility in the linker between the chelate and the dendrons. More importantly, this system also suffered from slow water exchange, limiting the relaxivity gains from the τ_R effect.

Work conducted by S. Aime and co-workers[58] has confirmed the importance of the rigidity and degree of globularity of the macromolecular moiety. Work on the synthesis of high molecular weight, slowly tumbling Gd(III) complexes which would bind to human serum albumin (HSA), led to the synthesis a PEG-5000 derivative of the hexadentate chelate H_4TREN-HOPO-TAM (r_1 = 8.8 mM^{-1} s^{-1}, 20 MHz, 25°C for the non-coupled system) as illustrated in **figure 2.17**. Only a small increase in τ_R was reported for the PEG-derivatised system (r_1 = 9.1 mM^{-1} s^{-1}, 20 MHz, 25°) probably due to rapid internal motions within the polymer chain. However, interpretation of this result is tempered by the fact that the parent low molecular weight system had a q-value of 2, whereas this was reduced to a value of 1 for the macromolecular system. This change was attributed to the partial displacement of water molecules by the PEG oxygens.

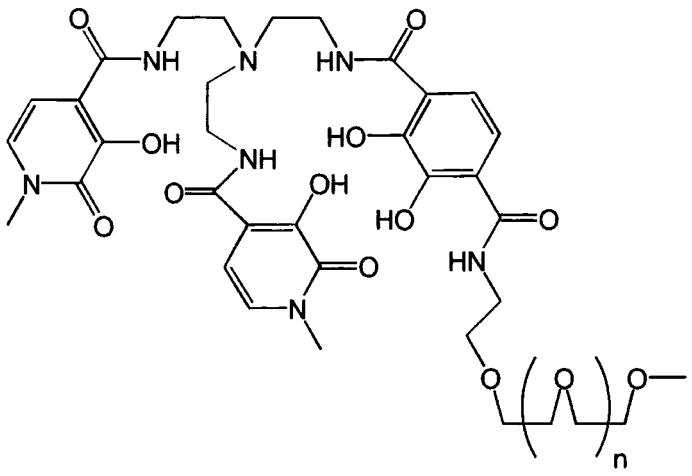

Figure 2.17 – H_4TREN-HOPO-TAM-PEG-5000, median n = 121

Work conducted within this group has shown similar results.[163] An experiment in which tetrasubstitution of Gd[gDOTA]$^-$ with PEG chains, initially with average M_w = 2000, and then 6000 each, led to relaxivities of *ca.* 9 mM^{-1} s^{-1} in both cases. This illustrates the lack of effect on relaxivity of the linear PEG, despite the large increase in molecular weight. This may be attributed to the chaotic segmental motion of the polymer chain and its lack of coupling to the chelate centre.

Similar work by Toth and co-workers illustrated the same phenomenon with regard to limited decreases in τ_R after PEG-derivatisation in the case of [Gd.DTPA-BA] (**figure 2.18**).[187] This work has been directed towards the elucidation of how the attachment of a linear PEG chain would effect the exchange rate between inner and outer sphere water in the 8-coordinate gadolinium complex of the ligand illustrated below.

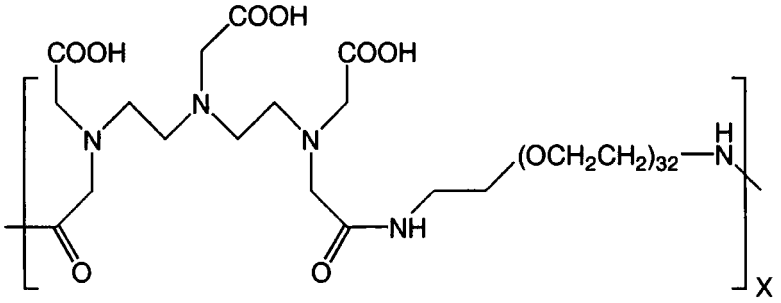

Figure 2.18 – DTPA-BA-PEG

The rate and mechanism of water exchange was unaffected in this poly(aminocarboxylate) q = 1 complex, in contrast to the [Gd.TREN-HOPO-TAM]

complex discussed above. Importantly, the relaxivity of the PEG functionalised complex was only 1.5 times that of the non-functionalised analogue. Again this was attributed to fast internal motion within the polymer chains.

In general dendimers have low solution viscosities because intermolecular chain entanglement is less likely than in linear polymers. The relationship between intrinsic viscosity (η) and molecular weight shows a maximum viscosity in the range 3 to 5 kDa. This has been shown for PAMAM,[118] poly(propyleneimine)[119] and polyether dendrimers.[120]

There are safety concerns regarding the use of high molecular mass contrast agents in the body. Large molecules are more likely to antagonise the immune system than smaller ones, possibly causing dangerous anaphylactic shock. Biocompatible macromolecules such as polyethylene glycol (PEG), or dendrimers of analogous structure, seem to offer the best solution to this problem, as they will tend not to bind to proteins and are not taken up into the reticuloendothelial system. Indeed PEG is known to be non-toxic, non-antigenic, biocompatible and non-biodegradable.[121]

2.9 Aim of this Thesis

Initially, it is very important when designing a new contrast agent to understand thoroughly the relationship between the molecule's function, and its structure and environment. The preceeding discussions have described these relationships in some detail. An understanding of the inter-relationship between these parameters has also been dealt with. The aim of this thesis was to utilise these tools to design an improved MRI contrast agent.

This was to be achieved by slowing the rate of rotation of the system in solution, which has been shown to lead to an enhanced relaxivity. This required that the contrast agent have a high molecular weight, but also that the increase in molecular weight be distributed as symmetrically as possible around the core of the molecule in a globular arrangement, with the key gadolinium chelate at the core. This was envisaged to allow maximum modulation of relaxation, of the slowly rotating coordinated water molecules, by the paramagnetic gadolinium ion.

Additionally, it was important to base the high molecular weight system on a well-understood low molecular weight analogue. This was to ensure parameters such as the coordination environment, q-value and chelate stereochemistry were fixed within a range where good relaxivity values and stability could be expected. To this end, target molecules were identified as various tetrasubstituted $(Gd[DOTA])^-$ chelates, the syntheses of which are outlined in the following chapters. This core structure was then covalently attached to four amine-terminated, water-soluble dendrons to form what was envisaged to be a series of globular dendrimers with long rotational correlation times and high relaxivities.

2.10 Schematic Summary of Important Parameters

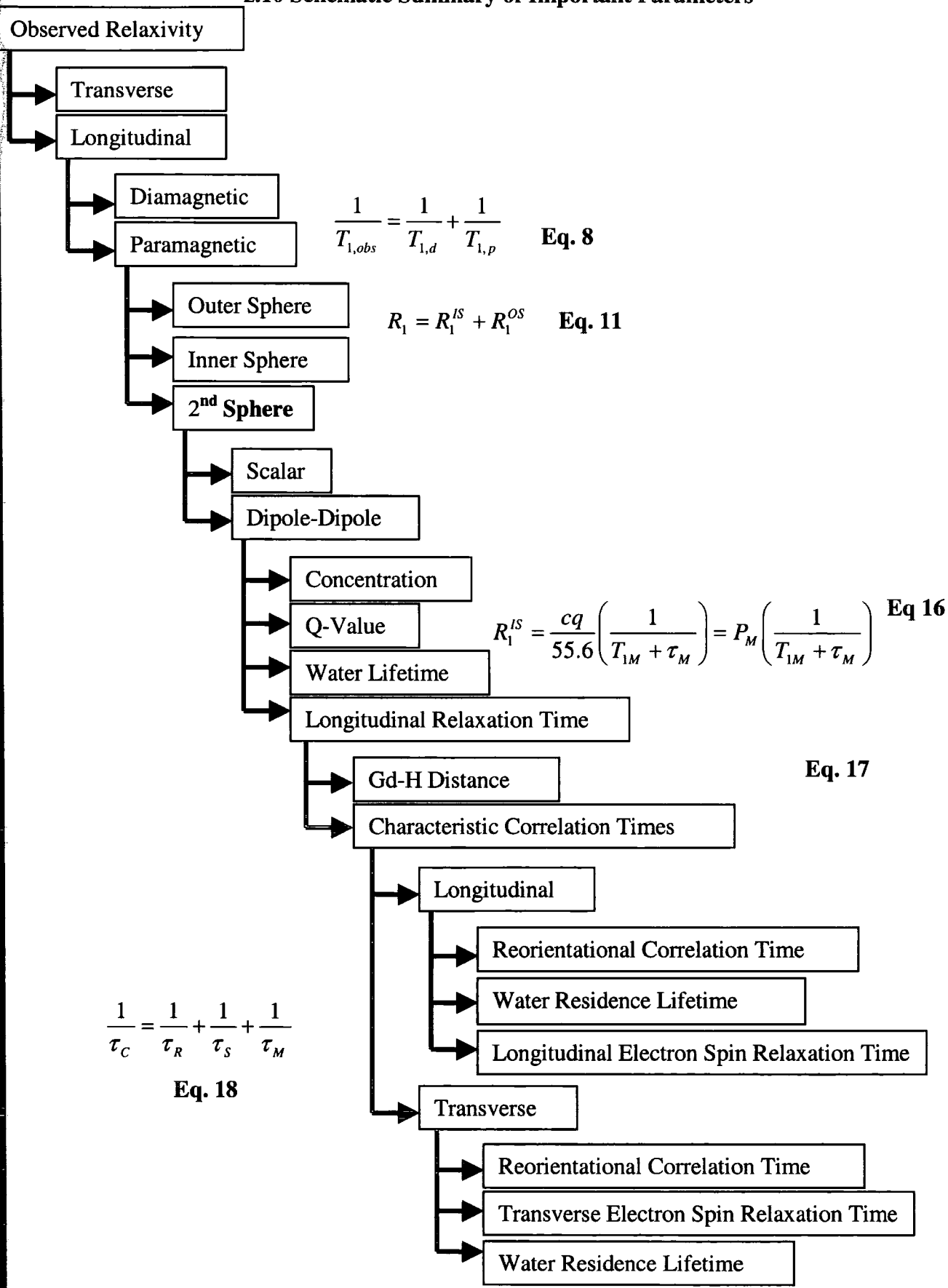

$$\frac{1}{\tau_C} = \frac{1}{\tau_R} + \frac{1}{\tau_S} + \frac{1}{\tau_M}$$

Eq. 18

Chapter 3

Synthetic Approaches to Gadolinium Chelates

This chapter initially discusses the target molecules and the reasons why they were chosen. It then goes on to outline the synthetic routes which were followed, and rationalises their synthetic outcomes.

3.1 Structural Features

As previously discussed, the DOTA ligand is an attractive system due to a range of features of its complexes with lanthanide ions, and gadolinium (III) in particular. The [Gd.DOTA]$^-$ complex is very stable and non-toxic under biological conditions, it has a labile axial water binding site and the general dependence of its relaxivity on its stereochemistry is understood. With these structure-function relationships in mind, new chelate systems based on DOTA have been designed with a view to improving relaxivity values compared to [Gd.DOTA]$^-$ itself.

Symmetrically tetra-substituted complexes were designed with a view to incorporating relatively high molecular weight moieties. Amide coupling was chosen to attach the high molecular weight moiety to the core due to its relative ease and stability, especially with respect to changes in pH. This obviously limited the nature of the groups on the pendant arm of the core DOTA complex to carboxylic acids and amines. Symmetrical substitution was considered important to maximise the electronic relaxation time, and to ensure that the Gd(III) ion was at the centre of any tumbling motion.

There are two positions within DOTA where the attachment of pendant groups can be envisaged – on the ring ethylene groups and on the acetate pendant arm methylene groups. Attachment of substituents to the $12N_4$ ring requires their introduction prior to the synthesis of the $12N_4$ ring moeity. This is a rather long and difficult process. It is much easier to use a suitably substituted acetate-derived alkylating agent when adding the pendant arms to cyclen itself, which is commercially available.

3.2 Cyclen Alkylation with α-Haloacid Derivatives

The first reported synthesis of α-substituted DOTA was in 1984 (**figure 3.1**).[122] (*S*)-2-Chloropropanoic acid (**1**) was used to alkylate cyclen (**2**) yielding 1,4,7,10-

tetraazacyclododecane-1,4,7,10-tetra(α-methyl acetate) (DOTMA, **3**). After crystallisation, DOTMA was isolated as the pure (*RRRR*) isomer.

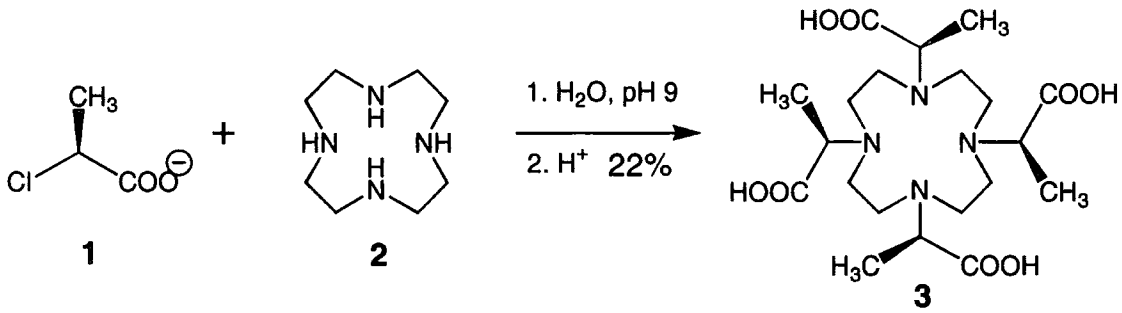

1 **2** **3**

Figure 3.1 – DOTMA Synthesis

The Eu(III), Tb(III) and Yb(III) complexes of DOTMA were found to be similar to those of DOTA. The ytterbium and europium complexes each possessed one bound water molecule in solution. (*RRRR*) [Eu.DOTMA]$^-$ was found to exist as two species in solution following luminescence studies, examining the $^5D_0 \rightarrow {}^7F_0$ transition in the emission spectrum. (*RRRR*) [Yb.DOTMA]$^-$ was also found to exist as two species by NMR. These findings are consistent with the presence of m and M isomers.

Studies conducted on [Gd.DOTMA]$^-$ have revealed that although it has a smaller q-value than [Gd.DOTA]$^-$ (0.7 and 1.0 respectively), it exhibits slightly higher relaxivity (R_1 = 3.8 and 3.5 $mM^{-1}s^{-1}$ at 37°C respectively).[123] This phenomenon was originally attributed to the increased rigidity of the complex leading to a longer electronic relaxation time. It was later appreciated that the rise is associated with a faster exchange rate and a slightly higher τ_R value. Other work on the substitution of the pendant acetate arms of DOTA has confirmed its beneficial effects in terms of both stability and relaxivity.[57,124]

A further example of the use of a ring *N*-alkylation is provided by the synthesis of the tetra(carboxyethyl) DOTA derivative (gDOTA, **5**)[98] by Guerbet S.A. (France), which was discussed in chapter 1. Racemic dimethyl-2-bromopentanedioate (**4**) was used to tetraalkylate cyclen, overnight, with very little evidence of elimination (**figure 3.2**). Attempts to synthesise the enantiopure bromo compound failed.

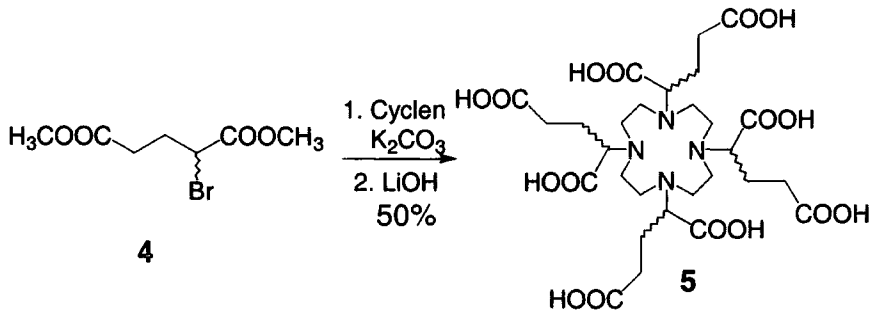

Figure 3.2 – gDOTA Synthesis

The syntheses outlined above relied on the use of a halogenated alkylating agent. α-Bromoacids may be prepared from readily available amino acids by diazotisation in the presence of bromide anions, using toluene as a solvent to disfavour any S_N1 process. However, alkylation reactions with α-bromo and α-chloro alkylating agents can result in extensive racemisation due to halide exchange, especially in the case of the α-bromo acid compounds, due to the greater nucleoplilicity of the bromide ion. The use of α-chloro and α-bromoacids can also result in elimination (**figure 3.4**).

An additional problem with α-haloacids is the replacement of the desired S_N2 alkylation mechanism by an S_Ni mechanism in the case of substrates possessing significant steric bulk (**figure 3.3**). [125] This occurs because the steric bulk increases the energy of the S_N2 transition state, making the sterically less hindered S_Ni reaction pathway more likely. This mechanism involves anchimeric assistance from the carboxylate group. Because the S_N1 pathway proceeds with inversion and the S_Ni pathway proceeds with retention of configuration, any combination of the two will produce at least partial racemisation.

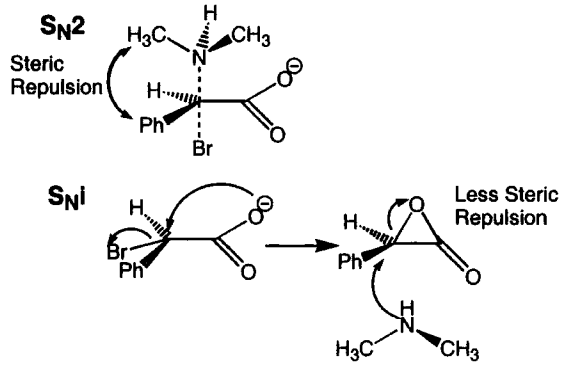

Figure 3.3 – S_N2 and S_Ni Pathways

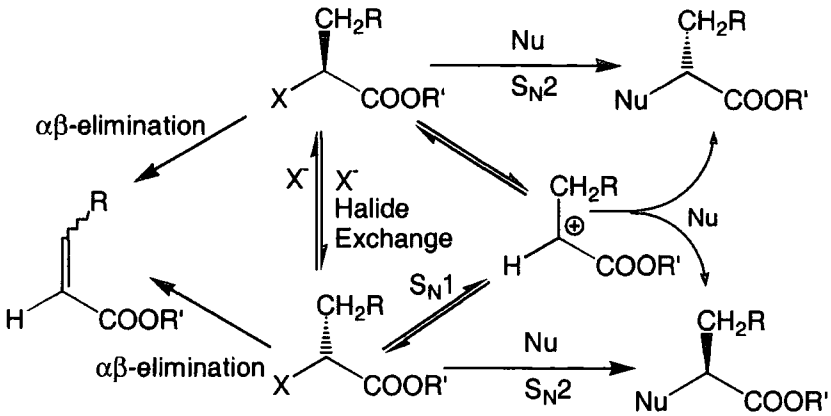

Figure 3.4 – S_N1, S_N2 and Elimination Pathways

3.3 Alkylation of Cyclen with Triflates

As well as an optically pure α-chloroester alkylating agent, cyclen has also been successfully alkylated with an optically pure α-trifluoromethylsulphonyloxyester alkylating agent **6** (a triflate), derived from benzyl lactate (**figure 3.5**).[126]

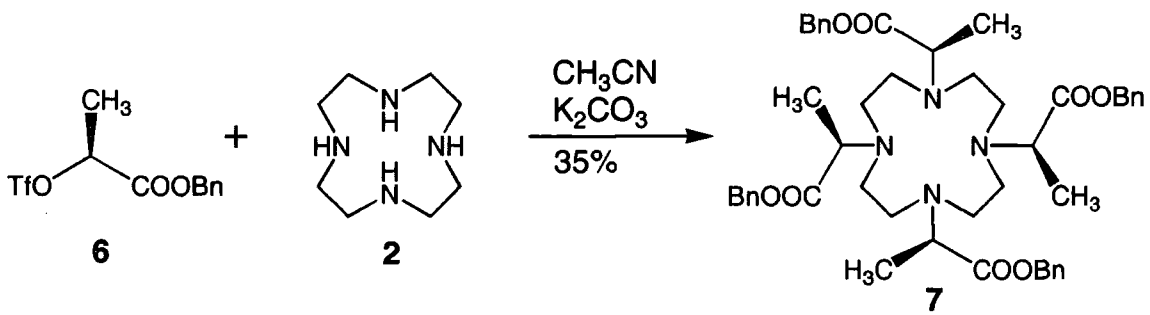

Figure 3.5 – Alkylation of Cyclen with a Triflate

There are several advantages to the use of triflates. They are powerful alkylating agents, which may be used under moderate conditions. Triflates give high yields in a clean S_N2 reaction with much shorter reaction times.[127] They are also quite stable, not being rapidly hydrolysed by atmospheric moisture.[128,129] Effenberger has shown that 2-triflyloxyesters cleanly undergo enantiospecific nucleophilic substitution with secondary amines to give α-aminoesters with inversion of configuration.[127,130] Triflates may easily be prepared from the corresponding enantiomerically pure alcohol.

For these reactions, secondary substrates generally react by an S_N2 mechanism, except that an S_N1 pathway may become more important in more polar media due to

cation solvation and stabilisation.[131] Reactions proceeding via an intermediate α-carbonyl cation have reduced S_N1 rates due to destabilisation of the carbocation by electron withdrawal (inductive destabilisation). Note however that β-aryl groups shift the character of the substitution towards the $E1_{CB}$ (conjugate base) mechanism.

However a note of caution regarding the use of triflate derivatives must be considered. Attempts to synthesise tetra(carboxyethyl) DOTA using (*S*)-dimethyl-2-triflyloxypentandioate and cyclen failed because the triflate rapidly underwent intramolecular cyclisation to yield 3-methoxycarbonyl-γ-lactone. Attempts to protect the carboxylic acid termini as less reactive tertiary amides instead of esters also failed.[98]

Of course, there are less reactive analogues of triflates. However, in the case of α-methylsulphonyloxy (mesyl) and α-toluenesulphonyloxy (tosyl) carboxylic acid derivatives, more drastic reaction conditions are required to attain an acceptable yield. Moreover, these conditions can lead to extensive concomitant elimination and also racemisation.[132] In addition to the triflyl group, the nosyl (*p*-nitrobenzenesulphonate) group has been demonstrated to give rise to a clean, optically pure substitution with amines (**figure 3.6**).[130]

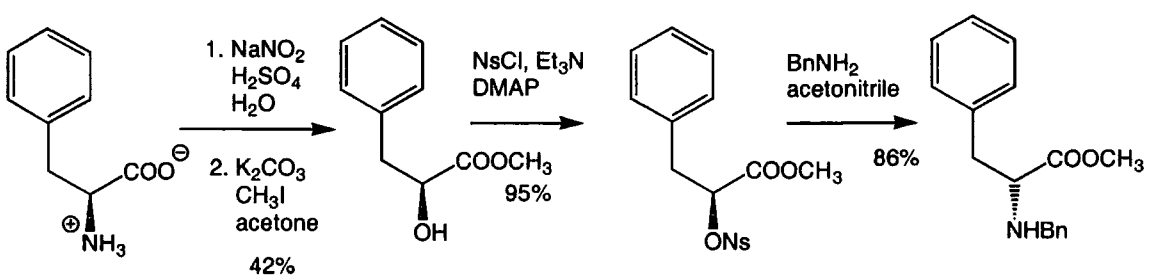

Figure 3.6 – Phenylalanine-derived Nosylate

3.4 Racemic Syntheses and Epimerisation

Because of the difficulties associated with stereoselective syntheses, previous work within the group has mainly dealt with the alkylation of $12N_4$ using racemic alkylating agents.[98,133] One successful alternative approach to obtaining a significant percentage of the (*RRRR*)/(*SSSS*) systems was the epimerisation of the mixture of isomers of the Gd complex, allowing conversion into the desired stereoisomeric pair.

It was established that the α-methylene protons on the acetate pendant arm of [Eu.DOTA]$^-$ were sufficiently acidic to allow hydrogen-deuterium exchange at pD 11 (100°C, 24 h).[134] It was anticipated that an α-substituted acetate pendant arm might display similar properties,[98] notwithstanding the reduced acidity associated with inductive destabilisation of the enolate anion. This meant that interconversion of isomers would occur leading to enrichment of the thermodynamically favoured isomer. The steric demand of the alkyl substitution in [Eu.gDOTA]$^{5-}$ was expected to be minimised in the *(RRRR)/(SSSS)* pair. After 4 weeks at pH 12.5 only the *(RRRR)/(SSSS)* isomeric pair was present in solution. However it was established that this process did not involve an enolisation process. It occurred because the *(RRRR)/(SSSS)* pair was the most difficult to decomplex, and under the conditions employed, the other isomers underwent decomplexation preferentially, with the irreversible precipitation of $Gd(OH)_3$.

However, it was established that epimerisation is possible at low pH (*ca.* 3) with the Lewis acidity of the lanthanide itself promoting interconversion. The following mechanism was proposed.[98] Because the *(RRRR)/(SSSS)* pair is the most stable, it tends not to decomplex once formed. The other isomeric pairs however continuously enolise very slowly until the equilibrium distribution is attained (**figure 3.7**).

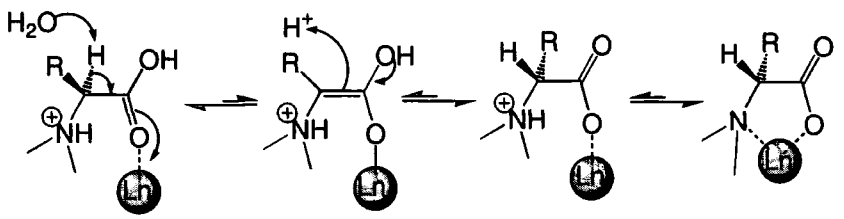

Figure 3.7 – Mechanism of Epimerisation

As an alternative method, fractional crystallisation of the mixture of ligand stereoisomers allows isolation of each diastereomer.[49]

3.5 Choice of Pendant Arms

However, it was anticipated that the use of triflates could provide a means of producing enantiopure DOTA derivatives without the need for epimerisation. Work conducted within the group has highlighted the importance of the identity of the base during the cyclen alkylation reaction.[98] The alkylation of cyclen with (*S*)-diethyl-2-

triflyloxybutandioate was carried out. After *N*-alkylation, the resultant ammonium cation must be deprotonated. Each deprotonation process on the progressively more alkylated cyclen corresponds to a nitrogen centre with a higher pK_a. Consequently, triethylamine is not a strong enough base to deprotonate the later ammonium cations formed during the alkylation process. The reaction proceeds only as far as trialkylation. Stronger carbonate bases are therefore necessary to allow tetraalkylation. It was additionally found that a mixture of diastereomers was present, indicating that a pure S_N2 reaction had not occurred. It is possible that the elevated temperatures (50°C) used in the reaction may have introduced some S_N1 character to the reaction.

The stereochemical consequences are of importance to the choice of substituent on the acetate pendant arm. An increase in the percentage of twisted square antiprismatic geometry, m, around the Gd(III) centre would be expected to enhance the relaxivity of the complex. There are two possible ways of achieving this. As discussed previously, the stereochemistry of the α-substituents on the pendant arms of DOTA determines the ratio of the twisted square antiprism to regular square antiprism isomer (m:M). The synthesis of optically pure (*RRRR*) or (*SSSS*) α-substituted $[Gd.DOTA]^-$ would therefore be expected to yield complexes with a greater percentage of m-isomer and therefore higher relaxivities.

Because the increased water exchange rate and relaxivity of the m-isomer has been attributed to steric crowding around the water-binding site, it would also be interesting to examine whether increased steric bulk on the pendant arm has an enhancing effect on relaxivity. In addition, increases in steric bulk would be expected to reduce the lability and isomeric interconversion of the complex *via* pendant arm rotation. This would be expected to have a stabilising effect on the electronic environment of the metal cation, perhaps lengthening its electronic relaxation time. For these reasons, pendant arms based on relatively bulky phenyl groups were examined. The structure of such a target molecule is shown in **figure 3.8**, and approaches to its synthesis are discussed in the following sections.

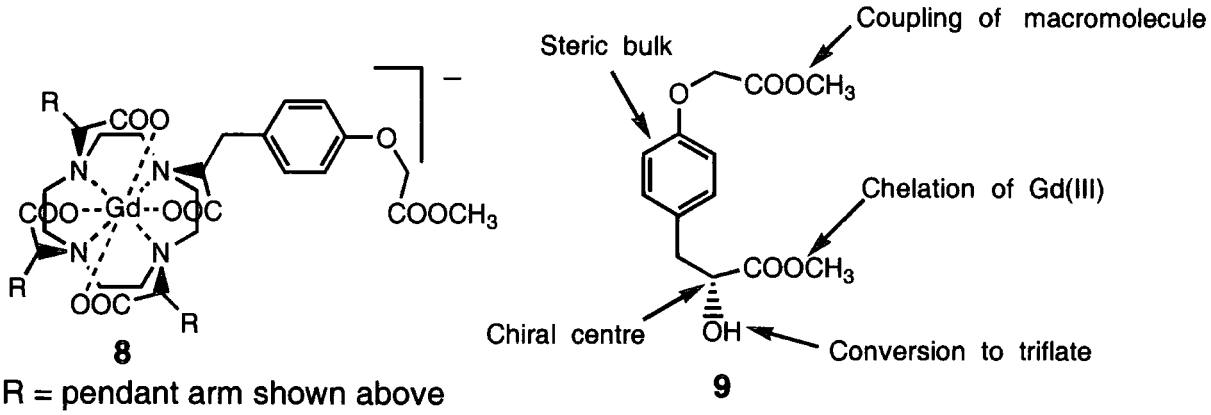

Figure 3.8 – Target Gd(III) Complex

The choice of alkylating agent precursor and the features of the target molecule are outlined above. α-Hydroxy esters may be synthesised by deamination from enantiopure, readily available amino acids, tyrosine in this case. The standard deamination conditions involve reaction of an aqueous solution of the amino acid with sulphuric acid and sodium nitrite. The reaction involves generation of the nitrosyl cation, NO^+, which converts the amino group to an α-azido acid. Anchimeric assistance by the carboxylate group facilitates the departure of the leaving group followed by nucleophilic attack of water. The reaction proceeds predominantly with retention of configuration. The analogous reaction on phenylalanine produces the desired product alcohol in 78% chemical yield with 91% retention of configuration.[135]

Dinitrogen tetroxide is an alternative nitrosation agent, which because it is used at -78°C, results in a reduction in elimination and rearrangement reactions.[136] The resultant nitrate esters are easily and quantitatively reduced to the corresponding alcohol under mild conditions. Amidine bases such as DBU (1,5-diazabicyclo[5.4.0]undec-5-ene) may be used to deprotonate the amine substrate. The reaction proceeds predominantly with retention of configuration. The results of these synthetic procedures are now discussed.

3.6 Model Triflate System

Racemic 2-hydroxy-3-phenylpropanoic acid (β-phenyllactic acid, **10**) was chosen as a model system to test the feasibility of using a trifluoromethylsulphonyl (triflyl) alkylating agent for reaction with $12N_4$ (**figure 3.9**).[126] Dickins had already successfully carried out the reaction within the group. The acid was converted to its methyl ester **11** in high yield,

and then treated with trifluoromethylsulphonic anhydride (triflic anhydride) in the presence of 2,6-lutidine, $^{i}Pr_2EtN$ or Et_3N as sterically hindered bases.[137-139] Yields of the alkylating agent **12** were good.

Initially, however, reaction of the triflyl species with $12N_4$, using amine bases with dichloromethane as solvent, was inefficient due to incomplete alkylation (*ca.* 40-50% trialkylation). The trialkylated product was chromatographically separable from the tetraalkylated product **13**. Isolated yields were moderate at 50%. The formation of trialkylated product was suppressed by the use of potassium carbonate as a base, with a more polar solvent (acetonitrile instead of dichloromethane) and at lower temperatures (-15°C instead of ambient temperature). Isolated yields improved to 70%. By-products included both *cis*- and *trans*-cinnamic methyl esters by elimination and methyl β-phenyllactate by hydrolysis. This indicated that the approach was suitable for further investigation with the desired *para*-substituted system (**figure 3.8**).

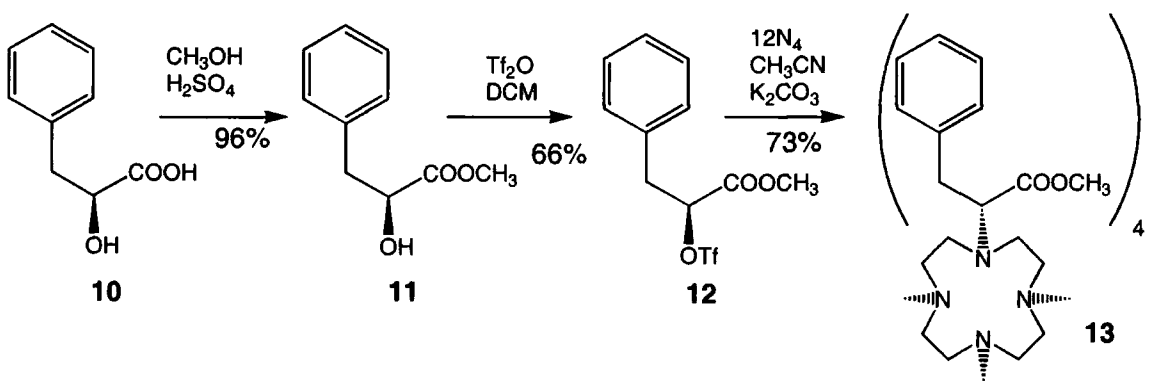

Figure 3.9 – Synthetic Scheme for Model Triflate System

3.7 Synthesis of Enantiopure Alcohols by Deamination

There are several possible methods to synthesise a single enantiomer triflyl alkylating agent for $12N_4$. As a precursor, an enantiopure alcohol was needed. Initially, an enantiomerically pure starting material was chosen. The amino acids constitute a cheap, readily available group of such compounds, with an extensive, well-understood chemistry. Several methods for the stereoselective conversion of enantiopure α-amino acids to α-hydroxy acids are available. Tyrosine was chosen as the most suitable amino acid as it has the necessary sterically bulky phenyl group, as well as a *para*-substituent

which it was possible to derivatise. Two suitable starting materials were identified – Boc-tyrosine **14** and tyrosine methyl ester hydrochloride **18** (**figure 3.10**). These were both converted into Boc-tyrosine methyl ester **15** by standard protection reactions,[140,141] in order that the phenolic hydroxyl group alone was available for reaction. Note that methyl esterification of Boc protected tyrosine was carried out using EDC as a dehydrating agent in view of the sensitivity of the Boc group to acidic conditions.

The phenol group was then alkylated in moderate yield with methyl bromoacetate in acetonitrile at 40-50°C, using potassium carbonate as base to yield **16**. It was important to exclude water from the reaction due to the sensitivity of the methyl ester to base hydrolysis. However despite taking precautions to exclude moisture, a significant amount of deesterification occurred. Methyl bromoacetate was slightly problematic due to its volatility and lachrymatory properties.

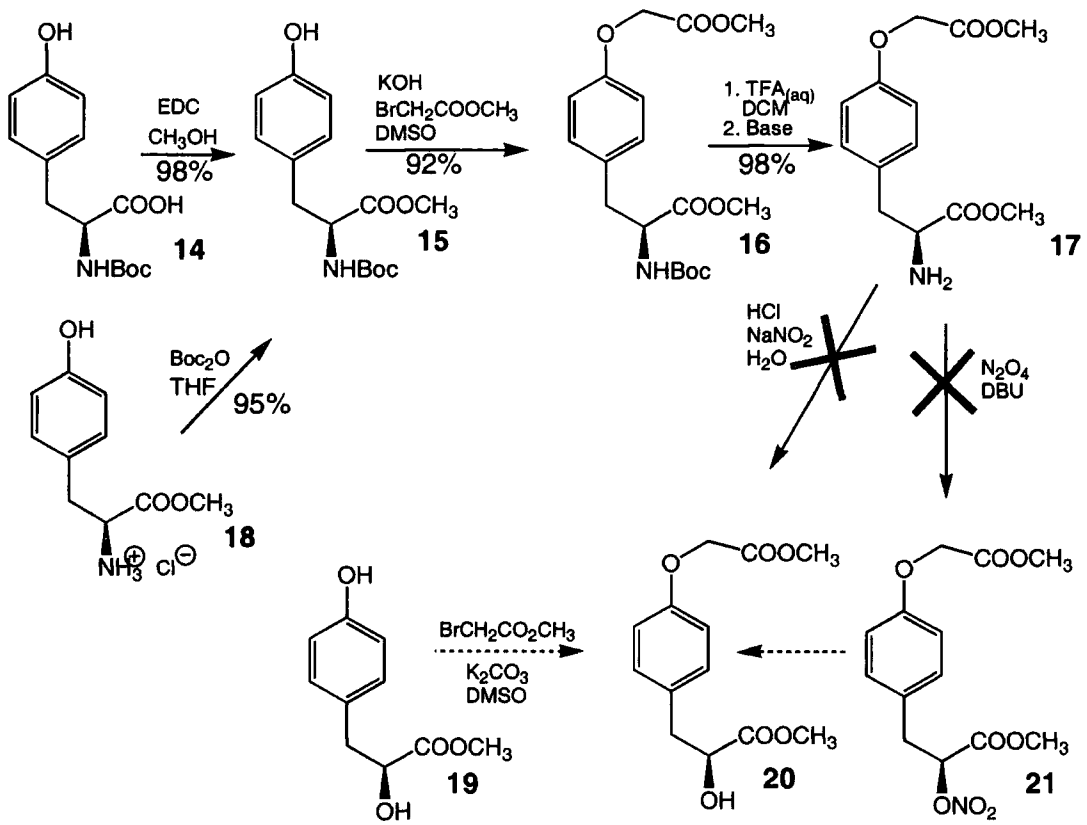

Figure 3.10 – Synthetic Scheme for Deamination Approach

Further investigation into improved alkylation procedures identified a procedure with short reaction times (30 min) at ambient temperature, using powdered potassium hydroxide as base in DMSO.[142] This procedure is postulated to involve reaction on the

surface of the potassium hydroxide due to its low solubility in DMSO. The reaction conditions are mild. As hoped, the speed of this reaction minimised deesterification, as well as methyl bromoacetate volatilisation, and gave a yield of 92%.

The next reaction removed the Boc protection group. This was accomplished in high yield with a wet solution of trifluoroacetic acid in DCM.

Then the key conversion of amine **17** to hydroxyl **20** was attempted. The amine was treated with sodium nitrite and hydrogen chloride in aqueous solution. Unfortunately the main product was the mono de-esterified starting material, along with a complex inseparable mixture of other products. Studies on this reaction have revealed that neighbouring group participation can result in aryl migration for substrates with electron-rich aryl systems, such as *p*-methoxyphenyl, and therefore presumably this system (see **section 3.10**).[135] However a modest chemical yield of 53% with 80% stereochemical retention was reported in this study for the *p*-methoxy substrate. This was not achieved with the *p*-alkoxyphenyl analogue **17**. An alternative deamination procedure using dinitrogen tetraoxide[136] was also attempted but failed, yielding a complex mixture of products, probably due to the same factors as above. Routes involving the stereospecific conversion of amines to alcohols were abandoned due to the difficulties encountered in the reaction.

3.8 Friedel-Crafts Approach to *p*-Substitution of Methyl Phenyllactate

Unfortunately no suitable enantiomerically pure, *p*-substituted phenyllactic or phenylacetic acid based starting materials were available to replace tyrosine. Therefore the option of performing *p*-substitution on phenyllactic acid itself was investigated. A Friedel-Crafts reaction[143] was chosen to add a 4-carbon chain with a terminal carboxyl-function (**figure 3.11**). This function could then be used to attach high molecular weight molecules.

The obvious Friedel-Crafts electrophile was succinic anhydride.[144] However, it failed to react with phenyllactic acid **10**. It appeared that a more reactive acylating agent was necessary. Also, the favourability of acid catalysed elimination to the conjugated cinnamate and the danger of acid catalysed racemisation made necessary the protection of the hydroxyl functionality. Phenyllactic acid was esterified with methanol (**11**), and then

acylated in high yield at the alcohol position using acetic anhydride and pyridine (**23**).[141] Initially a simple species was chosen to acylate the ring. The substrate was treated with acetyl chloride and aluminium chloride in 1,1,2,2-tetrachloroethane for 20 h and was successfully acetylated. Chromatography yielded the desired *p*-acyl product (14%), the deprotected alcohol analogue (3%) and the de-esterified analogue (35%). These were combined and methyl esterified to produce methyl-2-acetoxy-3-(4-acetylphenyl)propanoate **24**, with the acyl protecting group removed by transesterification. Overall the yield was 45%.

A haloform reaction was then attempted to convert the *p*-acyl group into an easily derivatised carboxylic acid **25**.[145] It was not expected that any bromination of the ring would occur due to the deactivating effect of both the acyl substitution in the starting material, and the carboxylate in the product. Initially the temperature was maintained below 10°C, but no reaction occurred. Upon repeating the reaction at ambient temperature, conversion to the carboxylic acid occurred, but so too did oxidation of the α-hydroxy acid to an α-keto acid. The main product of this reaction was (*p*-carboxyphenyl)pyruvic acid.

Although this route was not successful, later work revealed the utility of pyruvic acid derivatives in a stereoselective reduction to yield the enantiopure alcohol. The option of protecting the alcohol with a base- and oxidation-resistant group was not further investigated due to the success of a second acylation procedure which yielded an easily derivatised group directly.

Methyl-3-bromoformylpropanoate and methyl-3-chloroformylpropanoate were both successfully employed as more reactive analogues of succinic anhydride in the Friedel-Crafts acylation of methyl-2-acetoxy-3-phenylpropanoate.[146] Partial deprotection of the products necessitated the methyl esterification of the carboxyl groups and concomitant transesterification of the acetoxy group to the alcohol. A mixture of *ortho* and *para* products was chromatographically isolated and then the *para* product **26** was recrystallised repeatedly from acetonitrile. The overall yield was 12% due to the inefficiency of the crystallisation process.

The alcohol was then converted to a triflyl leaving group (**27**) in the usual manner in good yield. After isolation, the triflyl derivative was used in an alkylation reaction of

$12N_4$, but there was a very limited amount of alkylation, and the major product was the cinnamate ester elimination product. The difficulty of purification and lack of reactivity led to the abandonment of this route.

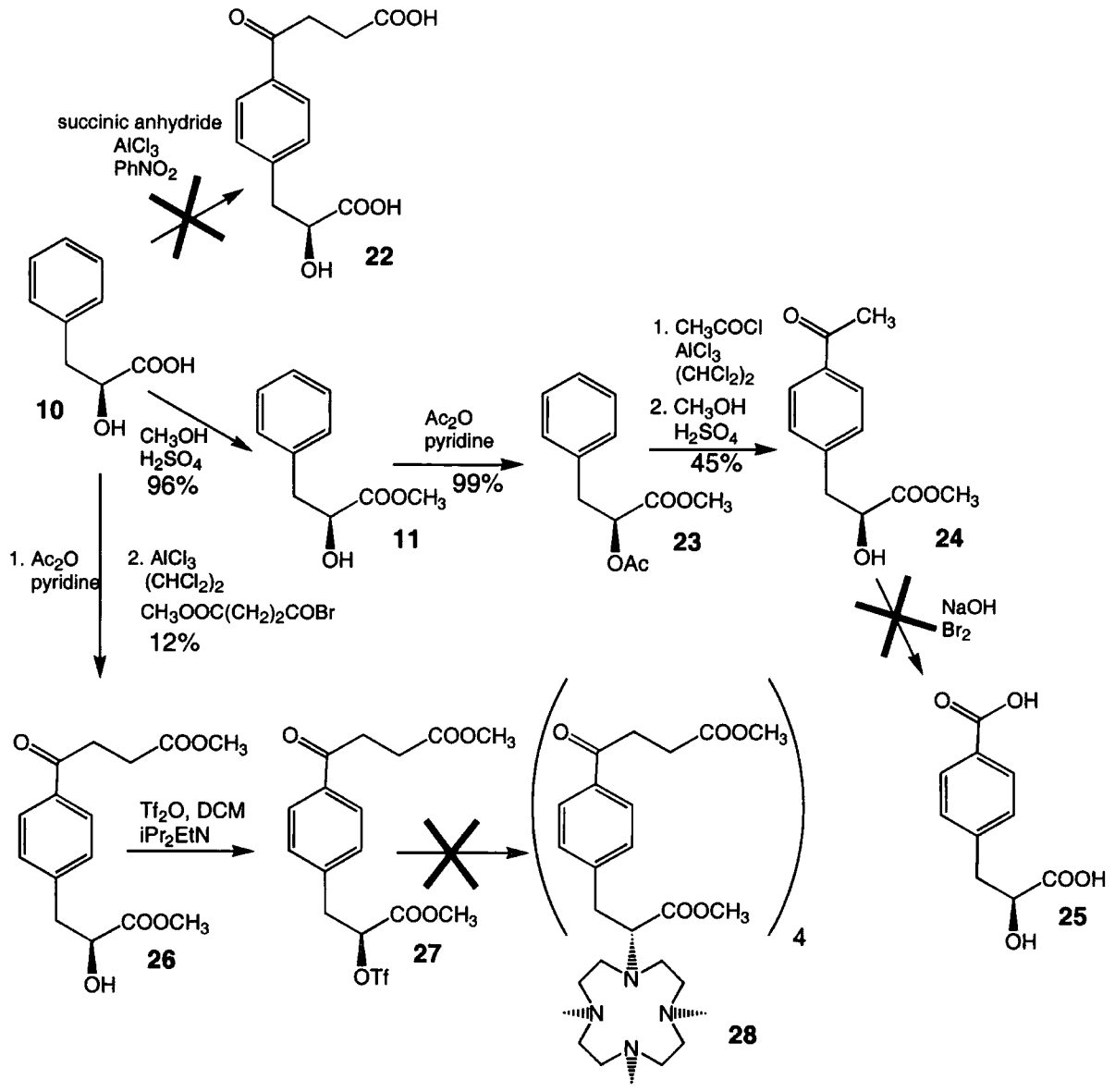

Figure 3.11 – Friedel Crafts Approach

In contrast to the *p*-alkoxy systems (see **section 3.10**), *p*-acylation of phenyllactate ester produced a phenyl substitution pattern, which was unlikely to lead to aryl participation in the reaction. The electron withdrawing effect of the carbonyl group reduced the aryl nucleophilicity significantly. Triflate **27** however proved not to be a very

efficient alkylating agent. Again cinnamates were formed by elimination in preference to *N*-alkylation. The reason for this may be due to an $E1_{cb}$ mechanism (**figure 3.12**)[193].

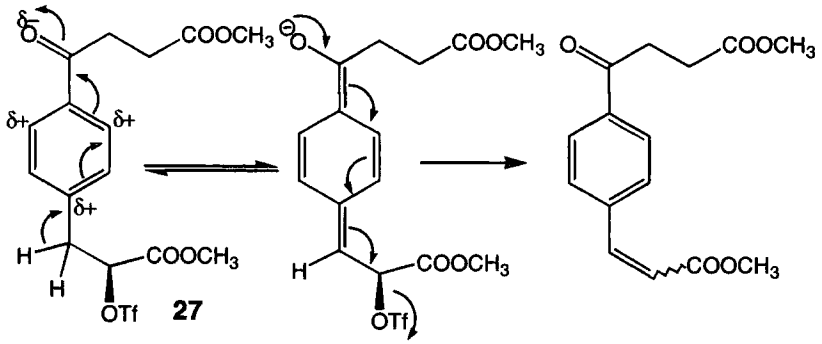

Figure 3.12 – Formation of E and Z Cinnamates via $E1_{cb}$ Mechanism

The electon withdrawing effect of the *p*-alkanoyl group causes a partial positive charge to form on the *ipso*-carbon of the phenyl ring. This would be expected to enhance the acidity at the benzylic position. Also, the benzylic carbanion formed by deprotonation under the reaction conditions would be stabilised by an extended conjugated system including the acyl group.

3.9 Racemic Routes via Benzylic Bromination

As well as the use of enantiomerically pure alkylating agents, routes to racemic analogues were also assessed. In light of the difficulties encountered in the use of triflyl alkylating agents, racemic halogenated alkylating agents were investigated. The halogenation of *p*-(hydroxyphenyl)acetic acid derivatives is shown schematically in **figure 3.13**.

The methyl (4-hydroxyphenyl)acetate **29** system differs from the methyl-3-(4-hydroxyphenyl)lactate system in the greater amount of steric hindrance both in the alkylating agent itself and in the target molecule, tetraalkylated $12N_4$. Three approaches to the target molecule were attempted. Initially, the phenol group was alkylated with methyl bromoacetate to yield the desired structural motif **30**, with a protected carboxylate for subsequent linkage to a high mass unit. This was then subjected to benzylic bromination under free radical conditions using AIBN, with NBS in carbon tetrachloride as a source of low concentration bromine to yield **31**. Trial and error led to the discovery that reaction only occurred when the NBS was added initially to the solution of the substrate, and only after bringing to reflux was the AIBN added. Chromatographic

purification was inefficient, yielding *ca.* 27% dibrominated by-product and 18% of the impure monobrominated product. The low yield and difficulty in purification led to the investigation of other analogous substrates for bromination.

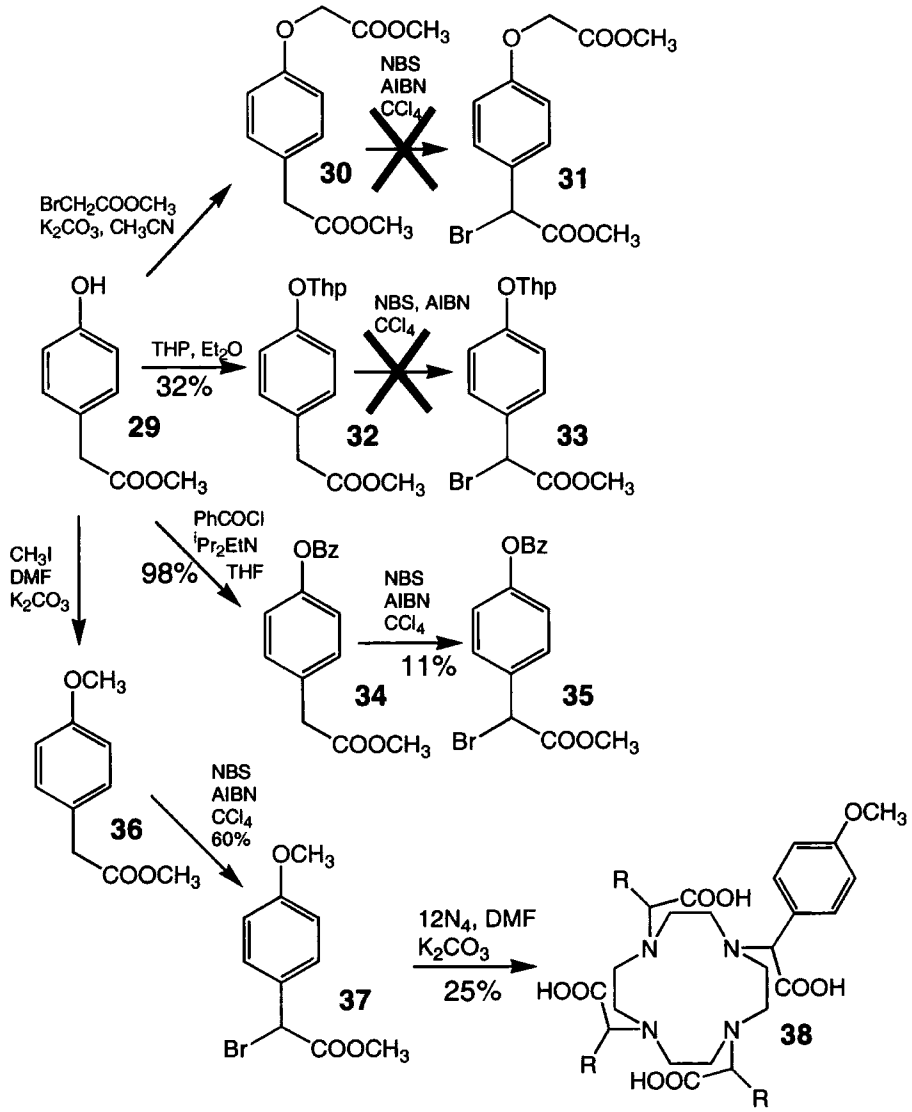

Figure 3.13 – Benzylic Bromination Approach

The second type of route involved the initial protection of the phenolic hydroxyl group, screening several different groups. The tetrahydropyranyl group (**32**)[141,147,148] was found to be unsuitable, as it appeared to be unstable under the bromination reaction conditions, cleaving and allowing polymerisation between the resultant phenol and the brominated product. Even when diisopropylethylamine was added to remove any acid which may have been formed during bromination, the reaction was not successful.

Protection as a methyl ether (**36**) was carried out in good yield using methyl iodide and potassium carbonate in DMF.[149,150] The product underwent bromination quite cleanly with NBS/AIBN in 60% yield (**37**). Alkylation of $12N_4$ was then carried out successfully in DMF with potassium carbonate as base. The tetraalkylated product **38** was isolated in 25% yield. Attempts to remove the methoxy protection using sodium ethanethiolate[151] were unsuccessful, leading to the formation of a pungent tar. This route was abandoned.

A benzoyl ester was then adopted as an alternative, more easily removed protective group. Reaction between methyl-4-(hydroxyphenyl)acetate and benzoyl chloride was clean and quantitative. Repeated treatment of the product **34** with NBS and AIBN yielded the monobrominated product **35**, which was purified by recrystallisation from diethyl ether. This product underwent reaction with $12N_4$ in DMF with potassium carbonate base to yield a mixture of tri and tetraalkylated $12N_4$. Attempts at separation of these two products failed however.

3.10 Stereoselective Pyruvate Reduction

At this point the alcohol-triflyl route was reconsidered. A new approach was based on the stereospecific reduction of an α-keto acid, rather than using an enantiomerically pure starting material. Although enzymatic routes were considered,[152] they were expensive and not suited to the substrate. Hydroxyphenylpyruvic acid **39** was stereoselectively reduced to (*S*)-2-hydroxy-3-(4-hydroxyphenyl)propanoic acid **40** using (+)-*B*-chlorodiisopino campheylborane ((+)-DIP-Cl™),[153] rapidly and in high yield (**figure 3.14**). This reagent reacts via a rigid bicyclic transition state assembly with neighbouring group participation of the carboxylate group. This causes the reductive hydrogen to be exposed to only one of the enantiotopic faces, giving high enantiomeric excesses, >95% e.e. in the case of this substrate (e.e. measured with europium (III) *tris*[3-(heptafluoropropylhydroxymethylene)-(+)-camphorate] chiral shift reagent).

Esterification was then carried out in methanol in high yield, giving the ester **41**.[154] Selective alkylation of the phenolic alcohol was initially attempted using one molar equivalent of sodium methoxide to deprotonate the phenol alone. This method

proved not to be suitable as alkylation of the aliphatic alcohol occurred. This method is also more likely to cause racemisation.

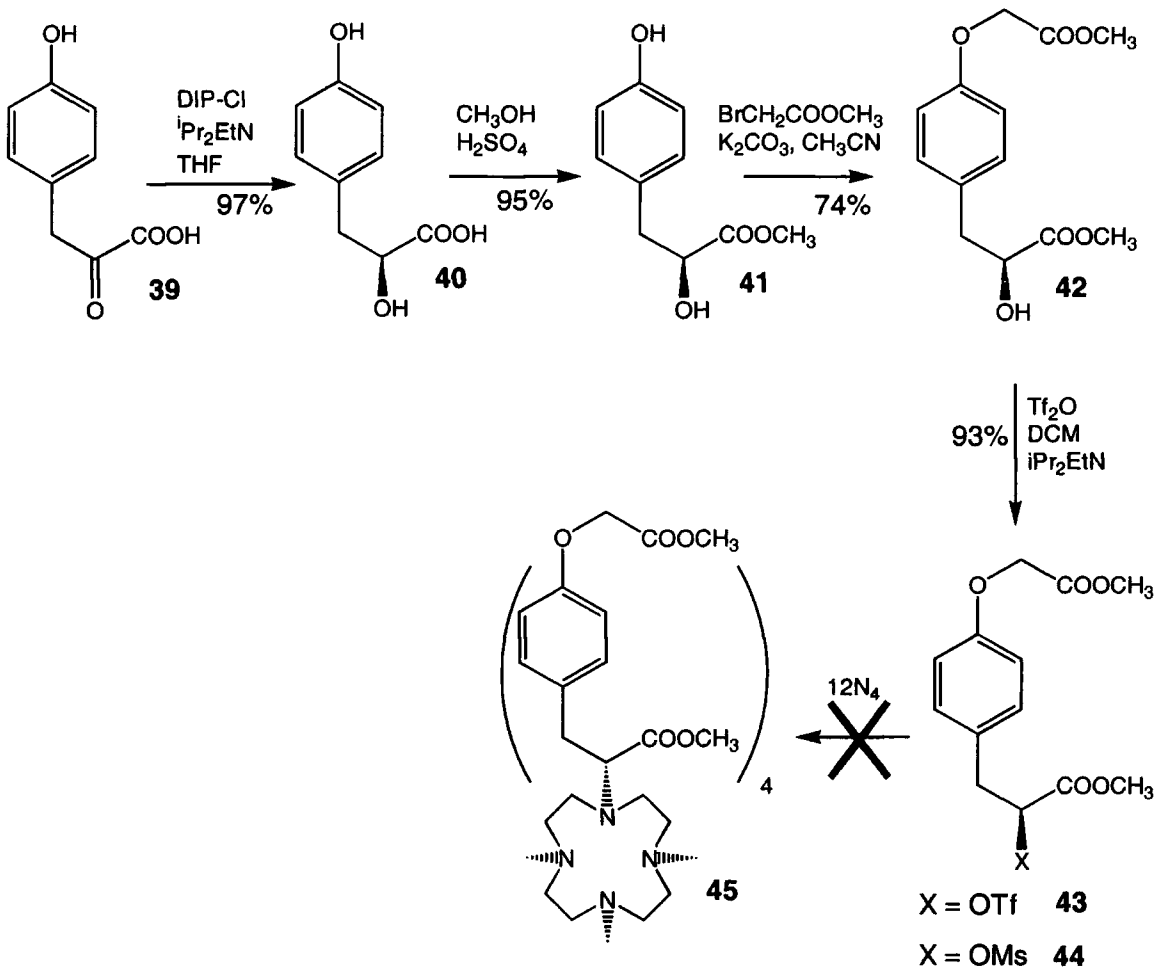

Figure 3.14 – Stereoselective Reduction of Pyruvate Derivative

The use of a two to threefold excess of methyl bromoacetate in the presence of three equivalents of potassium carbonate in dry acetonitrile eliminated dialkylation and gave reasonable yields of methyl-2-hydroxy-3-(4-methoxycarbonylmethoxyphenyl) propanoate **42**, without any evidence of racemisation (e.e. again measured with europium (III) *tris*[3-(heptafluoropropylhydroxymethylene)-(+)-camphorate] chiral shift reagent). The free alcohol group was then converted to a triflate group with triflic anhydride in high yield (**43**).

Alkylation of $12N_4$ was then attempted with the triflyl derivative. The reaction produced mainly methyl-4-carboxymethoxycinnamate, and there was extensive loss of

the ester methyl groups. The tri- and tetraalkylated products were visible by mass spectroscopy, and a trace of $12N_4$-based product mixture was isolated chromatographically. This was insufficient for further purification and reaction however. After repeated failure to isolate viable quantities of tetraalkylated $12N_4$ **45**, an alternative, less reactive alkylating agent was used. Treatment of methyl-2-hydroxy-3-(4-methoxycarbonylmethoxyphenyl)propanoate with mesyl chloride yielded the desired mesylate derivative **44** in high yield.[155] It was noted, however, that in solvents which were more polar than DCM, such as ethyl acetate, the mesylate product reacted with the diisopropylethylammonium chloride salt *via* nucleophilic substitution by the chloride anion. The formation of the resultant methyl-2-chloro-3-(4-methoxycarbonylmethoxy phenyl)propanoate may be avoided by chromatographic removal of the salt whilst still dissolved in DCM, with elution of the mesyl product using 50% ethyl acetate in hexane.

Alkylation of $12N_4$ using methyl-2-mesyl-3-(4-methoxycarbonylmethoxy phenyl)propanoate **44** was attempted using diisopropylethylamine as base and acetonitrile as solvent. Mono- and disubstitution were detected, but no further reaction was observed. However the use of a stronger base, potassium carbonate, and heating to 60°C promoted further alkylation, and over 2 weeks shifted the distribution of products to tri- and tetraalkylated derivatives of $12N_4$ only. Again, potassium carbonate may have aided the reaction by deprotonating the product of the first and subsequent alkylation steps. These partially substituted products may have been stronger bases than diisopropylamine due to chelation of any proton on the ring nitrogen by the pendant arm carbonyl. However, the drawback of potassium carbonate was that the lengthy reaction time allowed deesterification to occur which reduced the yield significantly. DMSO was tried as an alternative solvent, but no alkylation was detected, indeed the $12N_4$ was recovered.

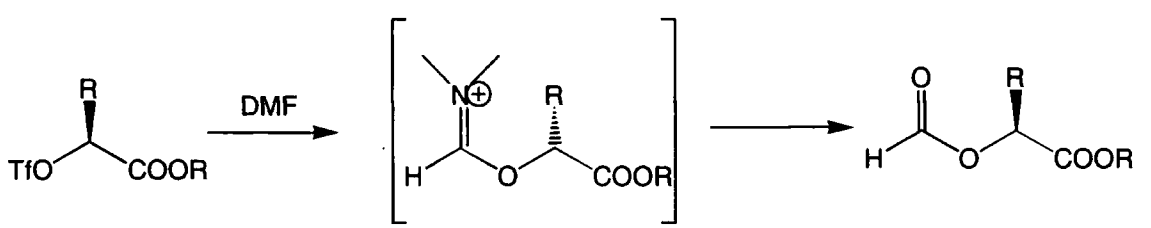

Figure 3.15 – Alkylation of DMF by Triflates

Use of DMF was little better, proceeding only as far as a small trace of tri-substituted product, with no evidence of tetra-substitution. An additional problem with

DMF is that it may act as a nucleophile towards α-triflyloxyesters (**figure 3.15**).[156,157] Another danger, which applies to both DMF and DMSO, is that they are very polar and can promote racemisation of the triflate.[158]

The potassium carbonate/acetonitrile system did eventually yield a mixture of tri- and tetra-substituted $12N_4$ (60 mg), but again insufficient material was obtained to allow an effective separation.

Attempts to synthesise DOTA-derived complexes with aryl-based pendant arms were hampered by many factors. In the case of this stereoselective route, both the triflate **43** and mesylate **44** derivatives of the enantiopure alcohol **42** were generated in high yield. Although methyl-3-phenyl-2-trifluoromethylsulphonyloxypropanoate **12** underwent reaction in good yield with cyclen, the *p*-alkoxy substituted analogue **43** did not. Repeated attempts at the reaction generated mainly cinnamates (**figure 3.16**). The origin of the failure in this reaction would not be expected to be steric in nature as the phenyl substituted triflate has approximately the same steric demand as the *p*-alkoxy substituted analogue. Electronic effects due to *p*-substitution are more likely to be the cause.[191,192]

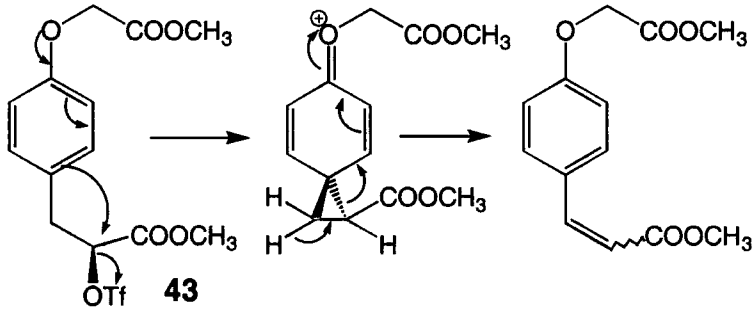

Figure 3.16 – Formation of Cinnamate via Aryl Group Participation

p-Substitution with an alkoxy group increases the nucleophilicity of the aryl group, making it more reactive towards the highly electrophilic triflate centre. The spiro intermediate structure may then undergo proton loss from the methylene group in the cyclopropane ring to regenerate the aryl group, and form a cinnamate ester. The stereochemistry of the product depends on which of the methylene protons is lost. This anchimerically assisted elimination process would be expected to occur far more readily in this system than in the simpler phenyl substituted system.

Note that initially the benzylic protons in the simpler phenyl system are more acidic than those in the *p*-alkoxy analogue because one of the canonical forms of the *p*-alkoxy system places partial negative charge on the *ipso* carbon, which destabilises the anionic conjugate base. However, the same protons in the spiro compound are much more acidic for three reasons. Firstly, their loss relieves ring strain in the cyclopropyl moiety. Secondly, it restores the original aromatic system, but in a more stable cinnamyl conjugative pattern. Thirdly, the spiro compound does not have a destabilising partial negative charge adjacent to the pseudo-benzylic centre. The enhanced tendency of this triflate to undergo elimination is at odds with the usual stability of α-triflyloxy esters, due to the substitution pattern on the phenyl group. The tendency of these systems to undergo phenyl migration and participation has already been discussed in the case of tyrosine deamination (**section 3.7**).

The mesylate analogue proved to be more successful as an alkylating agent for cyclen. This is thought to be the case because of the mesylate group's lower electrophilicity. This may have limited the tendency of the aryl group to act nucleophilically towards the electrophilic centre. However, this system was not reactive enough to alkylate each of the four nitrogens on cyclen. This drawback became an insurmountable problem when no adequate conditions could be found to separate the tri- and tetraalkylated products.

Full separation was necessary because the presence of the trisubstituted lanthanide complex in later investigations would have a major influence on relaxivity measurements. This would be a complex with two inner sphere water molecules (*i.e.* q = 2), and would therefore have very different characteristics. Although the option of attempting to separate the uncharged trisubstituted complex from the anionic tetrasubstituted complex was considered, the amount of product available was too small to be useful.

Because of the difficulties encountered in the synthesis and isolation of systems with *p*-substituted aryl pendant arms, a readily available supply of gDOTA, synthesised in house by S. Kean and K. Senanayake (**figure 3.2**),[49] was used to make the gadolinium core complex for the dendritic structures under study.

Chapter 4

Synthetic Approaches to High Molecular Weight Dendrimers

This chapter initially discusses the choice of target systems, their features and develops a synthetic strategy. It then goes on to discuss specifically the outcomes of the synthetic routes which were followed.

4.1 Poly(ether-amide) Dendrimers – Background

The field of dendrimer chemistry has gained greatly in importance since the first 'cascade' molecule, as they were then known, was synthesised in 1978.[100] Dendrimers exhibit a number of unique physical properties due to their well-defined, highly branched monodisperse architectures, their globular shape and their multiple peripheral functionalities.[99,159] The construction of symmetrical, highly branched dendrimers requires the appropriate choice of dendritic core and monomer to define the key properties of the dendrimer, i.e. its size, shape and porosity as well as the internal and surface functionality. Dendrimers may consist of one or more types of internal functionality. Examples of difunctional global dendrimers, which were synthesised by Newkome and co-workers, are presented in **figure 4.1**.[160]

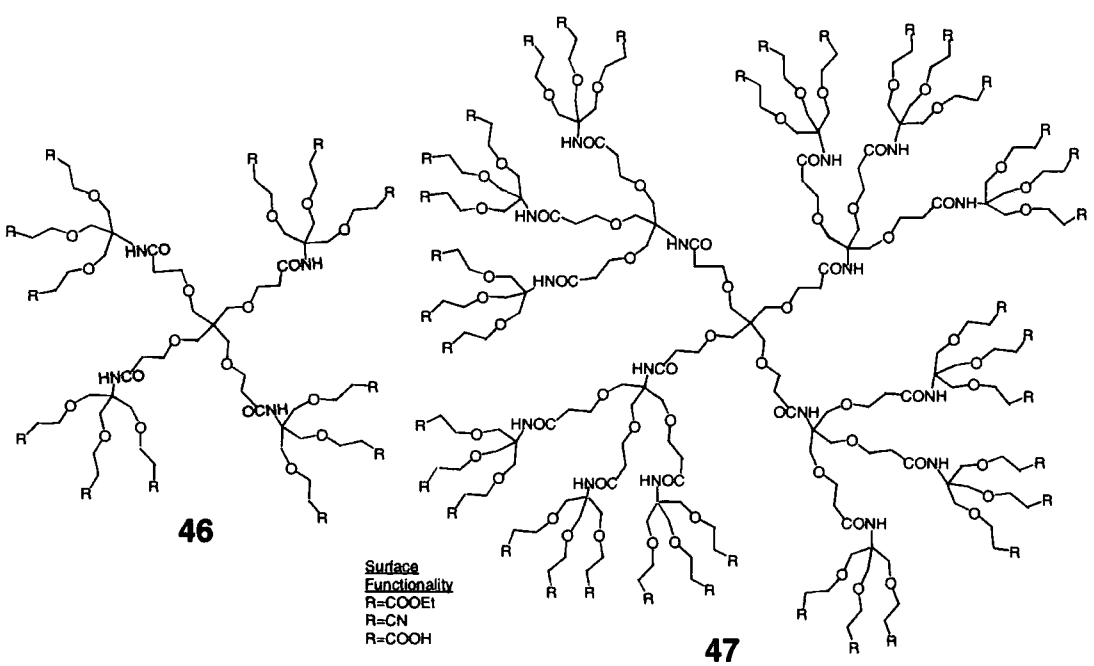

Figure 4.1 – Generation One and Two Poly(ether-amide) Dendrimers

These poly(etheramide) dendrimers (**46** and **47**) are based on pentaerythritol (**48**). This acts as the molecular core and defines the directionality of the system (directionality of four in this case). The monomer unit is based on *tris*-[(cyanoethoxy)methyl] aminomethane (**53**). Dendritic architectures are produced by the coupling of the core (**51**) and monomer units (**54**). The resultant dendrimers (**46** and **47**) possess quaternary branching points, maximal density of terminal functionality, equal bond distances between the surface functional groups and the cascade centre and the same chemical connection between all adjacent quaternary carbons, i.e. $-CH_2OCH_2CH_2CONH-$. They also have a symmetrical, three-dimensional globular structure. Note that although the structure is based on *tris*(hydroxymethyl)aminomethane (TRIS) (**52**), it has intervening linkers of the form $-CH_2CH_2CO-$, which effectively extend the arms of TRIS. This is necessary because the use of any similarly sized derivative of TRIS alone would lead to the rapid onset of dense packing and steric hindrance in the reiterative chemical process, which is used in the formation of higher generations. The synthetic procedure which was used is outlined in **figure 4.2**.

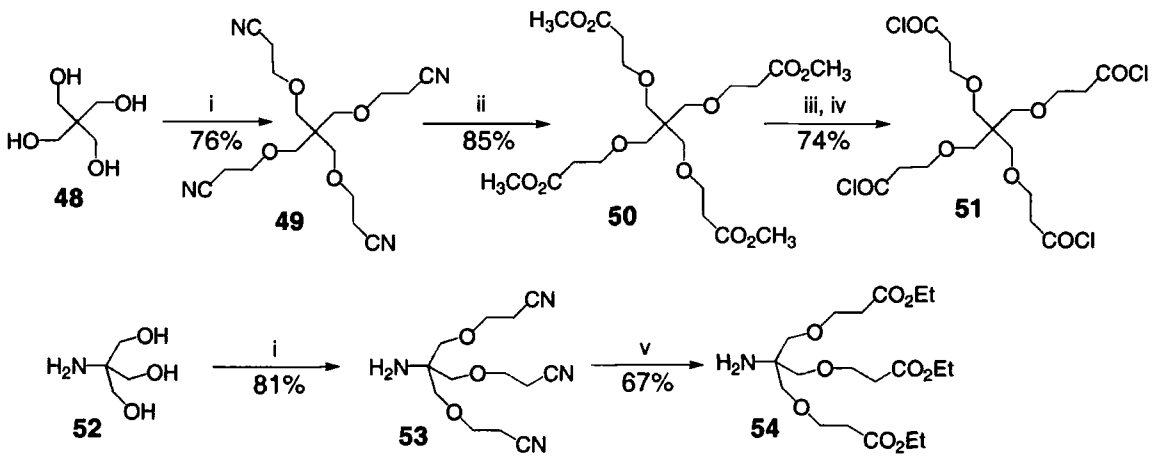

Reagents and conditions: (i) CH_2=CHCN, KOH, *p*-dioxane, 25°C, 24 h; (ii) MeOH, dry HCl, reflux, 2 h; (iii) 3 N NaOH, 70°C, 24 h; (iv) $SOCl_2$, DCM, reflux, 1 h; (v) EtOH, dry HCl, reflux, 3 h.

Figure 4.2 – Synthesis of Poly(ether-amide) Dendrons

The reaction between the *tetrakis*-(acyl chloride) (**51**) and the *tris*-(ethyl ester) (**54**) led to the generation-1 dendritic ester (**46**). After de-esterification this was again coupled to *tris*-(ethyl ester) (**54**) via a peptide coupling reaction (1-HOBt, DCC, 37%) to

form the second generation (**47**). Although the yield for this peptide coupling is quite low, it does show that the hindered primary amine (**54**) undergoes the reaction.

However even the carboxylic acid terminated dendrimers **46** and **47**, where R = COOH, were only slightly water-soluble. This makes this dendritic system unsuitable for use as the high molecular moiety of a hydrophilic contrast agent, especially in light of the fact that carboxylate groups would increase the osmotic potential *in vivo*. However the use of this type of dendrimer as a linking group between the core Gd(III) complex and a more water-soluble dendritic system was investigated (see **section 4.3**). This is an attractive option because the trifurcated structure of this dendron allows the rapid build-up of dendritic bulk.

Work carried out by the same group developed an alternative strategy based on this structure with terminal alcohol functionalities.[161] This dendrimer (**56**) proved to be water soluble due to its terminal hydroxyl groups. The option of using similar systems was then investigated. These are discussed in **section 4.2**.

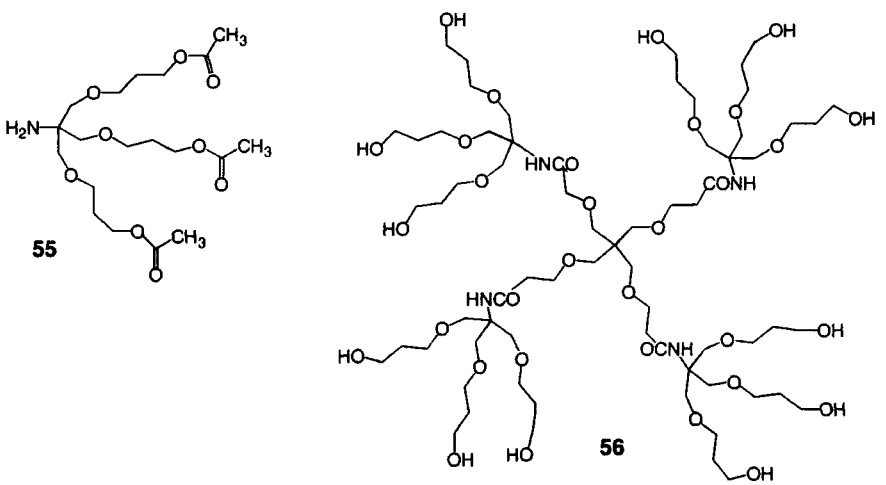

Figure 4.3 – Hydroxyl Terminated Poly(ether-amide) Dendrimer

4.2 Poly(ether) Dendrimers – Background

Because of its water solubility and non-ionic character, linear poly(ethylene glycol) (PEG) has found wide application in areas such as surfactants and biocompatible drug solubilisers.[162,163] Fréchet and co-workers have developed a convergent synthesis of aliphatic polyether dendrons with hydroxyl surface functionalities and similar solubility

properties to PEG (**figures 4.4 and 4.8**).[164] They may be considered to be dendritic analogues of PEG because they exhibit the same 2:1 ratio of carbon to oxygen in the branched repeat unit. The compact shape, high polarity and multiple terminal functionalities make them an attractive macromolecular adduct for Gd(III) complexes in contrast agent design. The synthesis also claims to be based on a monomer unit whose attributes include simple high-yielding activation and growth steps, with easy purification.

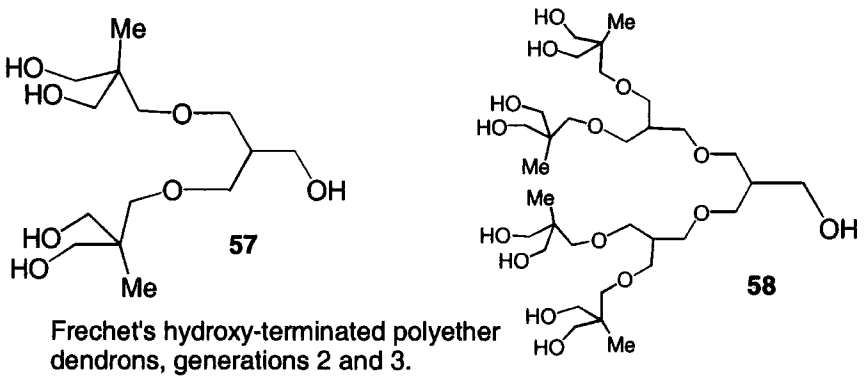

Frechet's hydroxy-terminated polyether dendrons, generations 2 and 3.

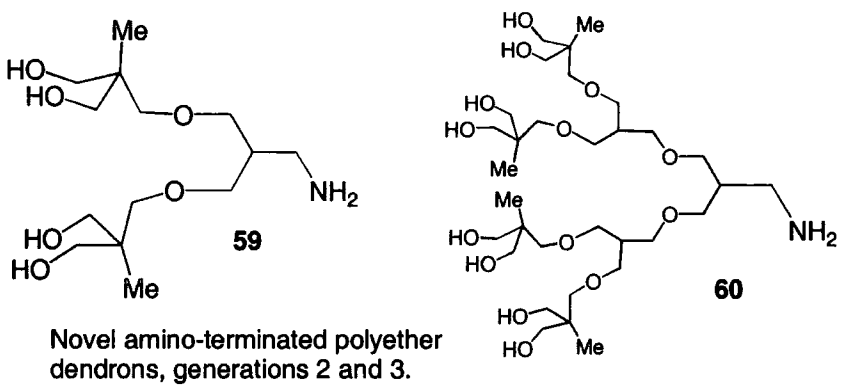

Novel amino-terminated polyether dendrons, generations 2 and 3.

Figure 4.4 – Novel Amino-terminated Dendrons from Frechet's Poly(ether) Dendrons

The focal group produced by Frechet's synthetic strategy is a primary alcohol (**57** and **58**). The most obvious method of coupling this functionality to a carboxy-terminated Gd(III) complex such as Gd(gDOTA)$^-$ is *via* an ester. However, esters undergo hydrolysis rather too easily, in particular *in vivo*. For this reason, a mild procedure for the transformation of the alcohol to an amine was required (**59** and **60**, see **section 4.5**). This would enable the use of more robust amide bonds for coupling to the Gd(III) complex.

4.3 Poly(ether-amide) Dendritic Linkers – Synthetic Strategy[160,161,165-168]

As has been discussed previously, the relaxivity of a contrast agent is dependent on its rotational correlation time, which is dependent on its mass. In order to increase the range of molecular masses available for study, a dendritic linker based on Newkome's poly(etheramide) methodology was envisaged. This would allow an extension to the direct coupling of the protected poly(ether) dendrons **75** and **78** to the Gd(III) core. The synthetic strategy is outlined in **figures 4.5** and **4.6**.

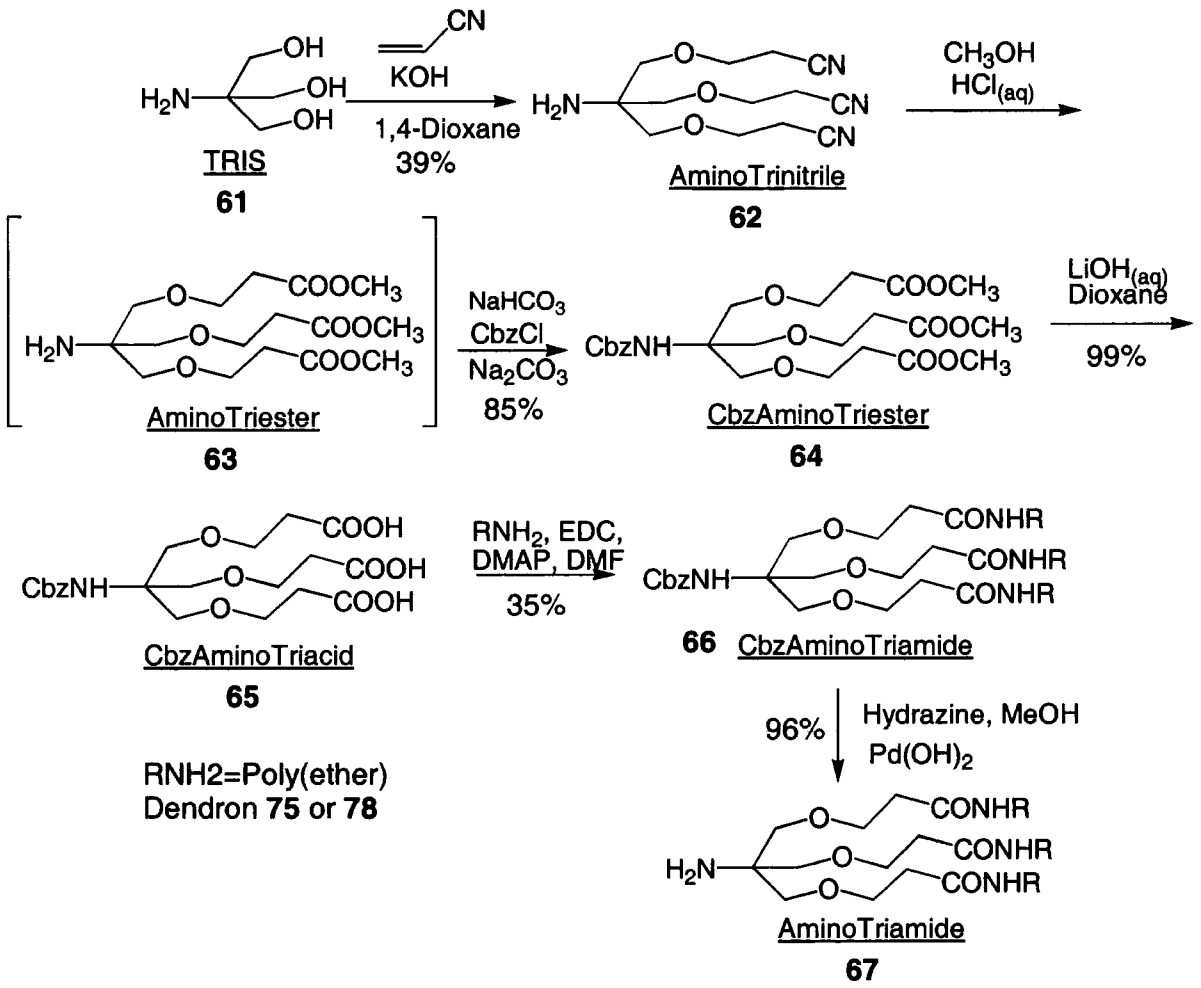

Figure 4.5 – Synthetic Strategy for Poly(ether-amide) Linker

Despite its utility, the 1,4 addition of oxygen nucleophiles to Michael acceptors is infrequently reported.[169,170] The hydroxide-catalysed addition of pentaerythritol to acrylonitrile has been carried out by Schanzer *et al.*,[171] and has been extended to other

polyols including TRIS by Dupuy *et al.*[172] The initial reaction in this sequence is based on the potassium hydroxide catalysed addition of TRIS (**61**) to acrylonitrile, to yield the key trifurcated structure. Subsequent functional group interconversion generates the aminotriester (**63**).

By protecting the aminotriester (**63**) as a benzylcarbamate (**64**),[167] and then hydrolysing the ester groups, the possibility of coupling the carboxyl groups to the amine focal group of a poly(ether) dendron (**75** or **78**) via an amide was envisaged. Subsequent facile deprotection of the benzylcarbamate group reveals the focal amine group (**67**) for further coupling to a tetracarboxy substituted Gd(III) chelate core. An example of this system, after ketal deprotection, is illustrated in **figure 4.6**.

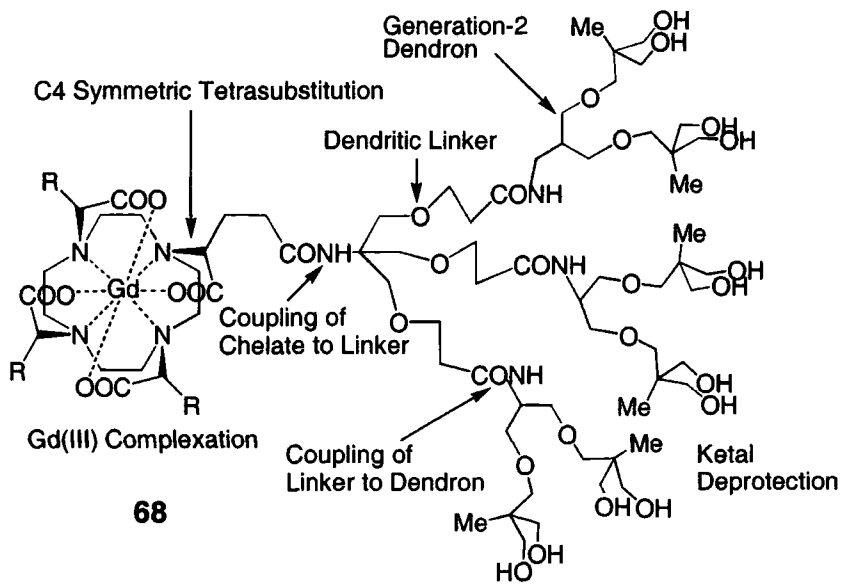

Figure 4.6 – Poly(ether-amide) Linked Poly(ether) Dendrimer based on gDOTA.

4.4 Poly(ether-amide) Dendrimers – Aqueous Solution Characteristics

An analogy may be drawn between the structure (**68**) and that of a globular electron-transfer heme protein mimic synthesised by Diederich and co-workers (**figure 4.7**).[165] A zinc porphyrin derivative with four carboxylate arms was attached to poly(ether-amide) dendrons by a peptide coupling methodology.

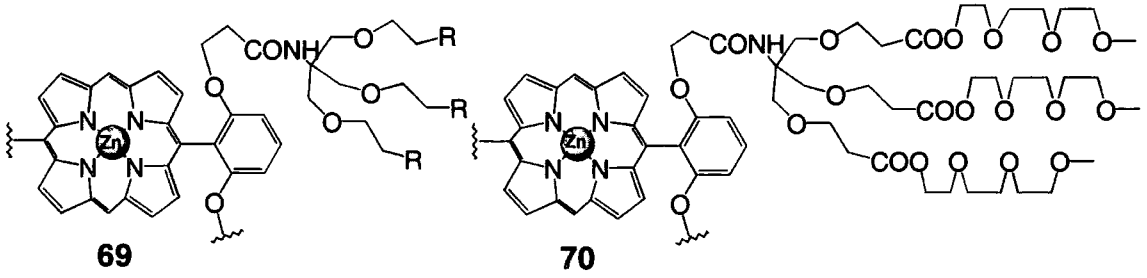

Figure 4.7 – Globular Electron-Transfer Heme Protein Mimics

The generation-1 compound **69**, where R=COOH, was further extended to the generation-2 and generation-3 analogues using the Newkome poly(ether-amide) system discussed in **section 4.1**. This system was not water soluble without deprotonation, as may be expected with reference to the Newkome system itself. Computer modelling suggested that the third generation dendrimer (M_w=19054) had a globular structure with dense packing.

The generation-1 poly(ether-amide) system with poly(ethylene glycol) monomethyl ether termination **70** displayed good water solubility, as did the generation-2 analogue terminated in the same manner. This is important with regard to our design for a contrast agent system with the same poly(ether-amide) dendritic linker. It shows that poly(ethylene glycol) (PEG) is sufficiently hydrophilic to induce water solubility in systems with both one generation and two generations of hydrophobic poly(ether-amide) dendrons.

Redox studies conducted on the iron analogues of these PEG-terminated systems showed that for the Fe(III)/Fe(II) couple in aqueous solution, the generation-2 dendrimer exhibited a potential 420 mV more positive than the generation-1 dendrimer. This large difference was attributed to differences in the solvation of the core electrophore. Whereas the relatively open branches in the generation-1 structure do not impede access by water molecules to the core, the more densely packed dendritic superstructure of the generation-2 analogue reduces contact between the heme unit and bulk solvent. As a result the more charged Fe(III) state is destabilised relative to Fe(II) and the redox potential is shifted to a more positive value.

This result is also important with regard to our contrast agent design. Access of water molecules to the Gd(III) catalytic centre is necessary to ensure rapid exchange of relaxed water into the bulk solution. At some point, increases in generation may begin to

retard the function of the contrast agent by inhibiting free diffusion of water from the central Gd(III) ion, through the interior to the bulk solvent.

4.5 Poly(ether) Dendron Synthesis

The synthesis of polyether dendrons as far as the third generation was carried out according to Fréchet (**figure 4.8**).[173] Because of the convergent nature of the synthesis, the first generation alcohol bears the peripheral functionalities. The synthesis commenced with the protection of two of the three identical alcohol functionalities of 1,1,1-*tris*-(hydroxymethyl)ethane as a ketal (**72**). This protecting group was chosen for several reasons. Most obviously, it prevents any nucleophilic behaviour by the protected hydroxyl groups. It is very stable to the strongly basic conditions which were used in subsequent steps. It facilitates chromatographic purification of the dendrons as it instils solubility in hexane. A single alcohol group remains for coupling to form the second generation. Finally, the protecting group can be quantitatively cleaved with a small amount of acid. A symmetrical ketone was chosen to avoid any undesirable complications during characterisation.

Yields of the *bis*-protected alcohol (**72**) were initially not very high. A variety of azeotropic solvent systems was used to remove water from the system during reaction. Both benzene[174] and toluene could be used with a Dean and Stark apparatus but the triol exhibited low solubility. Toluene also suffered from the disadvantage that its relatively high boiling point caused degradation of the product, especially in light of the long reaction times required. Dioxane and tetrahydrofuran exhibited no solubility problems. They were used in conjunction with a Soxhlet apparatus using calcium chloride as a drying agent. Two acids were assessed as catalysts. $BF_3.OMe_2$ complex suffered from hydrolysis under the reaction conditions, which necessitated repeated additions. This led to extensive borate deposition. The hydrogen fluoride by-product also led to the spasmodic failure of glassware. *p*-Toluenesulphonic acid (PTSA) was found to be more suitable. The combination of PTSA and benzene[174] led to some of the best yields (71%).

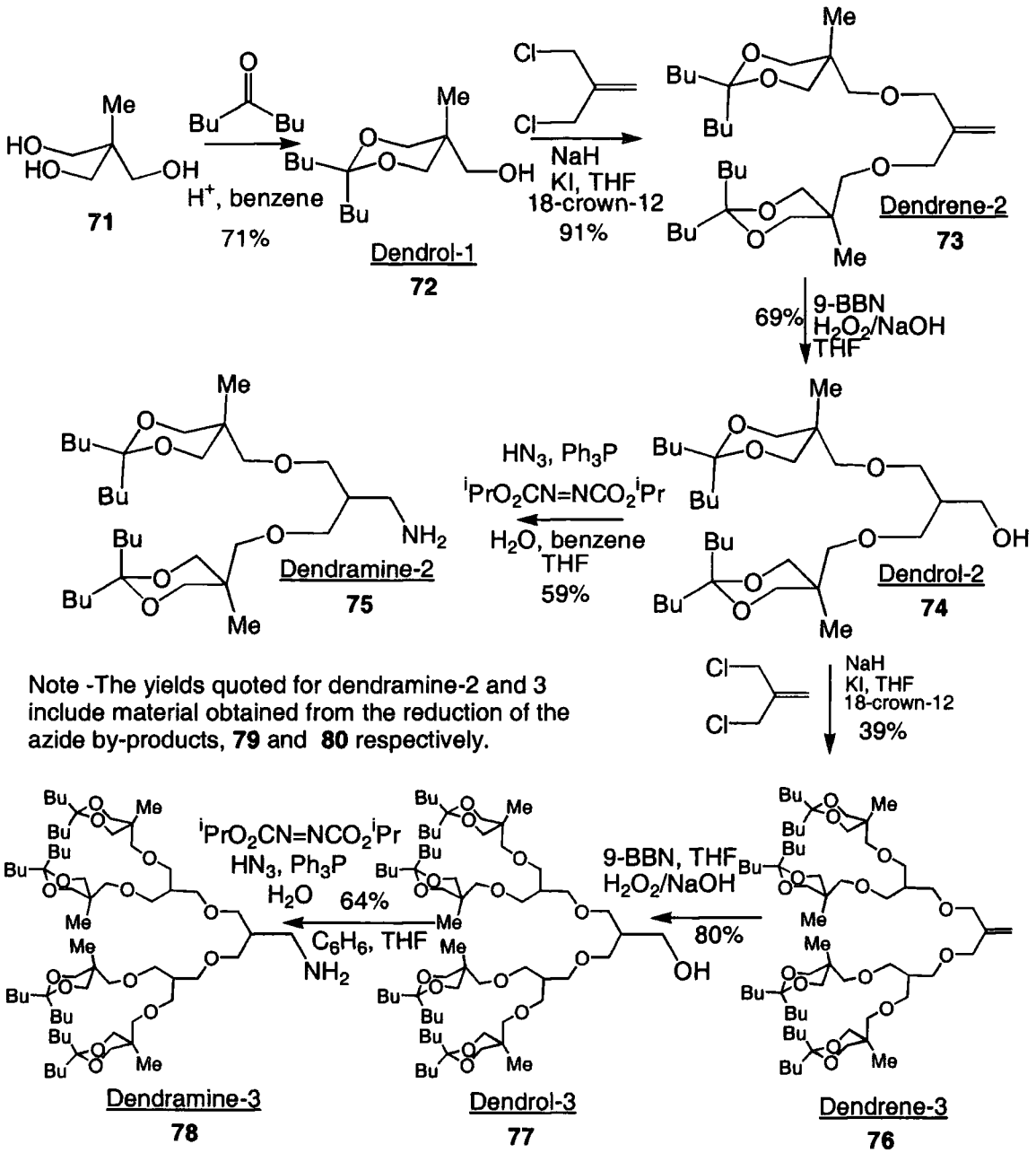

Figure 4.8 – Poly(ether) Dendron Synthetic Scheme

The monomer used in further generations was methallyl dichloride (3-chloro-2-chloromethylprop-1-ene). A Williamson coupling reaction was used to synthesise the second-generation alkene (**73**). The alkene functionality served as an activating group with respect to nucleophilic substitution for the two chloromethyl groups, as well as a masked hydroxyl group for use in the synthesis of the next generation. The symmetry of the molecule also ensured that the product was the same whether reaction occurred by an

S_N1, S_N2 or S_N2' mechanism (i.e. allylic rearrangement did not affect the regiochemistry of the substitution). In addition the lack of any proton β to the chloride prevented any elimination. Deprotonation of the first generation alcohol with sodium hydride in tetrahydrofuran imparted it with the necessary nucleophilicity for this reaction. To reinforce the allylic activation of the chloromethyl groups, a catalytic amount of potassium iodide was added to replace the chloride with iodide. 18-Crown-6 was added to aid solubilisation of the salt. The reaction required extended times to achieve disubstitution, and in the case of the third generation alkene (**76**), a significant amount of the monosubstituted product was isolated. Chromatographic purification on silica was rather difficult and resulted in only moderate yields.

In the subsequent activation step, the alkene functionality (**73**) was converted to an alcohol (**74**) by a hydroboration-oxidation reaction.[175] 9-Borabicyclo[3.3.1]nonane (9-BBN) was used in the hydroboration reaction as the steric bulk adjacent to the boron centre prevented the formation of any Markovnikov side product (note that Fréchet's initial use of borane-THF complex as a hydroborating agent resulted in the production of 5% of the wrong regioisomer). 9-BBN also has the advantage of being an easily handled crystalline solid and is also relatively stable to atmospheric oxygen and moisture.

After addition to the alkene, the trialkylborane product of the reaction was converted directly to the alcohol (**74**) with alkaline hydrogen peroxide. However, a major by-product of this reaction resulted from the cleavage of the ether bonds formed in the Williamson coupling reaction. The reduction of the oxidation time from 60 min to 15 min reduced the amount of these alcohol by-products. However, obtaining pure product chromatographically was very tedious. The products eluted in wide bands, which were not fully separable from each other. Very large volumes of solvent were necessary, typically over 10 dm^3 for batches of 1-5g. Impure fractions led to a large reduction in the average isolated yield of the second and third generation alcohols (**74** and **77**). Monitoring the composition of the fractions was also problematic as TLC was not sensitive or reliable enough. ^1H NMR was the only reliable method, which was rather time-consuming. Complete purification was important however, as any trace of the by-product alcohols present in subsequent coupling reactions would form asymmetrically substituted impurities which would be almost impossible to remove.

In addition, the octane-1,5-diol by-product from 9-BBN proved difficult to separate fully, further reducing the yield. In the case of the second generation alcohol (**76**), this diol could not be efficiently removed by distillation as the desired product was too volatile. A large proportion of the diol was removed by dissolving the crude product mixture in methanol and then adding a little water to force the dendrimer molecules to oil out. The wet methanolic solution of the diol was then decanted. This process prevented the large amount of diol from swamping the chromatographic separation, but again caused a significant drop in yield.

After purification, the second-generation alcohol (**74**) was coupled as before with a molecule of methallyl dichloride to yield the third generation alkene (**76**). Hydroboration-oxidation was again used to convert this to the alcohol (**77**). A large proportion of the diol by-product was removed by distillation in this case. However, yields were still low. No further increase in generation was attempted.

Conversion of the alcohol focal group functionality of both the second (**74**) and third generations (**77**) to amines was then carried out via a Mitsunobu reaction. This was to allow amide coupling to the carboxylic acid pendant arms of the dendritic core. Most alcohol to amine syntheses involve the conversion of the hydroxyl to a good leaving group such as a halide or a sulphonate under acidic conditions. This is then treated with an $-NH_2$ equivalent such as a metal azide to form the alkyl azide, which may then be reduced to the amine. This reaction sequence is not advisable in this case due to the acid-sensitivity of the ketal protecting group. An elaboration of a Mitsunobu reaction in a non-polar medium was chosen instead to convert the alcohol directly to an alkyl azide, using mildly acidic hydrazoic acid as the azide source.[194-196]

The treatment of alcohols **74** and **77** with hydrazoic acid, diisopropyl azodicarboxylate and an excess of triphenylphosphine in THF followed by the addition of water furnished a convenient one-pot sequence which produced the required amine in moderate yields (Figures 4.8 and 5.3). Initial conversion of the alcohols to the alkyl azides **79** and **80** was achieved by the Mitsunobu portion of the reaction. This was then followed *in situ* by a Staudinger reaction[176] of the azide with triphenylphosphine to yield an iminophosphorane intermediate.[197] This was subsequently hydrolysed to the appropriate amine (**75** or **78**).

The reaction yielded 33% amine, 33% azide and the remainder was the starting material. Increased reaction times and temperatures merely led to the formation of an isopropyl carbamate adduct by attack of the amine on diisopropyl azodicarboxylate.

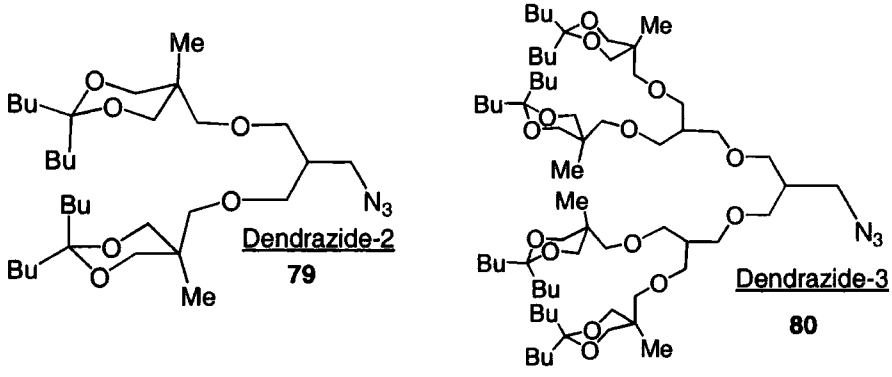

Figure 4.9 – Intermediate Azide Dendrons

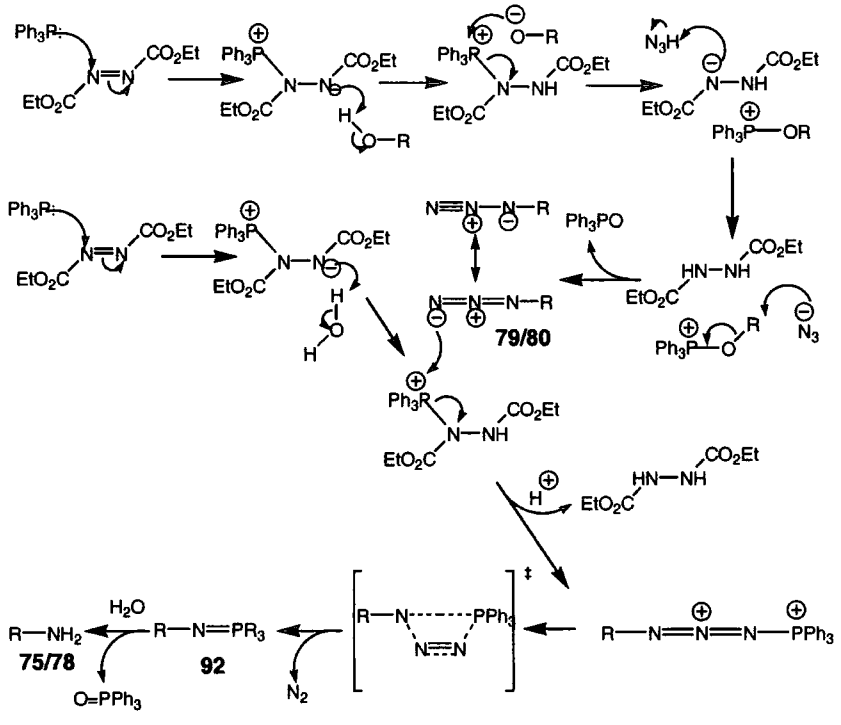

Figure 4.10 – Mechanism of Mitsunobu and Staudinger Reactions

The azide, alcohol and amine had very different R_f values on silica and were easily separated. The alcohol was recycled and the azide by-products (**79** and **80**) were reduced to the desired amines with hydrazine hydrate and palladium hydroxide on carbon in methanol.[177] This method gave quantitative yields, was carried out in normal glassware and did not involve the use of pressurised hydrogen gas. Purification of the amines was

also relatively easy as the catalyst was simply filtered off and the product extracted into hexane.

The greatest challenge associated with the synthesis of the various poly(ether) dendrons was that of inefficient purification and concomitant low yields. Techniques were utilised such as the oiling out of the partially purified dendritic product from wet methanolic solution, or the removal of certain impurities prior to chromatography by crystallisation (i.e. triphenylphosphine oxide and diisopropyl dicarbamate). The product dendrons were removed from the bulk of the crystalline triphenylphosphine oxide and dicarbamate by-products by dissolving in warm hexane.

These processes aided subsequent chromatographic separation. A second problem was the instability of the ketal protecting group. Even the trace quantities of HCl present in $CDCl_3$ due to decomposition processes were enough to cause hydrolysis. All NMR samples were either dissolved in CD_2Cl_2, or $CDCl_3$ which had been neutralised with potassium carbonate. However, the ketal protected products, with the exception of the amine functionalised analogues, were unstable to the atmosphere and decomposed within 1-2 months.

One key step in the reaction sequence is incompatible with the substrate. The oxidation of the 9-BBN adduct with basic peroxide resulted in the partial degradation of the ether functionality, which was not desirable in the synthesis of a PEG analogue. It is hypothesised that the degradation step may proceed via a captodatively stabilised radical at the ether undergoing cleavage. The key to poly(ether) synthesis was repeated reactions to generate enough product to overcome the significant losses at each step.

4.6 Poly(ether-amide) Linker - Synthesis

The initial Michael addition of the triol *tris*(hydroxymethyl)aminomethane (TRIS) (**61**) to acrylonitrile was the key reaction in the formation of the trifurcated dendritic structure (**67**, **figure 4.5**).[178,179] However, the reaction was found to be inefficient. An initial ratio of 1:3.25 (TRIS:acrylonitrile) gave isolated yields of the aminotrinitrile (**62**) of only 20%. The nitrile group underwent hydrolysis to the acid and the amide under the reaction conditions. The acid was impossible to extract from aqueous solution. Very large quantities of by-products due to partial *O*-substitution and *N*-substitution were isolated.

The protection of the amino group in TRIS was investigated to improve yields from the Michael reaction by preventing *N*-addition. Reaction of TRIS with di-*tert*-butyldicarbonate (Boc anhydride)[180] was unsuccessful, probably due to the steric hindrance of the amine group. An alternative, more reactive *tert*-butoxycarbonylating agent, 2-(*tert*-butoxycarbonyloxyimino)-2-phenylacetonitrile (Boc-ON) was found to be more successful (**figure 4.11**).[181-183] Initial use of an aqueous dioxane solvent system led to significant *O*-attack and incomplete conversion of the TRIS. However, the use of dry DMF[184] gave a good yield of Boc-TRIS (77%) (**81**).

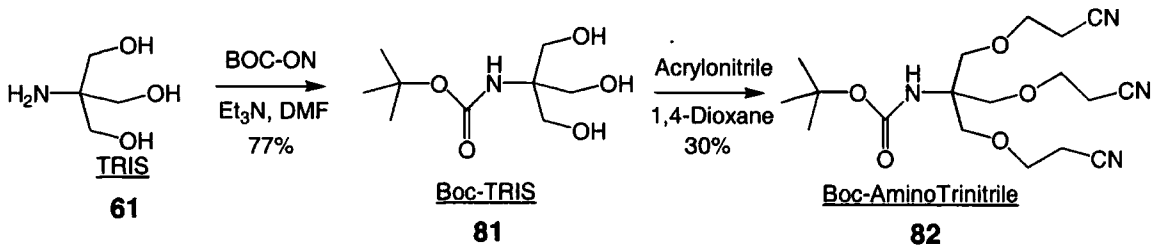

Figure 4.11 – Boc Protection of TRIS

Acrylonitrile was then treated with Boc-TRIS under the previously described Michael reaction conditions. However, the reaction resulted in the extensive conversion of the Boc protecting group to an isocyanate group,[185] as well as some Boc cleavage to the amine. Despite the usually high stability of Boc protection to aqueous base, the structure of this particular molecule may have made the conversion to the isocyanate (**83**) more facile (**figure 4.12**).

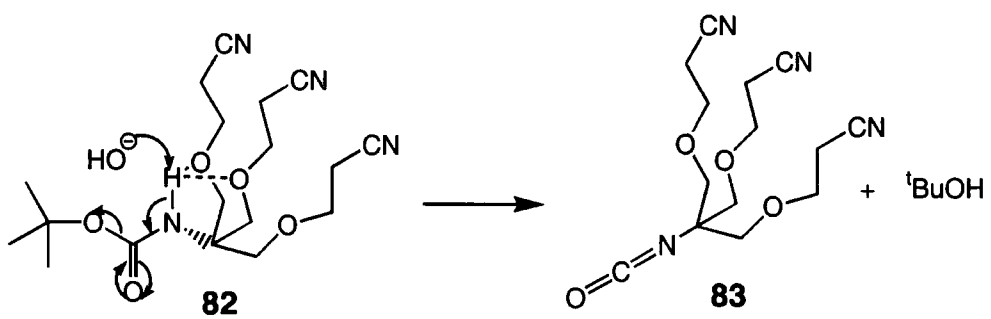

Figure 4.12 – Proposed Mechanism for Formation of Isocyanate By-Product

Stabilisation of any partial positive charge on the carbamate proton by oxygen chelation in the transition state, during hydroxyl attack would be expected to increase the effective acidity of the proton, allowing removal under aqueous basic conditions.

Resonance stabilisation of the negative charge on the nitrogen through the adjacent carbonyl group would also be expected to act in a stabilising manner. As hydrolysis of the isocyanate by-product (**83**) in the presence of nitrile groups would be problematic, no attempt was made to convert it to the amine. Although this reaction was not repeated due to its inefficiency, it did yield 30% of the desired product.

Both the Boc protected aminotrinitrile (**82**) and the unprotected aminotrinitrile (**62**) were successfully converted with good yields to the aminotriester (**63**) using dry methanol saturated with hydrogen chloride gas.[186,187] However, neutralisation of the protonated amine after the reaction, prior to isolation was problematic. The substrate was susceptible to extremely rapid ester hydrolysis at pH > 9. The reason for this was not clear, but it may be related to the reason why the Boc protected amine was converted in to the isocyanate, i.e. intramolecular chelation by the ether oxygens (**figure 4.13**). At pH 9-10, there is both protonated amine present, as well as a catalytic concentration of hydroxide. Effective intramolecular protonation of the ester carbonyl group by the alkyl ammonium group, and the chelation and stabilisation of the resultant cation would be expected to enhance the electrophilicity of the ester. This would allow the nucleophilic attack of a hydroxide anion. This attack is reversible, but the loss of ethoxide instead of hydroxide is not. This process may rapidly hydrolyse the ester groups. Note that re-esterification is also very rapid, so much so that mass spectroscopy of the acid is impossible in methanol. Transesterification is also rapid in ethanol.

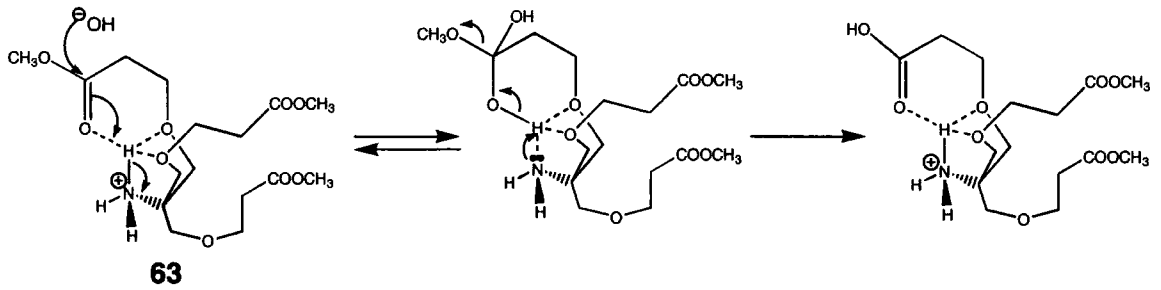

Figure 4.13 – Proposed Mechanism of Accelerated Ester Hydrolysis

For this reason the aminotriester (**63**) was not isolated and purified. The crude product was converted directly to the benzyl carbamate (Cbz) derivative (**64**) to protect the amine group.[188-190] Yields for this reaction were not very high, especially in light of

the very high yields which are usual for this protection. This was due to partial de-esterification under the reaction conditions.

The CbzAminoTriester (**64**) was de-esterified with lithium hydroxide in aqueous dioxane solution in high yield. The CbzAminoTriacid was then ready for amide coupling to the amine functionalised dendrons to yield systems of the general form **66**.

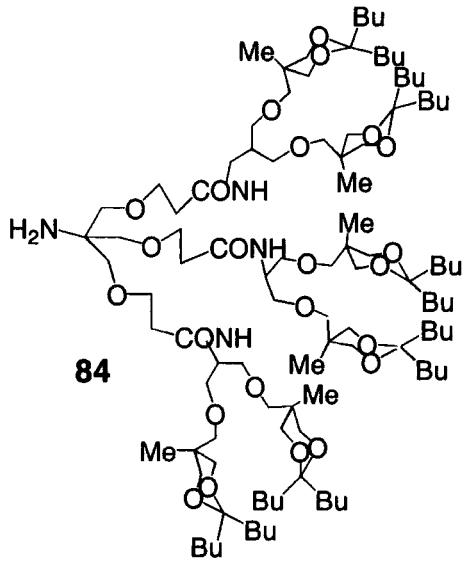

Figure 4.14 – Poly(ether-amide) Linked Generation-1 Poly(ether) Dendron

A standard amide coupling reaction was successfully carried out using 1-[3-(dimethylamino)propyl]-3-ethylcarbodiimide hydrochloride (EDC) and 1-hydroxybenzotriazole hydrate (HOBt) in DMF. Subsequently, reductive deprotection of the Cbz group with $Pd(OH)_2$ as catalyst and hydrazine hydrate as hydrogen source proceeded in very high yield. This generated the target trifurcated dendron (**84**), incorporating three generation-2 poly(ether) dendrons, for coupling to the chelate core.

4.7 Coupling to Chelate Core

Because of the lack of success in producing sufficient pure material of the target aromatic Gd(III) complexes (**chapter 3**), a readily available and well-understood system was used as an alternative. As discussed previously, the solution phase stereoismeric behaviour of $[Gd.gDOTA]^-$ has been studied in this group.[98] It is known that the desired (*RRRR/SSSS*) diastereomer may be generated in high yield from the statistical mixture of diastereomers by acid-catalysed epimerisation. The complex possesses four peripheral carboxylic acid groups distributed in the plane of the parent cyclic structure.

Initially the [Eu.gDOTA]$^-$ analogue was synthesised by boiling an equimolar amount of $EuCl_3$ and gDOTA at pH 3.5 overnight. ^1H NMR revealed the presence of just two diastereomers, the m and M configurations of the enantiomeric (*RRRR/SSSS*) pair. The same procedure was then used to synthesise the Gd(III) analogue.

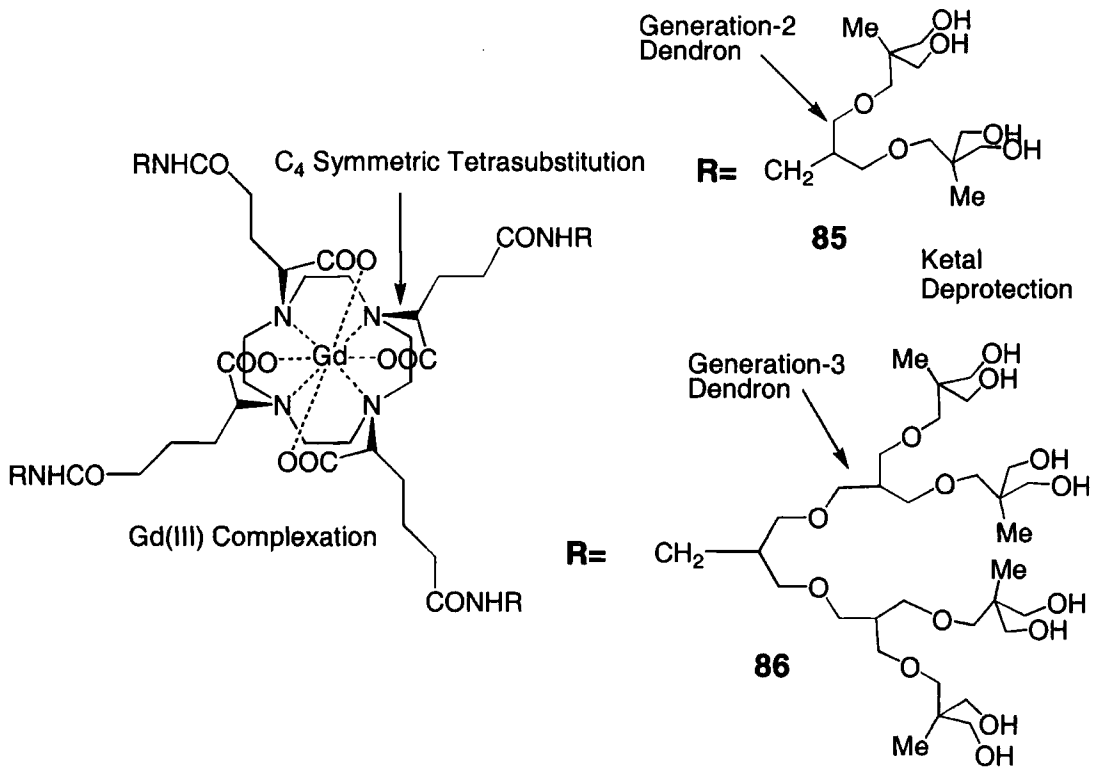

Figure 4.15 – Successfully Synthesised Contrast Agents

[Gd.gDOTA]$^-$ was then converted to its activated *N*-hydroxysuccinimide (NHS) tetraester by treatment with EDC and NHS in DMSO. The reaction was monitored by negative ESMS. Under the conditions used (DMSO, base) to generate the tetrasubstituted NHS ester of [Gd.gDOTA]$^-$, repeated attempts gave a distribution of mono-, di-, tri- and tetrasubstituted products. However, this appeared to be satisfactory with regard to the subsequent amidation with the generation-2 amine-functionalised poly(ether) dendron. Only the tetrasubstituted dendrimer product was visible by negative ESMS. The product was soluble in hexane, and therefore easily separated from the reaction mixture (crude yield = 46%). Removal of the ketal protecting groups in *p*-dioxane with a catalytic amount of hydrochloric acid yielded the water-soluble contrast agent target molecule (crude yield = 26%) (**85**, **figure 4.15**). However, the reaction did not occur with the

generation-3 amine to generate **86** under these conditions. An alternative aqueous system developed by K. Senanayake, using dendramine-3, which had been deprotected of its ketal groups prior to amide coupling was successful. The coupling was carried out with good conversion to the tetrasubstituted product using EDC and HOBt.

In the case of **86**, the steric hindrance and chemical reactivity due to the immediate environment of the amine group would not be expected to differ from that of the lower generation analogue **85**. However longer-range entanglement and steric hindrance due to the larger size of the molecule may have been to blame for its initial failure in the non-aqueous system. The successful changeover to water as solvent may have encouraged the elongation of the dendrimeric chains into space due to improved hydration properties.

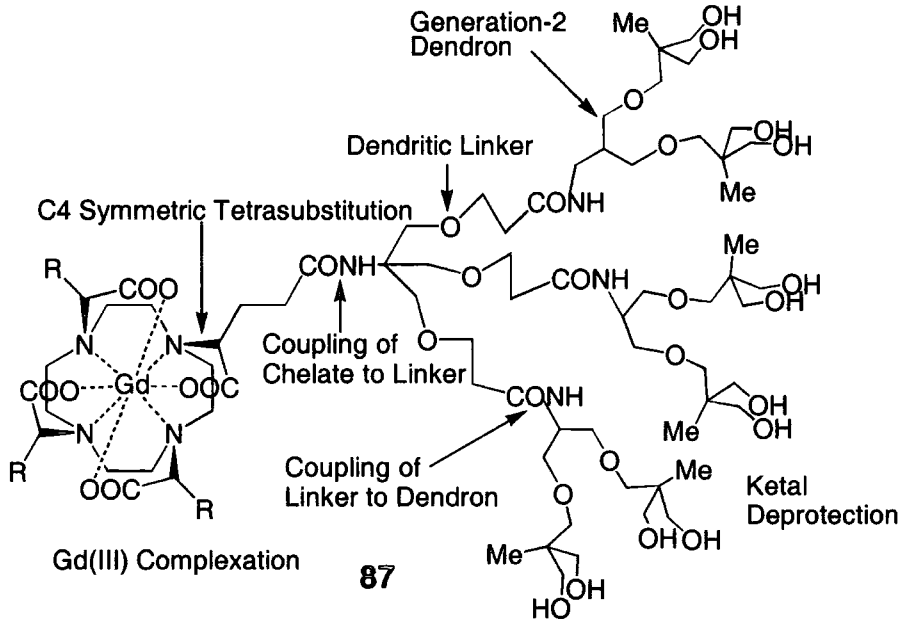

Figure 4.16 – Contrast Agent Incorporating Dendritic Linker

The coupling reaction with the first generation poly(ether-amide) linked poly(ether) dendron **84** to eventually produce **87** appeared not to be successful. No trace of amide formation was detected by ESMS.). In this case, local steric hindrance appeared to prevent efficient amidation of the NHS ester. An additional factor may have been the reduced nucleophilicity of the amine functionality due to the presence of β-ether oxygens. This is in spite of the success of a very similar reaction reported by Newkome, albeit with moderate yields. Diederich and co-workers observed a related trend in the ease of amide

coupling as follows (**figure 4.17**).[167] Whereas the generation-1 amine (**88**) underwent amide coupling (DCC, HOBt) with a yield of 40%, the second-generation analogue (**89**) yielded only 19% of the desired product. This difference in reactivity was attributed to steric hindrance and the resultant poor accessibility of the focal point of the dendron. The problem was solved by the insertion of a spacer group (Cbz-glycine) under forcing conditions, to give the glycyl derivative (**90**). [167]

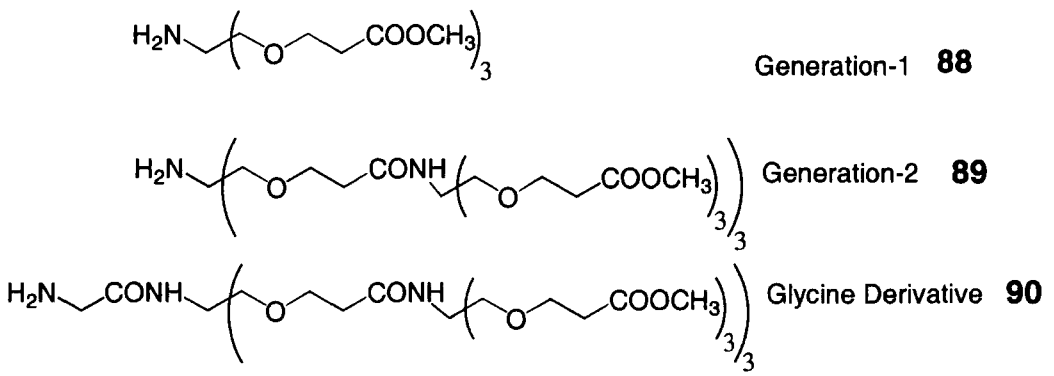

Figure 4.17 – Generation-1 and 2 poly(ether-amide) dendrons

In light of this, no attempt was made to synthesise the poly(ether-amide) linked generation-3 poly(ether) analogue for coupling.

The integrity of the complexes **85** and **86** was confirmed by mass spectroscopy (see following three pages). It was estimated from negative electrospray MS that there was *ca.* 10% of the (generation-1)(generation-2)$_3$ impurity in **85**, and as much as 25% of the analogous (generation-2)(generation-3)$_3$ impurity in **86**. This was due to the presence of small amounts of the lower generation analogue in the amide coupling to Gd[gDOTA]$^-$. There were insignificant amounts of analogues of even lower mass present. This estimation of relative amounts is based on similar sensitivity of the negative ESMS technique to each of the molecules, which is justifiable because of their similar sizes and structures, ionisation not being necessary due to their overall negative charge.

The negative ESMS spectra of the ketal-protected generation-2 Gd(gDOTA) complex is reproduced overleaf, showing some (generation-1)(generation-2)$_3$ impurity at m/z = 2686. The deprotected analogue (**85**) is shown on the subsequent page, followed by the generation-3 deprotected complex (**86**), which also shows a significant amount of the (generation-2)(generation-3)$_3$ impurity at m/z = 3150.

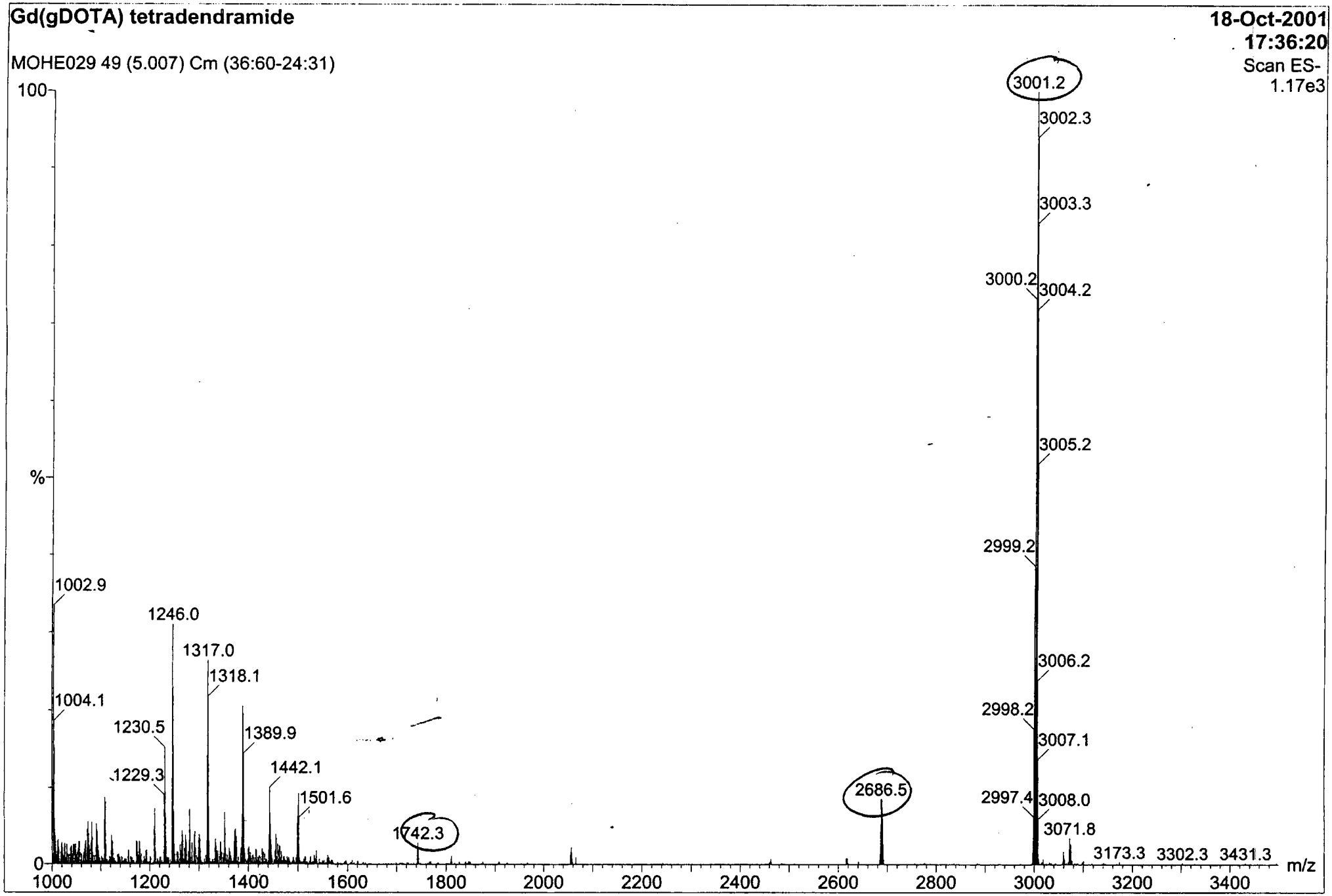
Gd(gDOTA) tetradendramide
18-Oct-2001
17:36:20
MOHE029 49 (5.007) Cm (36:60-24:31)
Scan ES-
1.17e3
100
%
0
3001.2
3002.3
3003.3
3000.2
3004.2
3005.2
2999.2
3006.2
2998.2
3007.1
2997.4
3008.0
3071.8
3173.3
3302.3
3431.3
1002.9
1246.0
1317.0
1318.1
1004.1
1230.5
1389.9
1229.3
1442.1
1501.6
1742.3
2686.5
m/z
1000
1200
1400
1600
1800
2000
2200
2400
2600
2800
3000
3200
3400

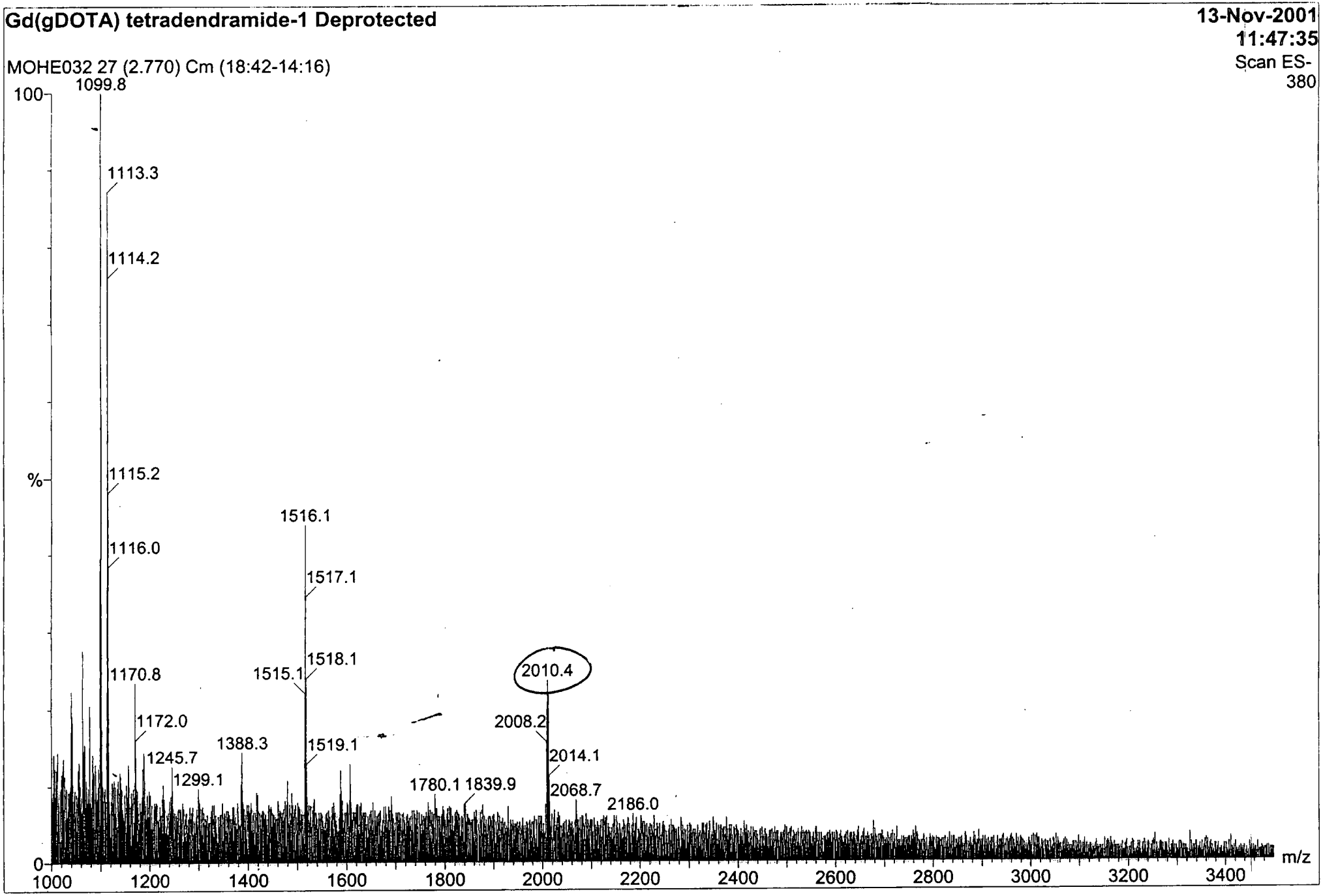
Gd(gDOTA) tetradendramide-1 Deprotected
13-Nov-2001
11:47:35
MOHE032 27 (2.770) Cm (18:42-14:16)
Scan ES-
380
100
%
0
1099.8
1113.3
1114.2
1115.2
1116.0
1170.8
1172.0
1245.7
1299.1
1388.3
1515.1
1516.1
1517.1
1518.1
1519.1
1780.1
1839.9
2008.2
2010.4
2014.1
2068.7
2186.0
1000
1200
1400
1600
1800
2000
2200
2400
2600
2800
3000
3200
3400
m/z

coupling reaction

20-Mar-2002
12:06:31
Scan ES-
1.25e3

KsGdgDOTADE1 23 (2.364)

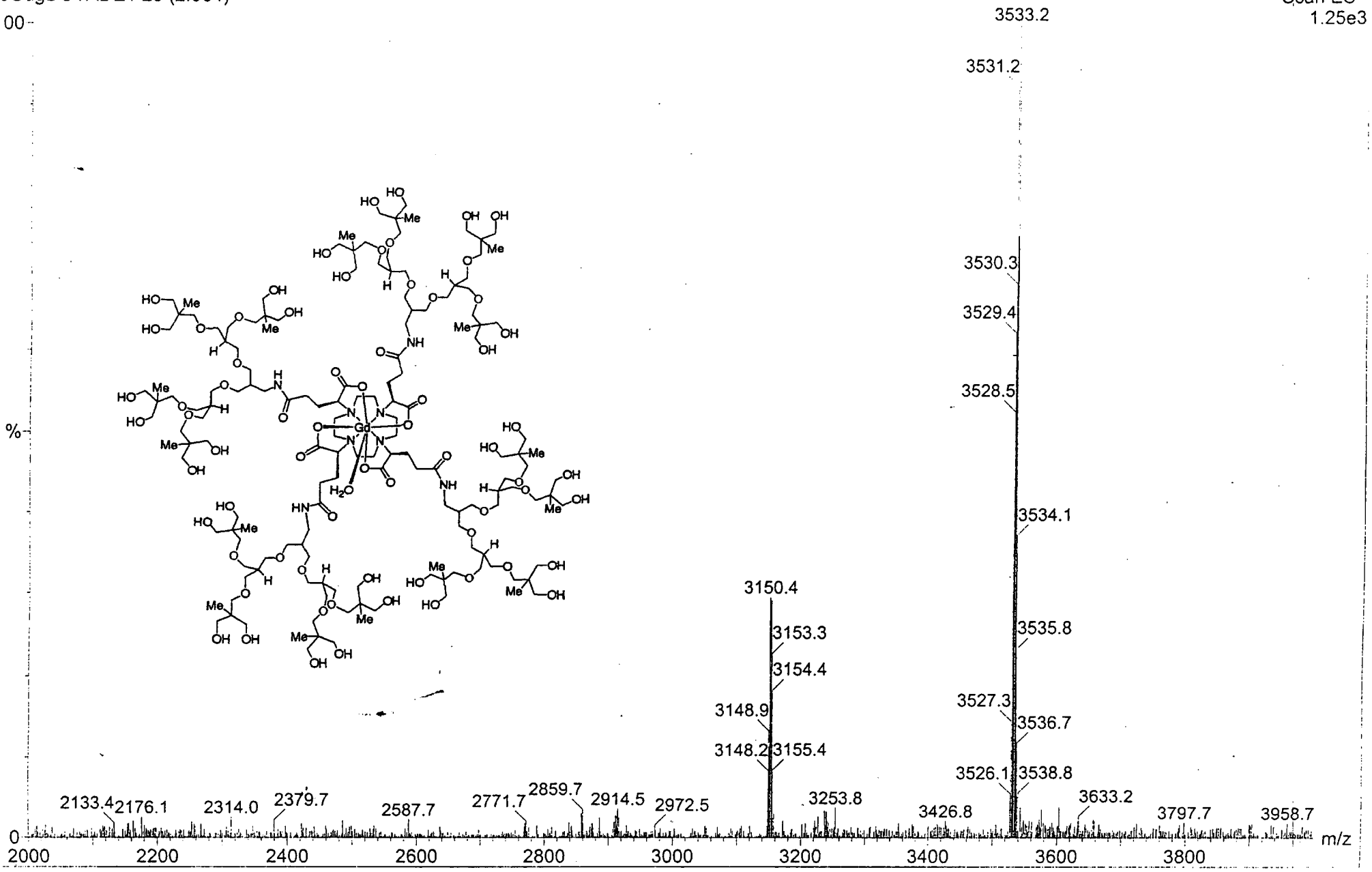

Chapter 5

Results and Discussion

This chapter discusses the relaxivity experiments conducted on contrast agents **85** *and* **86**, *and summarises the results of the work. It then suggests further work to be conducted in light of these results.*

5.1 Determination of Relaxivity Values

The relaxivity of the dendritic gadolinium complex (**85**) was determined at a field strength of 65 MHz in aqueous solution over a range of temperatures. The inversion recovery method was used, the pulse sequence being 180°-τ-90° as explained in **section 1.3h**. This experiment records spectra at a variety of delay times (τ) resulting in a number of spectra ranging from maximum negative intensity to maximum positive intensity. The intensity data are fitted by the NMR computer to this equation to get a value of T_1.

The sample was contained in a micro-sample NMR tube to maximise sensitivity. The longitudinal relaxation rate R_1 (s^{-1}) is the reciprocal of T_1 (s). To calculate the paramagnetic contribution to this rate (R_{1p}), the diamagnetic contribution due to water was subtracted. This was measured experimentally to be 0.38 s^{-1}at 298 K in pure water.[201] After obtaining the R_{1p} value it was necessary to accurately measure the concentration of gadolinium(III) in solution so that the relaxivity could be calculated ($r_{1p} = R_{1p}/[Gd]$).

This was achieved by removing a volume of the sample gadolinium complex solution prior to relaxivity measurement, and adding to it an equal volume of 5.0 M nitric acid. This was intended to dissociate the complex at room temperature. However, it was found that heating at 60°C for 24 h was necessary. This confirmed, in a qualitative manner, the high kinetic stability of the complex with respect to acid dissociation. The reduction in relaxivity of the system was monitored over 3-4 days until no further change was observed. This was taken to signify full dissociation of Gd(III). The concentration of Gd(III) could then be calculated by re-measuring T_1 and using the fact that the relaxivity of Gd(III) in 2.5 M aqueous nitric acid at 298 K is 11.7 mM^{-1} s^{-1}.[201] Using this method, a value of 17.8 ± 0.5 mM^{-1} s^{-1} was calculated. This value compares to a value of R_{1p} = 7.8 ± 0.1 mM^{-1} s^{-1} (298 K, 65 MHz) for $[Gd.gDOTA]^-$ itself. The relaxivity value obtained

for this dendritic chelate clearly demonstrates that the functionalisation of the complex with dendrimeric high molecular mass moieties leads to an enhanced relaxivity, as was expected.

Relaxivity measurements on the analogous generation-3 Gd[gDOTA]$^-$ tetradendramide **86** (298 K, 65 MHz) gave a slightly higher value of 21 ± 0.5 mM^{-1} s^{-1}. Although this value is better than that of the generation-2 compound, it is only slightly greater. The reason for this lack of improvement was investigated by NMRD profiling (see **section 5.3**).

5.2 Variable Temperature Relaxivity Measurements

The 65 MHz VT NMR instrument was calibrated initially by examining the difference in chemical shift between the two resonances of ethylene glycol over a range of temperatures, and the following calibration curve was generated (**figure 5.1**).

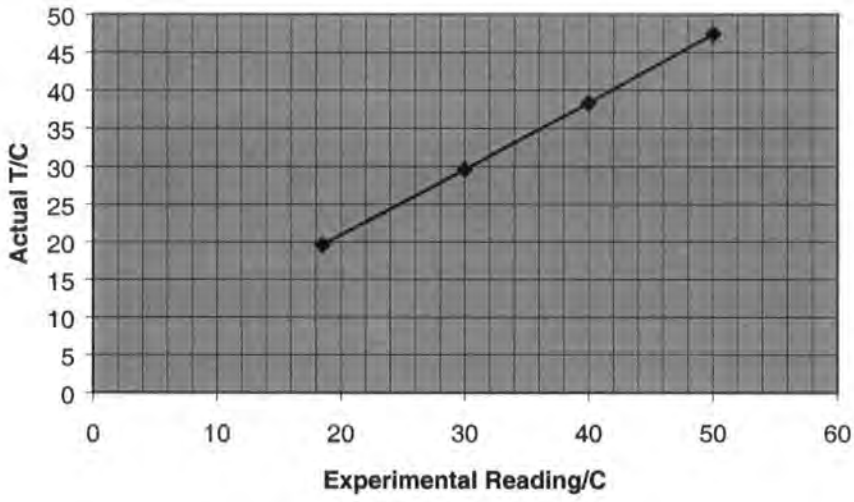

Figure 5.1 – Temperature Calibration of 65 MHz VT NMR

These data were then used to measure relaxivities of an aqueous solution of $GdCl_3.6H_2O$ (5.48 mM) at a range of temperatures as shown in **figure 5.2**. The relaxivities of [Gd.gDOTA]$^-$ at three temperatures were plotted on the same graph and combined with the relaxivities of the generation-2 Gd(III) complex **85**.

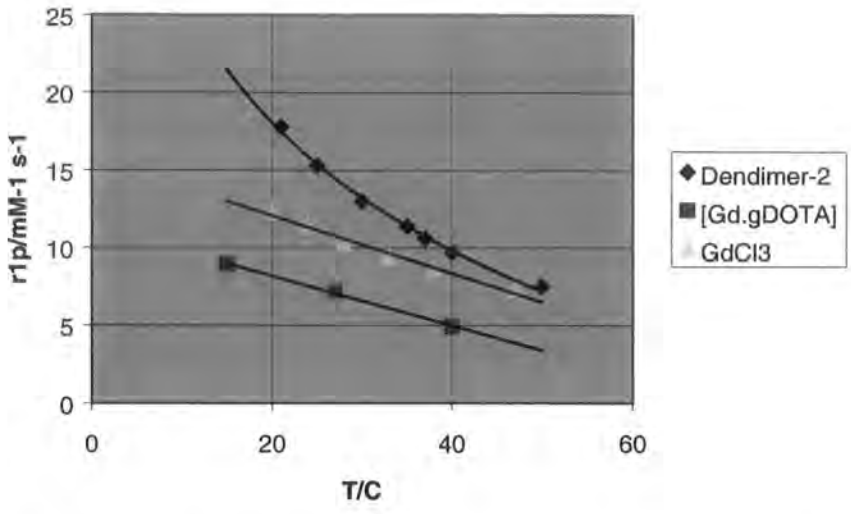

Figure 5.2 – Temperature Dependence of Relaxivity, 65 MHz.

The data show that the relaxivity of both $GdCl_3$ and $[Gd.gDOTA]^-$ shows an inverse, linear proportionality to temperature, whereas that of the dendritic complex is non-linear. This indicates qualitatively that the relaxivity has a dependence on more than one parameter (τ_R and τ_M). Also, it has significantly higher relaxivities than $GdCl_3$ at lower temperatures, but approaches that of $GdCl_3$ above 50°C.

5.3 NMRD Profiling

As well as being difficult to synthesise, the generation-2 $[Gd(DOTA)]^-$ tetradendramide complex was both difficult to purify and difficult to analyse with respect to purity as the only method of characterisation which proved viable was ESMS. Due to these difficulties and the limited amount of the generation-2 $[Gd(DOTA)]^-$ tetradendramide complex available, it was not possible to carry out NMRD profiling on this system **85**. However measurements were carried out on the higher generation-3 analogue **86**. The relaxivity was measured and the data fitted by M. Botta at the University of Turin on a Stelar field-cycling relaxometer, at 25°C and pH=7.2 from 0.008 to 20 MHz. The NMRD profile obtained is shown in **figure 5.3**. An additional point measured at 65 MHz measured at Durham was also considered in the fitting of the data.

Initial attempts to fit the data in terms of the usual inner sphere-outer sphere model of contributions to relaxivity gave very poor results. However the high relaxivity

observed at lower fields requires a large number of hydrogen-bonded water molecules relatively close to the Gd centre. This second sphere contribution was taken into account by including in the fitting three new parameters: *nl*, the average number of second sphere water molecules, their average distance from the metal centre, r_{2s}, and their effective correlation time $\tau_{C'}$ (including rotational, exchange and electronic contributions). Additionally, initial values typical of anionic, q=1, tetrasubstituted DOTA complexes were imposed for the following parameters; Δ^2, τ_V, r, a, and D.

$$\frac{1}{\tau_{C'}} = \frac{1}{\tau_{M'}} + \frac{1}{\tau_{R'}} + \frac{1}{\tau_S}$$

The three contributions from the inner, second and outer sphere water molecules are shown. One of the main aspects of the resultant profile is that the contribution of the inner sphere relaxivity is smaller than that of the second sphere water. There is clearly a well-defined shell of second sphere water molecules, which is the main contributor to the overall observed relaxivity. The fitting gives a value of 8 second sphere water molecules at an average distance of 4.0Å from the Gd(III) ion. The effective overall correlation time is 253 ps at 25°C. The value of the rotational correlation time is 400 ps, which is 5.5 times longer than that of $GdDOTA^-$, which is approximately the same factor by which their molecular weights differ.

However, a long value of the water exchange lifetime (ca. 500 ns) results from the best-fitting procedure. This is perhaps due to the presence of a relatively rigid network of hydrogen-bonded water molecules close to the coordination site of the inner sphere water, which may inhibit the ease of water exchange on the metal. This was disappointing in terms of the overall enhancement of relaxivity, but the profile did show clearly a significant increase in relaxivity at medium field strengths (10-100 MHz). This is consistent with a degree of optimisation of the rotational correlation time.

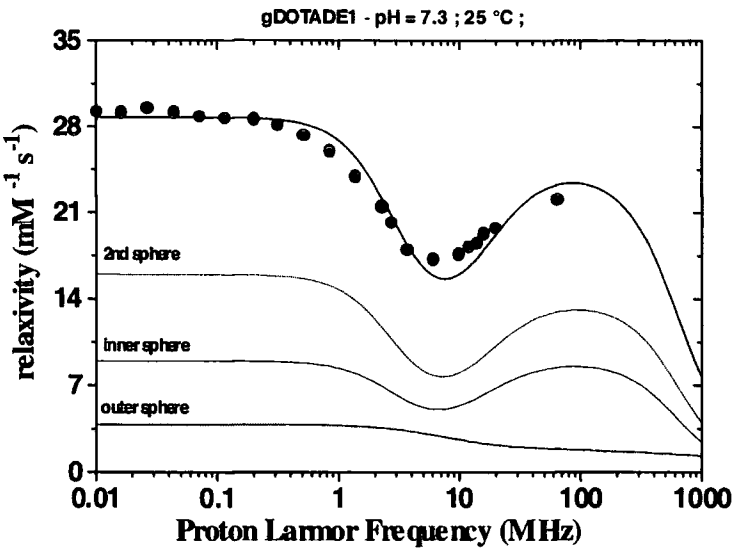

Figure 5.3 – NMRD Profile of Complex 90

The NMRD profile was also measured at 39°C. The results of this fitting combined with that at 25°C are shown in **figure 5.4**. There was a reduction in relaxivity over the full range of frequencies, in comparison with the corresponding profile at 25°C. This would be expected in a system where the rotational correlation time is the dominant factor. Note however that it is the second sphere water molecules which contribute most to the overall relaxivity and it is their rotational correlation time which is dominant. This is in spite of the rate of inner sphere water exchange increasing with temperature. The corresponding best fitting parameters are listed in **tables 5.1**, **5.2** and **5.3**.

In order to more accurately assess the value of τ_M, variable temperature ^{17}O NMR data were measured at 2.1 T and analysed in terms of the Swift-Connick equations (**figure 5.5**).[63] The value of τ_M calculated at 25°C is 590 ns ($\Delta H_M^{\#}$=34.6 kJ mol^{-1}), significantly longer than the value for the [GdDOTA]$^-$ complex (ca. 244 ns, 298 K). The electronic and rotational parameters were taken from the NMRD profile and fixed during the fitting procedure.

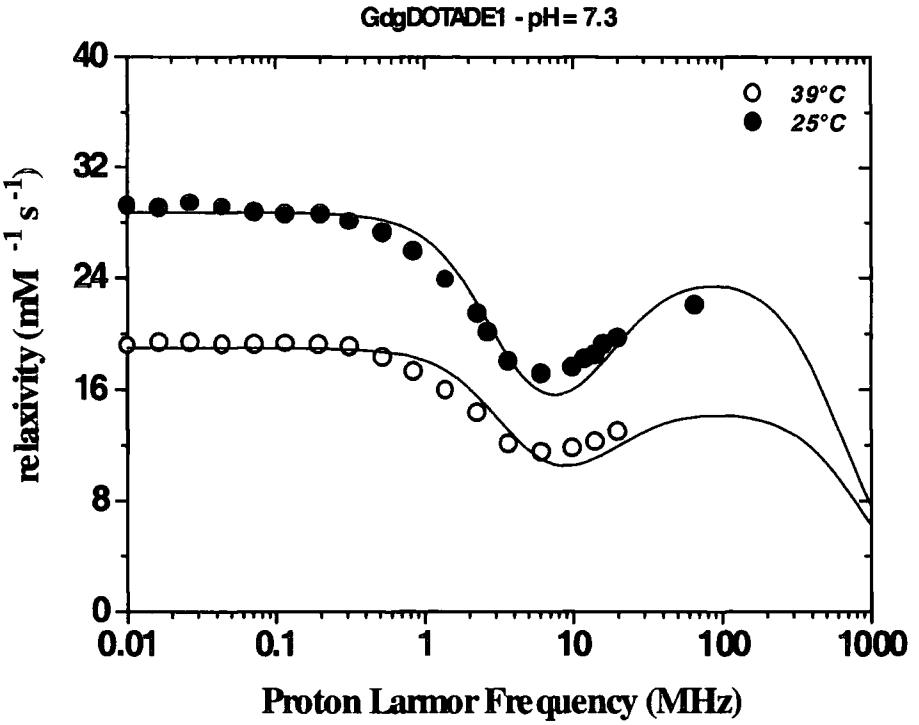

Figure 5.4 – NMRD Profile of Complex **86** at 25°C and 39°C.

This confirmed the large reduction in the rate of inner-sphere water exchange. Although a combination of an increased number of second sphere water molecules and a significant increase in the rotational correlation time combined to produce a respectable increase in relaxivity, the increase was suppressed by the reduced water exchange rate.

Additionally, the temperature dependence of the relaxivity of the generation-3 Gd(III) complex **86** was examined at 20 MHz by M. Botta at the University of Turin (**figure 5.6**). The parameters used to fit the curve were taken from the corresponding NMRD and ^{17}O profiles. The fact that the fit is quite good is strong support for the reliability of the relaxivity values calculated, in spite of the fact that the presence of a strong second sphere term is often regarded as making a meaningful interpretation of the data very difficult. The fact that the same set of parameters can reproduce three different sets of data well, is consistent with the validity of the conclusions.

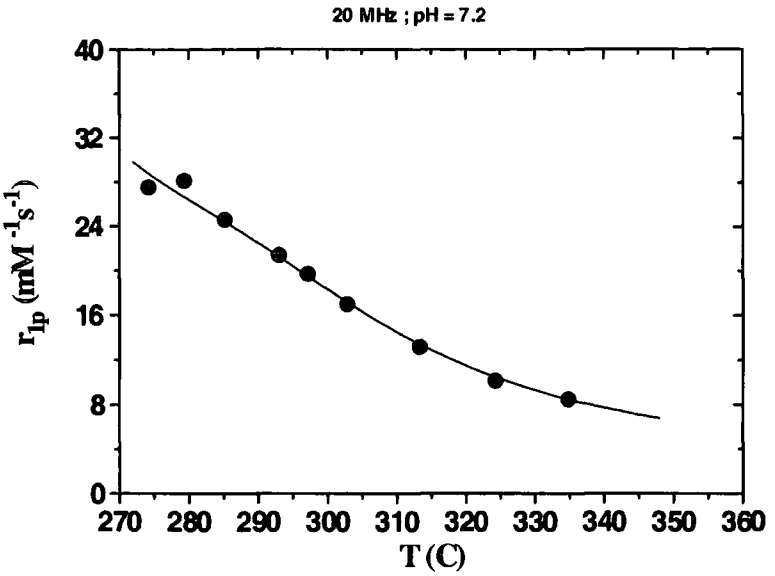

Figure 5.5 – ^{17}O VT NMR Measurements of Complex **86**

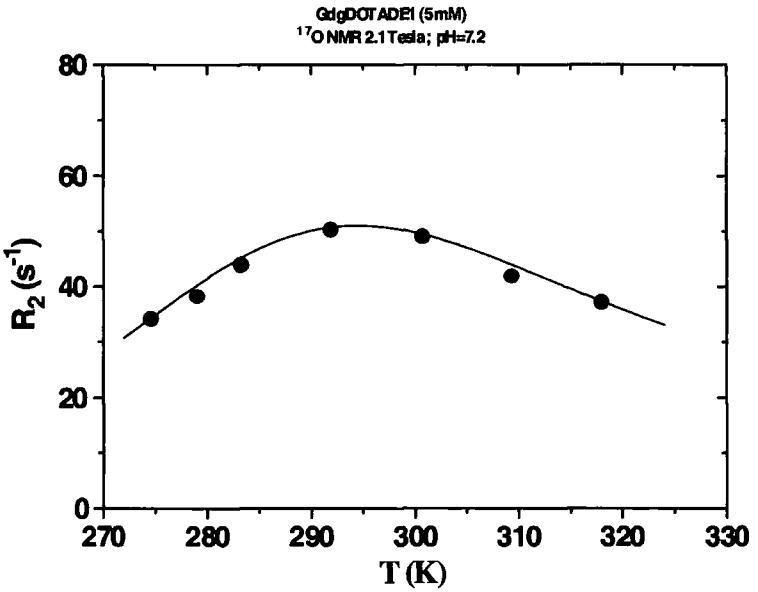

Figure 5.6 – Temperature-dependence of the Relaxivity of Complex **86**

5.4 Relaxivity at 400 MHz

The relaxivity of complex **85** was determined to be 7.9 ± 0.1 mM^{-1} s^{-1} at 20°C and 400 MHz. This lower relaxivity at high field strengths is characteristic of all high molecular weight contrast agents.

Best Fitting Parameters of the NMRD Profiles

Parameter	25°C	39°C
Δ^2 ($s^{-1};\times10^{-19}$)	4.1	4.9
τ_V (ps)	15	14
τ_R (ps)	310	220
τ_M (ns)	570	400
q	1	1
r (Å)	2.98	2.98
a (Å)	4	4
D ($cm^2s^{-1};\times10^5$)	2.24	3.13
q'	8	8
r' (Å)	4.0	4.4
τ' (ps)	250	190

Table 5.1 - VT NMR Measurements of Compound 86

Best Fitting Parameters of the VT ^{17}O R_2 (5 mmol/L solution)

Parameter	20 MHz
Δ^2 ($s^{-1};\times10^{-19}$)	4.1

τ_V (ps)	14
ΔH_V (*k*J/mol)	21
τ_R (ps)	310
ΔH_R (*k*J/mol)	40
τ_M (ns)	570
ΔH_M (*k*J/mol)	35
q	1
r (Gd-O; Å)	2.48

Table 5.2 - VT NMR Measurements of Compound 86

T-dependence of the relaxivity: Best Fitting Parameters

Parameter	20 MHz
Δ^2 (s^{-1};$\times 10^{-19}$)	4.1

τ_V (ps)	14
ΔH_V (*k*J/mol)	20
τ_R (ps)	310
ΔH_R (*k*J/mol)	40
τ_M (ns)	564
ΔH_M (*k*J/mol)	36
q	1
r (Å)	2.98
a (Å)	4
D ($cm^2s^{-1};\times10^5$)	2.24
ΔH_D (*k*J/mol)	-27
q'	8
r' (Å)	4.0
τ' (ps)	250
$\Delta H_{\tau'}$ (*k*J/mol)	16

Table 5.3 – Best-Fitting NMRD Parameters

5.5 Conclusions

The synthesis of two high molecular weight, dendritic poly(ether) Gd[gDOTA]$^-$ complexes was carried out. The relaxivity of the generation-2 complex (Mw = 2013) (**85**) was determined to be 17.8 ± 0.5 mM^{-1} s^{-1}, significantly higher than that of the parent $[GdgDOTA]^{-1}$ complex (7.8 ± 0.1 mM^{-1} s^{-1}). This successfully showed that symmetrical functionalisation with high molecular mass fragments significantly enhances relaxivity. The relaxivity of the analogous generation-3 complex (Mw = 3535) **86**, was still higher at 21.0 ± 0.5 mM^{-1} s^{-1}, but not as high as expected. The reason for this was revealed by NMRD profiling, using a new data fitting model which takes into account the second water coordination sphere. The results were surprising in that the second sphere water

molecules contributed more to the overall relaxivity than the inner sphere water. This was because there appears to be a well-defined shell of ca. 8 second-sphere water molecules, at an average distance of 4Å from the Gd(III) ion.

The effective overall correlation time was calculated to be 253 ps at 25°C, and the rotational correlation time was a factor of five greater than that of [GdgDOTA]$^-$, showing that the molecular rotation had been slowed significantly. Comparison of this result with the very poor increases in relaxivity upon attachment of linear PEG to similar systems, shows that the distribution and rigidity of the high molecular weight moieties is just as important as the actual mass being added. However the reason why there wasn't an even greater improvement in the relaxivity of the generation-3 complex was due to there being a surprisingly long water exchange lifetime ca. 500 ns. This limited the relaxivity due to the inner sphere water molecules sufficiently that the second sphere contribution became dominant. The limitation of the water exchange rate may actually be due to the fact that there is a well-defined, efficacious second sphere water network. The same attractive forces which hold the second sphere water in place, may also cause the inner sphere water to bind more strongly to the Gd(III) cation. Therefore, the resultant network of water molecules is beneficial to the second sphere effect, but detrimental to the inner sphere effect. This result was disappointing in light of the work carried out by Toth on the PEG-derivitised poly(aminocarboxylate) complex illustrated in **figure 2.18**, which did not show any change in the rate or mechanism of water exchange. The reason for this phenomenon is not clear, but may be due to the greater rigidity imparted by the closely packed dendritic structure of **85** and **86**. However, the desired improvement in the rotational correlation time was achieved, and this doctoral work has provided several avenues for building on the results obtained.

5.6 Recommendations for Further Work

Although the expectation is that the reduction in water exchange rate is due to changes in the solvation environment at the gadolinium centre upon attachment of the dendron moieties, the possibility of a change in the stereochemistry of the complex to the square antiprismatic system should be investigated. Synthesis of the Eu(III) and Tb(III) analogues, followed by ^{1}H NMR analysis would elucidate the stereochemistry.

If – as is likely – the distribution of isomers is not perturbed by greatly by the attachment of the dendron moieties, one could envisage a range of structures incorporating functional groups such as carboxylate and phosphate on the pendant arms (**figure 5.7**), which may change the hydration environment of the Gd (III) centre such that rapid water exchange conditions may be re-established. This would allow the full benefit of the enhanced rotational correlation time to be attained.

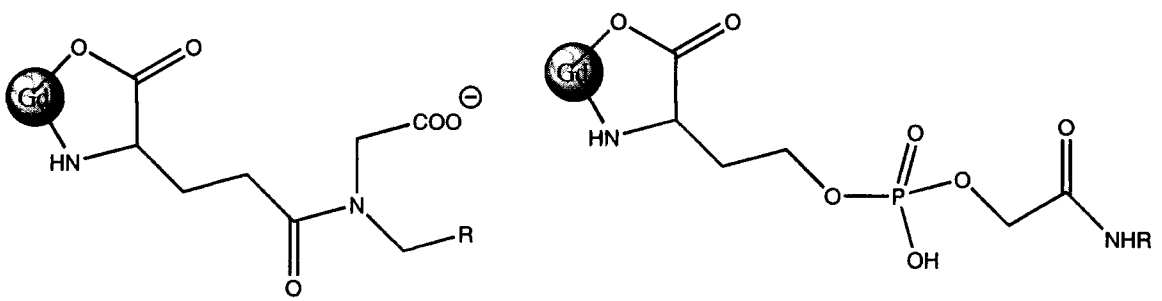

Figure 5.7 – Recommendations for Future Synthetic Work

The incorporation of polar groups into the area of the molecule near the inner sphere water would be expected to have a significant effect on the microenvironmental polarity and the organisation of hydrogen bonding. Groups such as phosphate and carboxylate may yield interesting results.

Additionally, any increase in the steric crowding around the inner-sphere water binding site would be expected to destabilise the hydrated state and therefore increase the rate of water exchange. Any of the aryl-based pendant arms, whose attachment to the $12N_4$ system was attempted in this thesis, would be expected to increase this steric crowding. However, the problems associated with these systems when undergoing S_n2 displacement with the sterically encumbered secondary amine nucleophile have been outlined, and depend on the nature of the *para*-functionalisation. Alternative, more promising approaches to these systems could be as follows.

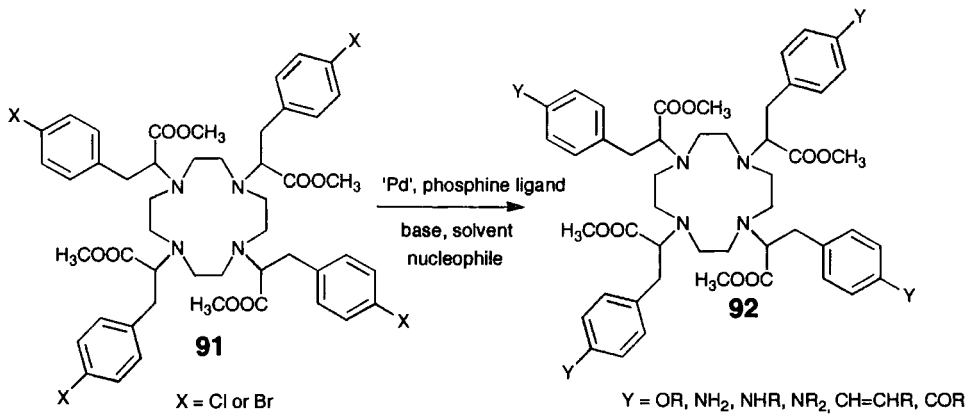

Figure 5.8 – Buchwald/Hartwig approach to *para*-substitution

para-Halo substituted analogues of the tetrasubstituted $12N_4$ compound **13**, such as **91** in **figure 5.8**, may be more easily accessible than systems where the group X corresponds to an acyl or alkoxy group (**28** and **45** respectively). *para*-Substitution with an electronically near-neutral halogen atom would not be expected to encourage elimination to the cinnamic system, either via the $E1_{CB}$ mechanism, as was the case for the *p*-acyl group, or via enhanced phenyl nucleophilicity, as was the case for the *p*-alkoxy group.

As an alternative to a halogen, a mesyl or tosyl group would be readily accessible from the easily prepared, enantiomerically pure **41**. These sulphonate groups also undergo Buchwald/Hartwig type chemistry, and would not be expected to exhibit sufficient mesomeric electron-donation to cause enhanced rates of elimination to the cinnamate.

The actual derivisitation of the aryl halide or sulphonate could include oxygen, nitrogen, sulphur or carbon-based nucleophiles. The range is extensive, and would enable the chemist to tune the properties of the system.

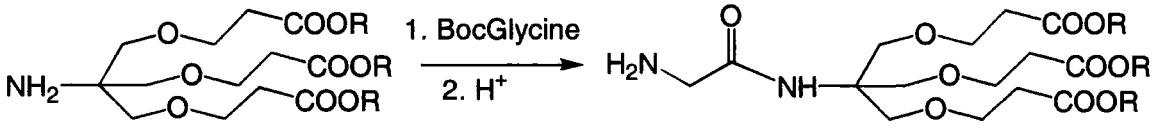

Figure 5.9 – Glycyl Derivitisation of the Trifurcated Linker

Another area of the thesis for which it would be advantageous to carry out some more work would be the trifurcated linker dendron (**figure 5.9**). The main problem with this

system was that the focal amino group was too sterically hindered to undergo facile coupling to the carboxy-terminated Gd chelate. *N*-functionalisation with, for example a glycyl group (see **90**), would make the reaction easier. The synthesis of systems based on this trifurcated linker would be of interest for two reasons. Firstly, increased molecular weight would be possible where the R group was a poly(ether) dendron of either generation-2 or 3. Secondly, the polarity of the microenvironment in the vicinity of the first and second sphere water molecules would be different to that present in **85** and **86**, and may lead to an increase in the inner sphere water exchange rate.

Chapter 6

Experimental

This chapter describes in detail the synthetic procedures, which were followed and provides the relevant characterisation data.

6.1 Experimental Methods

Reagents and Solvents

Reagents and solvents were purified using standard techniques. Solvents were dried as follows: acetonitrile, dichloromethane and amines over calcium hydride; ethers over sodium with benzophenone as indicator and alcohols from the corresponding magnesium alkoxide using iodine as a catalyst. *N,N*-Dimethylformamide and dimethylsulfoxide were used directly from Aldrich Sure-Seal® bottles. All water was of high purity with conductivity $\leq 0.06\mu S\ cm^{-1}$, obtained from the Purite® purification system.

Chromatography

Column chromatography was carried out using flash silica (Merck silica gel 60, 230-400 mesh).

Spectroscopy

^{1}H NMR spectra were recorded at 199.99 MHz on a Varian Mercury 200 instrument, at 299.99 MHz on a Varian Unity 300 instrument and at 399.99 MHz on a Varian VXR400 instrument. ^{13}C NMR spectra were recorded on the same instruments at 50.3 MHz, 74.4 MHz and 100.6 MHz respectively. Infra-red spectra were recorded on a Perkin Elmer 1600 FTIR spectrometer. Samples were run on sodium chloride discs as thin films, or as potassium bromide discs. Mass spectra were recorded using a VG Platform II electrospray mass spectrometer with methanol, water or acetonitrile as the carrier solvent.

Analysis

Melting points were determined on a Reichert Köfler Block and are uncorrected. Elemental analyses were determined on a Carlo ERBA 1106 instrument.

6.2 Experimental Procedures

Methyl-(*S*)-3-phenyllactate (11)[205]

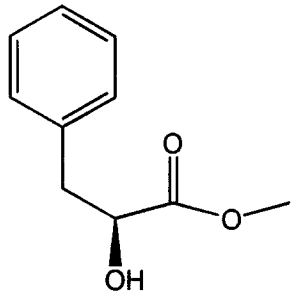

A solution of 3-phenyllactic acid (5.0 g, 30 mmol) and a catalytic amount of sulphuric acid in methanol (200 mL) was heated at reflux for 48 h. After neutralisation with sodium hydrogencarbonate and filtration, the methanol was removed *in vacuo* and the product extracted into ethyl acetate (3 x 50 mL) from water. After drying over magnesium sulphate and filtration, the solvent was removed *in vacuo* to yield a white crystalline solid (5.18 g, 96%), m.p. 39-42°C.

ν_{max} (neat)/cm^{-1} 3283 (OH), 1751 (C=O), 1104 (C-O); δ_H (300 MHz, $CDCl_3$) 2.75 (1H, d, ^3J 6.5, OH), 2.88 (1H, dd, ^2J 14.0, ^3J 7.0, CH_2), 3.05 (1H, dd, ^2J 14.0, ^3J 4.5, CH_2), 3.69 (3H, s, $COOCH_3$), 4.37 (1H, td, ^3J 4.5 and 7.0, CH), 7.12-7.23 (5H, m, Ph); δ_C (50 MHz, $CDCl_3$) 40.8 (CH_2), 52.7 ($COO\underline{C}H_3$), 71.6 ($C\underline{H}(OH)$), 127.1, 128.7, 129.7 and 136.6 (phenyl), 174.8 (C=O); *m/z* (ES+, methanol) 203 ($[M+Na]^+$, 100%); Found: C, 66.55; H, 6.80. $C_{10}H_{12}O_3$ requires C, 66.65; H, 6.71%, $[\alpha]_D^{22}$ 14° (*c* = 1, methanol).

Methyl-(*S*)-3-phenyl-2-triflylpropanoate (12)

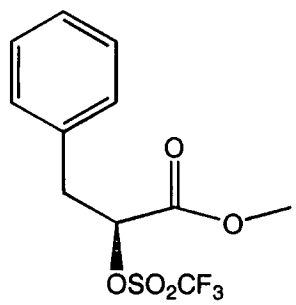

To a solution of methyl-(*S*)-3-phenyllactate, **11** (1.0 g, 5.6 mmol) in dry dichloromethane (20 mL) at -78°C was added via syringe, triethylamine (1.18 mL, 8.49 mmol) and

trifluoromethanesulphonic anhydride (5.0 g, 17.7 mmol) with stirring under argon. After 20 h, the solvent was removed in vacuo and the remaining brown-black liquid was extracted into hexane (5 x 20 mL) and decolourised with activated carbon. The hexane was then removed *in vacuo* to yield a clear liquid (1.17 g, 66%).

δ_H (300 MHz, $CDCl_3$) 3.23 (1H, dd, ^2J 15, ^3J 9, OH), 3.34 (1H, dd, ^2J 15, ^3J 4, CH_2), 3.83 (3H, s, CH_3), 5.26 (1H, dd, ^3J 9 and 4, CH), 7.21-7.35 (5H, m, Ph); *m/z* (ES+, methanol) 313 ($[M+H]^+$, 100%), $[\alpha]_D^{22}$ -9° (*c* = 0.5, methanol).

1,4,7,10-Tetra-1-(1'-methoxycarbonyl-2'-phenylethyl)-1,4,7,10-tetraazacyclododecane (13)

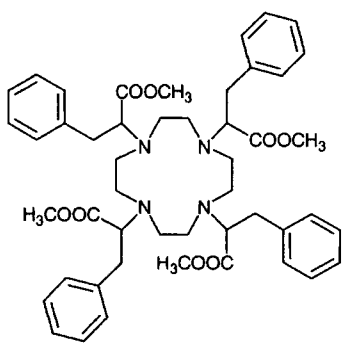

To 1,4,7,10-tetraazacyclododecane (0.12g, 0.70 mmol) and K_2CO_3 (0.69 g, 5.0mmol) in dry acetonitrile (10ml) was added with stirring methyl-(*S*)-3-phenyl-2-triflylpropanoate, **12** (1.51g, 4.84 mmol) under argon. After 10 days at –15 °C, the ESMS spectrum revealed the presence of the tetrasubstituted product alone. This was then extracted into dichloromethane from water, treated with activated carbon and dried over $MgSO_4$. Column chromatography (hexane:dichloromethane:methanol 75:24:1) yielded a solid (0.42 g, 73%).

δ_H (200 MHz, $CDCl_3$) 2.54-3.11 (24H, m, CH_2), 3.59 (12H, s, CH_3), 3.60-3.65 (4H, m, CH), 7.17-7.27 (20H, m, Ph); δ_C (50 MHz, $CDCl_3$) 36.2 (CH_2), 50.5 (CH_2), 51.3 (CH_3), 66.0 (CH), 126.6-129.8 (*o,m,p*-Ph), 138.9 (*ipso*-Ph), 178.0 (C=O); *m/z* (ES+, methanol) 821 ($[M+H]^+$, 100%); $[\alpha]_D^{22}$ 96° (*c* = 1, methanol).

Methyl-*N*-(*tert*-butoxycarbonyl)-L-tyrosinate (15)[206]

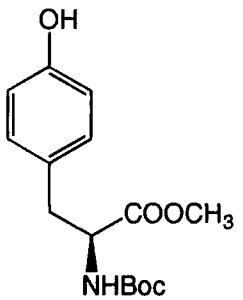

L-tyrosine methyl ester hydrochloride (6.83 g, 21.5 mmol) was dissolved in methanol (30 ml). To this was added potassium carbonate (2.9 g, 64.7 mmol) and di-tert-butyldicarbonate (4.69 g, 21.5 mmol) and the reaction heated at 45°C for 90 mins with stirring, and then allowed to stand overnight at room temperature. After methanol removal, the product was extracted from water with dichloromethane (5 x 25 ml), and dried over $MgSO_4$. Residual tert-butanol was removed *in vacuo* to yield a clear liquid (6.03 g, 95%).

ν_{max} (neat)/cm^{-1} 3380 br (OH), 1711 (ester), 1655 (carbamate), 1230 (C-O); δ_H (300 MHz, $CDCl_3$) 1.41 (9H, s, ^tBu), 2.96 (1H, m, CH_2), 3.01 (1H, m, CH_2), 3.70 (3H, s, $COOCH_3$), 4.54 (1H, m, CH), 4.99 (1H, s, br, NH), 6.83 (2H, d, ^3J 8 Hz, ArH), 7.11 (2H, d, ^3J 8 Hz, ArH); δ_C (75 MHz, $CDCl_3$) 30 (CH_3), 39 (*quat*-C), 53 ($COO\underline{C}H_3$), 58 (CH_2), 81 ($C\underline{H}(OH)$), 130, 131, 158 and 160 (phenyl), 175 (C=O); *m/z* (ES+, methanol) 296 ($[M+H]^+$, 100%), $[\alpha]_D^{22}$ 4.5° (*c* = 10, methanol).

Methyl-*N*-(*tert*-butoxycarbonyl)-*O*-(methoxycarbonylmethyl)-L-tyrosinate (16)

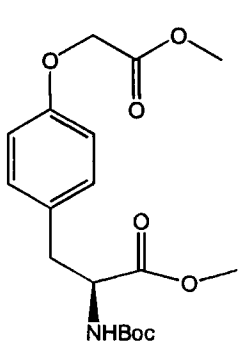

To dry dimethylsulphoxide (20ml) was added powdered KOH (3.36 g, 60 mmol) and methyl-2-(2,2-dimethylethoxyamido)-3-(4-hydroxyphenyl) propanoate, **15** (4.32 g, 14.6 mmol) was added and allowed to stir for 30 mins. To this was then added methyl bromoacetate (2.8 ml, 30 mmol) with stirring for 6 h. The product was then extracted into dichloromethane (3 x 25 ml) from aqueous K_2CO_3, dried over $MgSO_4$ and the solvent removed *in vacuo* to yield a clear liquid. Crystallisation from ethyl acetate/hexane yielded white crystals, m.p. 162°C (4.91 g, 92%).

ν_{max} (KBr)/cm^{-1} 3450 (NH), 1740 (C=O), 1658 (carbamate); δ_H (300 MHz, $CDCl_3$) 1.38 (9H, s, ^{t}Bu), 2.95 (1H, m, CH_2), 3.01 (1H, m, CH_2), 3.75 (3H, s, $COOCH_3$), 3.76 (3H, s, $COOCH_3$), 4.46 (1H, m, CH), 4.58 (2H, s, OCH_2), 5.00 (1H, d, ^3J 9, NH), 6.79 (2H, d, ^3J 9 Hz, ArH), 7.04 (2H, d, ^3J 9 Hz, ArH); *m/z* (ES+, methanol) 368 ([M+H]$^+$, 100%), Found: C, 61.02; H, 7.62; N 3.21. $C_{18}H_{25}NO_7$ requires C, 58.90; H, 6.81; N, 3.81%; $[\alpha]_D^{22}$ 3.5° (*c* = 1, methanol).

Methyl-*O*-(methoxycarbonylmethyl)-L-tyrosinate (17)

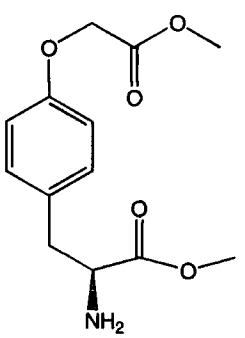

Methyl-*N*-(*tert*-butoxycarbonyl)-*O*-(methoxycarbonylmethyl)-L-tyrosinate, **16** (4.91 g, 13.4 mmol) was dissolved in 50% w/v aqueous solution of trifluoroacetic acid with stirring for 20 h. The residual acid was neutralised and extracted with saturated aqueous sodium bicarbonate and all volatiles were removed *in vacuo*, to yield a clear liquid (5.03 g, 98%).

ν_{max} (KBr)/cm^{-1} 3454 (NH), 1750 (C=O), 1658; δ_H (300 MHz, $CDCl_3$) 2.90-3.26 (2H, m, Ar$\underline{CH_2}$), 3.76 (3H, s, CH_3), 3.80 (3H, s, CH_3), 4.17-4.30 (1H, m, CH), 4.60 (2H, s,

OCH_2), 6.83-7.24 (4H, m, ArH); *m/z* (ES+, methanol) 268 ($[M+H]^+$, 100%); $[\alpha]_D^{22}$ 5° (*c* = 1, methanol).

Methyl-(*S*)-2-acetoxy-3-phenylpropanoate (23)

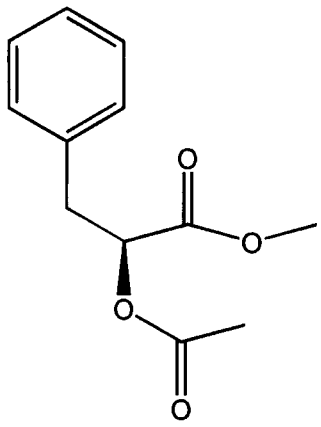

To a solution of methyl-(*S*)-2-acetoxy-3-phenylpropanoate (0.90 g, 5.0 mmol) in acetic anhydride (10 mL) was added dry pyridine (4 mL). After 18 h, methanol (20 mL) was added. After 1 h water (10 mL) was added. All volatiles were removed *in vacuo* and the product was extracted into ethyl acetate (3 x 25 mL) from water. The organic solution was dried over magnesium sulphate and the solvent removed *in vacuo* to yield a clear oil (1.10 g, 99%).

ν_{max} (neat)/cm^{-1} 3088, 3063, 3031 and 2954 (CH), 1748 (C=O), 1233 (C-O); δ_H (200 MHz, $CDCl_3$) 2.07 (3H, s, CH_3CO), 3.09 (1H, dd, ^2J 14.5, ^3J 8.4, CH_2), 3.17 (1H, dd, ^2J 14.5, ^3J 5.0, CH_2), 3.71 (3H, s, $COOCH_3$), 5.22 (1H, dd, ^3J 5.0 and 8.4, CH), 7.20-7.30 (5H, m, Ph); δ_C (63 MHz, $CDCl_3$) 20.5 (CH_2), 37.3 ($\underline{C}H_3CO$), 52.2 ($COO\underline{C}H_3$), 72.9 (CH), 126.9, 128.4, 129.2 and 135.9 (phenyl), 170.1 and 170.2 (C=O); *m/z* (ES+, methanol) 223 ($[M+H]^+$, 45%), 245 ($[M+Na]^+$, 100%), $[\alpha]_D^{22}$ -0.35° (*c* = 1, methanol).

Methyl-(*S*)-2-acetoxy-3-(4-acetylphenyl)propanoate (24)

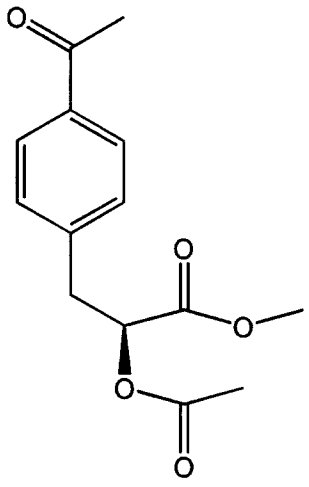

To a solution of acetyl chloride (1.2 mL, 17 mmol) and aluminium chloride (5.0 g, 48 mmol) in 1,1,2,2-tetrachloroethane (10 mL) was gradually added under argon with stirring a solution of methyl-(*S*)-2-acetoxy-3-phenylpropanoate, **23** (2.22 g, 10 mmol) in 1,1,2,2-tetrachloroethane (6 mL). After 20 h, the reaction mixture was poured into ice/acidified water (HCl) mixture and immediately extracted into ethyl acetate (4 x 30 mL), washed with water (1 x 30 mL), decolorised with activated carbon, filtered and the solvents removed *in vacuo*. Flash column chromatography (silica, 2% ethyl acetate in dichloromethane) yielded methyl-2-acetoxy-3-(4-acetylphenyl)propanoate (0.36 g, 14%), methyl-2-hydroxy-3-(4-acetylphenyl)propanoate (0.07 g, 3%) and 2-acetoxy-3-(4-acetylphenyl)propanoic acid (0.88 g, 35%). These three products were then combined, dissolved in methanol (50 ml) with a catalytic amount of sulphuric acid and heated at reflux for 48 h. After neutralisation with sodium hydrogencarbonate and filtration, the solvent was removed *in vacuo* and the product extracted into ethyl acetate (3 x 30 mL) from water to yield a white solid (0.93 g, 45%).

ν_{max} (neat)/cm^{-1} 3004, 2955 (CH), 1747 (ester C=O), 1683 (ketone C=O), 1235 (C-O); δ_H (400 MHz, $CDCl_3$) 2.01 (3H, s, CH_3CO), 2.52 (3H, s, $ArCOC\underline{H}_3$), 3.09 (1H, dd, ^2J 14, ^3J 8, CH_2), 3.18 (1H, dd, ^2J 14, ^3J 5, CH_2), 3.66 (3H, s, $COOCH_3$), 5.19 (1H, dd, ^3J 5 and 8, CH), 7.26 (2H, d, ^3J 8, Ar), 7.90 (2H, d, ^3J 8, Ar); δ_C (100 MHz, $CDCl_3$) 20.3 (CH_2), 26.4 ($Ar\underline{C}O$), 37.0 ($\underline{C}H_3CO$), 52.2 ($COO\underline{C}H_3$), 72.2 (CH), 128.4, 129.4, 133.8 and 141.3

(phenyl), 169.6 and 170.0 (ester C=O), 197.5 (ketone C=O); *m/z* (ES+, methanol) 265 ($[M+H]^+$, 20%), 287 ($[M+Na]^+$, 90%), $[\alpha]_D^{22}$ 10.5° (*c* 1.5 in methanol), m.p. 84-88 °C.

Methyl-(*S*)-4-[4-(2-acetoxy-2-methoxycarbonylethyl)phenyl]-4-oxobutanoate (26)

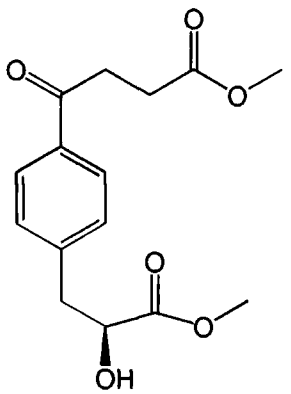

To a solution of methyl-3-bromoformylpropanoate (60 mmol) and aluminium chloride (27.0 g, 260 mmol) under argon in 1,1,2,2-tetrachloroethane (25 mL) was added gradually with stirring a solution of methyl-(*S*)-2-acetoxy-3-phenylpropanoate, **23** (6.87 g, 31 mmol) in 1,1,2,2-tetrachloroethane (25 mL). The solution was maintained at 50 °C for 20 h. The reaction was quenched with a mixture of ice and acidified water (HCl), and immediately extracted with ethyl acetate (3 x 50 mL). After drying with magnesium sulphate and filtering, the solvent was removed. The resultant mixture of products was fully de-esterified in an aqueous methanolic solution of sodium hydroxide for 20 h. After acidification to pH=1 with hydrochloric acid, the product was extracted into ethyl acetate (3 x 30 mL), dried over magnesium sulphate and filtered. Removal of the solvent yielded a black solid which was dissolved in methanol (150 mL), a catalytic amount of sulphuric acid was added and the solution heated at reflux for 48 h. After neutralisation with sodium hydrogencarbonate, filtration and removal of solvent *in vacuo*, a black oil resulted. This was purified by flash column chromatography (silica, ethyl acetate/hexane 1:5 → ethyl acetate/hexane 1:2) to yield a yellow oil which consisted of the *ortho*- and *para*-products. Crystallisation from acetonitrile (x 4) yielded the *para*-product as a white crystalline solid, m.p. 137-138°C (1.05 g, 12%).

Diacid: ν_{max} (KBr)/cm^{-1} 3425 (CHOH), ca. 3000 (COOH), 2924 (C-H), 1745 (CH(OH)COOH), 1696 (CH_2COOH), 1679 (ArC=O), 1437, 1419 and 1402 (COH), 1238

(C-O); δ_H (300 MHz, CD_3OD) 2.69 (2H, t, ^3J 6.6, $C\underline{H}_2COOH$), 2.97 (1H, dd, ^2J 13.8, ^3J 8.1, $ArC\underline{H}_2$), 3.17 (1H, dd, ^2J 13.8, ^3J 4.5, $ArC\underline{H}_2$), 3.29 (2H, t, ^3J 6.6, $ArCOC\underline{H}_2$), 4.38 (1H, dd, ^3J 8.1 and 4.5, $C\underline{H}(OH)$), 7.40 (2H, d, ^3J 8.4, *o*-Ar$\underline{H}$), 7.93 (2H, d, ^3J 8.4, *m*-Ar$\underline{H}$); δ_C (50 MHz, CD_3OD) 27.8 ($\underline{C}H_2COOH$), 33.2 ($ArCO\underline{C}H_2$), 40.3 ($Ar\underline{C}H_2$), 71.1 (CH(OH)), 127.9 (*o*-Ar), 129.8 (*m*-Ar), 135.3 (*p*-Ar), 143.8 (*ipso*-Ar), 175.4 ($CH_2\underline{C}$=O), 175.6 (CH(OH)$\underline{C}$OOH), 199.0 (Ar$\underline{C}$=O); *m/z* (ES+, methanol) 289 ($[M+Na]^+$, 100%), 555($[M_2+Na]^+$, 30%); Found: C, 58.40; H, 5.24. $C_{13}H_{14}O_6$ requires C, 58.65; H, 5.30%; m.p. 155-158°C; $[\alpha]_D^{22}$ 0° (*c* = 1, methanol).

Diester: ν_{max} (neat)/cm^{-1} 3481 (CH$\underline{O}$H), 2954 (C-H), 1737 ($\underline{C}OOCH_3$), 1683 (Ar$\underline{C}$=O), 1223 (C-O); δ_H (300 MHz, $CDCl_3$) 2.76 (2H, t, ^3J 6.6, $C\underline{H}_2COOCH_3$), 3.02 (1H, dd, ^2J 14.0, ^3J 6.8, $ArC\underline{H}_2$), 3.19 (1H, dd, ^2J 14.0, ^3J 4.4, $ArC\underline{H}_2$), 3.30 (2H, t, ^3J 6.6, $ArCOC\underline{H}_2$), 3.71 (3H, s, $CH_2COOC\underline{H}_3$), 3.80 (3H, s, CH(OH)$COOC\underline{H}_3$), 4.49 (1H, dd, ^3J 6.8 and 4.4, $C\underline{H}(OH)$), 7.33 (2H, d, ^3J 8.1, *o*-Ar$\underline{H}$), 7.92 (2H, d, ^3J 8.1, *m*-Ar$\underline{H}$); δ_C (50 MHz, $CDCl_3$) 27.3 ($\underline{C}H_2COOCH_3$), 33.6 ($ArCO\underline{C}H_2$), 40.6 ($Ar\underline{C}H_2$), 52.1 ($CH_2COO\underline{C}H_3$), 52.9 (CH(OH)$COO\underline{C}H_3$), 71.2 (CH(OH)), 128.4 (*o*-Ar), 130.0 (*m*-Ar), 135.4 (*p*-Ar), 142.7 (*ipso*-Ar), 173.7 ($CH_2\underline{C}OOCH_3$), 174.5 (CH(OH)$\underline{C}OOCH_3$), 198.0 (Ar$\underline{C}$=O); *m/z* (ES+, methanol) 317 ($[M+Na]^+$, 100%), 611($[M_2+Na]^+$, 50%); Found: C, 61.10 ; H, 6.20%. $C_{15}H_{16}O_6$ requires C, 61.22 ; H, 6.16%; $[\alpha]_D^{22}$ 0° (*c* = 1, methanol).

Methyl-(4-tetrahydropyranyloxyphenyl)ethanoate (32)[147]

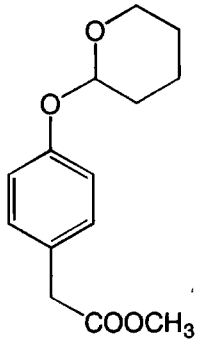

Methyl-4-hydroxyphenylacetate (8.00 g, 48.2 mmol) was dissolved in diethyl ether (100 mL) and the solution cooled to 0°C in an ice bath. Conc. $HCl_{(aq)}$ was added (10 drops), followed by 3,4-dihydro-2H-pyran (2.11 mL, 100 mmol). The solution was stirred at 0°C

for 40 min, and then for 24 h at ambient temperature. Flash column chromatography (silica, 10% ethyl acetate in hexane) yielded a clear oil (3.82g, 32%).

ν_{max} (neat)/cm^{-1} 3001 (CH), 1742 (C=O); δ_H (200 MHz, $CDCl_3$) 1.50-2.10 (6H, m, $OCH_2C\underline{H}_2C\underline{H}_2C\underline{H}_2$), 3.56 (2H, s, $ArC\underline{H}_2$), 3.60 (1H, m, OCH_2), 3.67 (3H, s, $COOCH_3$), 3.90 (1H, m, OCH_2), 5.40 (1H, m, $OC\underline{H}OCH_2$), 7.00 (2H, d, ^3J 8.7, ArH), 7.18 (2H, d, ^3J 8.7, ArH); δ_C (50 MHz, $CDCl_3$) 18.98 (CH_2), 25.45 (CH_2), 30.57 ($OCH_2O\underline{C}H_2$), 40.48 ($ArCH_2$), 52.04 ($COOCH_3$), 62.04 (CH_2O), 96.48 ($CH(O)_2$), 116.73 (Ar), 127.20 (Ar), 130.37 (Ar), 156.43 (Ar), 172.34 (C=O); *m/z* (ES+, methanol) 273 ($[M+Na]^+$, 10%), 289 ($[M+K]^+$, 10%).

Methyl-2-(4-benzoyloxyphenyl)ethanoate (34)

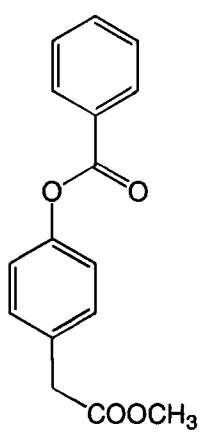

Methyl-4-hydroxyphenylacetate (5.0 g, 30.1 mmol) was dissolved in a solution of benzoyl chloride (3.5 mL, 30.1 mmol) and diisopropylethylamine (5.25 mL, 30.1 mmol) in dry THF (100 mL). The solution was stirred at ambient temperature for 24 h. The salt precipitate was filtered off and all volatiles removed *in vacuo* to yield the pure product as a white solid (7.97 g, 29.5 mmol, 98%).

ν_{max} (neat)/cm^{-1} 3003 (CH), 1740 (CH_2C=O), 1728 (ArC=O), 1508, 1277, 1215; δ_H (300 MHz, $CDCl_3$) 3.64 (2H, s, $ArC\underline{H}_2$), 3.70 (3H, s, $COOCH_3$), 7.19 (2H, d, ^3J 8.4, 2-Ar), 7.34 (2H, d, ^3J 8.4, 3-Ar), 7.50 (2H, t, ^3J 7.5, Ph), 7.63 (1H, t, ^3J 7.5, Ph), 8.19 (2H, d, ^3J 7.5, Ph); δ_C (50 MHz, $CDCl_3$) 40.79 ($Ar\underline{C}H_2$), 52.31 ($COO\underline{C}H_3$), 122.04, 128.81, 129.74, 130.39, 130.61, 131.83, 133.85 and 150.29 (Ar), 165.35 ($CH_2\underline{C}OOCH_3$) and 171.98

(ArCOOAr'); *m/z* (ES+, methanol) 293 ($[M+Na]^+$, 100%), 563 ($[M_2+Na]^+$, 50%); m.p. 49-50°C (lit.61-62°C).[202]

(±)-Methyl-2-(4-benzoyloxyphenyl)bromoacetate (35)

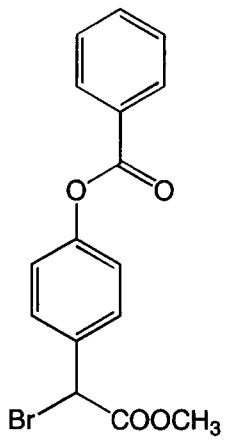

Methyl-4-benzoyloxyphenylacetate, **34** (7.95 g, 29.0 mmol) and *N*-bromosuccinimide (5.34 g, 30 mmol) were dissolved in carbon tetrachloride (50 mL) and brought to reflux. AIBN (0.10 g) was then added. After 24 h, the product was filtered and the crude was crystallised from diethyl ether to yield yellow crystals (1.14 g, 11%).

ν_{max} (neat)/cm^{-1} 3003 (CH), 1751 (CHBrC=O) and 1729 (ArC=O); δ_H (200 MHz, $CDCl_3$) 3.81 (3H, s, $COOCH_3$), 5.39 (1H, s, CHBr), 7.24 (2H, d, ^3J 9, 2-Ar), 7.48-7.71 (5H, m, Ph), 8.20 (2H, d, ^3J 9, 3-Ar); δ_C (50 MHz, $CDCl_3$) 45.63 (CHBr), 53.43 ($COO\underline{C}H_3$), 122.13, 128.60, 129.99, 130.19, 133.23, 133.76, 151.51 (Ar), 162.4 and 164.3 (C=O); *m/z* (ES+, methanol) 349 and 351 ($[M+H]^+$, 100%); m.p. 106-108 °C.

1,4,7,10-*tetrakis*[(*R*,*S*)-Methoxycarbonyl(4-methoxyphenyl)methyl)-1,4,7,10-tetraazacyclododecane (38)

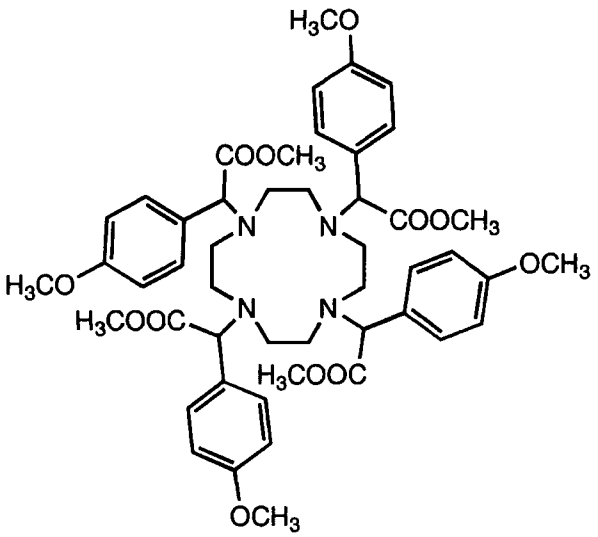

$12N_4$ (0.48 g, 2.8 mmol) was dissolved in dry DMF (10 mL) under Ar and potassium carbonate (3.88 g, 28.1 mmol) was added. Methyl-4-methoxyphenylbromoacetate, **35** (7.29g, 28.1 mmol) was added as a solution in DMF (10 mL) and the reaction stirred for 10 days. After removal of inorganic precipitates by filtration, the DMF was removed *in vacuo* and flash column chromatography (silica, 40% ethyl acetate in hexane) yielded the product as an oil (0.614 g, 25%).

ν_{max} (neat)/cm^{-1}; δ_H (300 MHz, $CDCl_3$) 2.45-2.58 (8H, m, NCH_2), 2.66-2.98 (8H, m, NCH_2), 3.56 (12H, m, $COOCH_3$), 3.72 (12H, m, $ArOCH_3$), 4.47, 4.37, 4.30, 4.28 (4H, m, NCHAr), 6.70-6.78 (8H, m, ArH), 7.60-7.15 (8H, m, ArH); δ_C (50 MHz, $CDCl_3$) 47.48, 47.91, 48.11 (NCH_2), 50.29 ($COOCH_3$), 54.18 ($ArOCH_3$), 66.28 (NCHAr), 112.46, 112.67 (ArH), 127.81, 127.66 (ArH), 129.16 (ArH), 158.08 (ArH), 171.89 (C=O); *m/z* (ES+) $[M+H]^+$, calc. 885.4286, obs. 885.4273.

2-(*S*)-Hydroxy-3-(4-hydroxyphenyl)propanoic acid (40)[203]

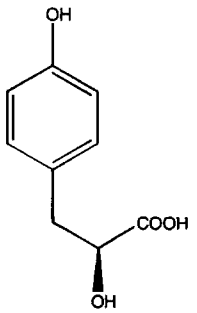

To a solution of (4-hydroxyphenyl)pyruvic acid (2.50 g, 13.8 mmol) in dry THF (30 mL) at 0°C was added dry triethylamine (1.95 mL, 13.8 mmol). After 5 min, (+)-*B*-chlorodiisopinocampheylborane (5.32 g, 16.6. mmol) was added. After 18 h, the reaction was quenched with water (10 mL), then a 6 M aqueous solution of sodium hydroxide (10 mL). After 30 min, the product solution was washed with hexane (5 x 30 mL), acidified to pH=0.5 with $HCl_{(aq)}$, extracted into ethyl acetate (3 x 30 mL), dried over magnesium sulphate and filtered. After solvent removal *in vacuo*, recrystallisation was carried out from diethyl ether and hexane, yielding a white solid (2.43 g, 13.3 mmol, 96.5%).

ν_{max} (KBr)/cm^{-1} 3479 (OH), 3315 (OH), 3026 (ArH), 2750 (COOH), 1722 (C=O); δ_H (300 MHz, CD_3OD) 2.80 (1H, dd, ^2J 14.1, ^3J 7.8, CH_2), 2.98 (1H, dd, ^2J 14.1, ^3J 4.5, CH_2), 4.26 (1H, dd, ^3J 7.8, ^3J 4.5, CH(OH)), 6.69 (2H, d, ^3J 8.4, m-ArH), 7.07 (2H, d, ^3J 8.4, o-ArH); δ_C (63 MHz, CD_3OD) 41.66 (CH_2), 73.89 (CH(OH)), 116.85 (m-Ar), 130.42 (i-Ar), 132.39 (o-Ar), 157.96 (p-Ar), 178.12 (C=O); *m/z* (ES+) 205 ($[M+Na]^+$, 100%); Found: C, 58.80; H, 5.53. $C_9H_{10}O_4$ requires C, 59.34; H, 5.53%); $[\alpha]_D^{22}$ -14°C (*c* = 1, methanol); m.p. 105-107°C (lit. 106-110°C).

Methyl-2-(*S*)-hydroxy-3-(4-hydroxyphenyl)propanoate (41)

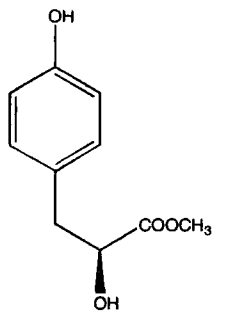

To a solution of (S)-1-Hydroxy-2-(4-hydroxyphenyl)propanoic acid, **40** (2.42 g, 13.4 mmol) in methanol (100 mL) was added one drop of conc. sulphuric acid and the solution heated at reflux with stirring. After 20 h, sodium hydrogencarbonate (5.0 g, 60 mmol) was added and stirred vigorously for 30 min. The mixture was filtered and the solvent removed *in vacuo* to yield a brown oil. Recrystallisation from THF yielded a white solid (2.50 g, 12.7 mmol, 95%).

ν_{max} (KBr)/cm^{-1} 3350 br (OH), 2952, 2926 and 2853 (CH), 1752 (C=O); δ_H (300 MHz, CD_3OD) 2.81 (1H, dd, ^2J 13.8, ^3J 7.5, CH_2), 2.93 (1H, dd, ^2J 13.8, ^3J 5.1, CH_2), 3.67 (3H, s, CH_3), 4.29 (1H, dd, ^3J 7.5, ^3J 5.1, C<u>H</u>(OH)), 6.69 (2H, d, ^3J 8.6, m-ArH), 7.02 (2H, d, ^3J 8.6, o-ArH); δ_C (75 MHz, CD_3OD) 39.69 (CH_2), 51.13 (CH_3), 72.14 (CH(OH)), 114.85 (m-Ar), 127.96 (i-Ar), 130.28 (o-Ar), 155.99 (p-Ar), 174.64 (C=O); *m/z* (ES+) 219 ([M+Na]$^+$, 70%); m.p. 122-124°C; $[\alpha]_D^{22}$ -10° ± 1 (*c* =1, ethanol).

Methyl-(*S*)-1-hydroxy-2-[4-(methoxycarbonylmethoxy)phenyl]propanoate (42)

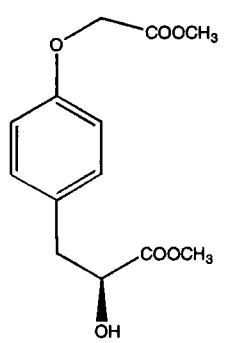

To a stirred solution of methyl-(*S*)-1-hydroxy-2-(4-hydroxyphenyl)propanoate, **41** (0.57 g, 2.92 mmol) in dry acetonitrile (10 mL) was added dry potassium carbonate (0.80 g, 5.84 mmol). After 1 h, methyl bromoacetate (0.32 mL, 3.50 mmol) was added. After 60

h, the mixture was filtered and the acetonitrile removed *in vacuo*. The product was then dissolved in DCM (20 mL) and filtered again. The DCM was then removed *in vacuo* and then the excess methyl bromoacetate was removed in a Kugelrohr (50°C, 0.2 mbar). Any remaining traces were neutralised by treating a vigorously stirred solution of the product in DCM (30 mL) with a 5% w/v aqueous solution of ammonia (10 mL) for 45 min. The organic layer was then isolated and washed with saturated aqueous sodium hydrogencarbonate solution (3 x 10 mL) and water (2 x 10 mL), dried over magnesium sulphate, filtered and the solvent removed in vacuo. Crystallisation from 50% ethyl acetate in hexane yielded plate-like crystals (3.98 g, 14.8 mmol, 74%).

ν_{max} (KBr)/cm^{-1} 3498 (OH), 3049, 3034, 3001 (ArH), 2955, 2930, 2914 (CH), 1750 (C=O); δ_H (300 MHz, CD_3OD) 2.86 (1H, dd, ^2J 13.8, ^3J 7.8, $ArCH_2$), 3.00 (1H, dd, ^2J 13.8, ^3J 4.8, $ArCH_2$), 3.68 (3H, s, $COOCH_3$), 3.76 (3H, s, $COOCH_3$), (1H, dd, ^2J 14.4, ^3J 4.2, $ArCH_2$), 3.78 (3H, s, $COOCH_3$), 3.80 (3H, s, $COOCH_3$), 4.31 (1H, dd, ^3J 7.8, ^3J 4.8, $CH(OH)$), 4.67 (2H, s, OCH_2COOCH_3), 6.83 (2H, d, ^3J 8.7, m-ArH), 7.14 (2H, d, ^3J 8.7, o-ArH); δ_C (63 MHz, $CDCl_3$) 47.85 ($ArCH_2$), 60.49 ($COOCH_3$), 60.65 ($COOCH_3$), 73.58 (OCH_2COOCH_3), 79.61 ($CH(OH)$), 117.11 (m-Ar), 139.93 (ipso-Ar), 138.86 (o-Ar), 165.00 (p-Ar), 176.91 ($CH(OH)COOCH_3$), 177.72 (OCH_2COOCH_3); *m/z* (ES+) $[M+NH_4]^+$, calc. 286.1291, meas. 286.1288; Found: C, 58.07; H, 6.03. $C_{10}H_{12}O_4$ requires C, 58.20; H, 6.01%); m.p. 52-54°C, $[\alpha]_D^{22}$ 5.0 ± 0.5 (*c* = 1, ethanol).

Methyl-(*S*)-1-methanesulphonyloxy-2-[4-(methoxycarbonylmethoxy)phenyl] propanoate (44)

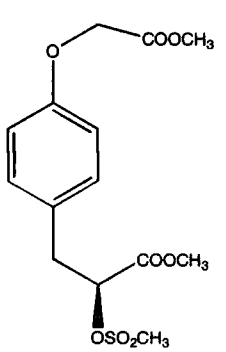

To a solution of methyl-(*S*)-1-hydroxy-2-[4-(methoxycarbonylmethoxy)phenyl] propanoate, **42** (0.20 g, 0.75 mmol) in dry DCM (2 mL) was added dry

diisopropylethylamine (0.20 mL, 1.13 mmol). The solution was cooled to 0°C and methanesulphonyl chloride (0.09 mL, 1.13 mmol) was added. The reaction was allowed to warm to ambient temperature. After 18 h, the solution was purified by gradient flash column chromatography (silica, 100% DCM → 33% ethyl acetate in hexane). The solvent was removed *in vacuo* to yield a clear oil (0.24 g, 0.70 mmol, 93%).

δ_H (300 MHz, $CDCl_3$) 2.82 (3H, s, OSO_2CH_3), 3.08 (1H, dd, ^2J 14.4, ^3J 8.4, $ArC\underline{H}_2$), 3.23 (1H, dd, ^2J 14.4, ^3J 4.2, $ArC\underline{H}_2$), 3.78 (3H, s, $COOCH_3$), 3.80 (3H, s, $COOCH_3$), 4.62 (2H, s, $OC\underline{H}_2COOCH_3$), 5.12 (1H, dd, ^3J 8.4, ^3J 4.2, $C\underline{H}(OSO_2CH_3)$), 6.86 (2H, d, ^3J 8.7, m-ArH), 7.17 (2H, d, ^3J 8.7, o-ArH); δ_C (63 MHz, $CDCl_3$) 37.33 (OSO_2CH_3), 38.57 ($Ar\underline{C}H_2$), 52.22 ($COO\underline{C}H_3$), 52.81 ($COO\underline{C}H_3$), 65.22 ($O\underline{C}H_2COOCH_3$), 78.58 ($\underline{C}H(OSO_2CH_3)$), 114.81 (m-Ar), 127.97(ipso-Ar), 130.66 (o-Ar), 157.15 (p-Ar), 168.81 (C=O), 169.20 ($COOCH_3$); *m/z* (ES+) 368 ($[M+Na]^+$, 85%); 384 ($[M+K]^+$, 100%).

AminoTrinitrile: 1,1,1-*tris*-(Cyanoethoxymethyl)aminomethane (62)

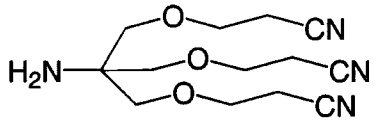

To a mixture of 1,4-dioxane (12.5 mL) and 40% w/v aqueous potassium hydroxide solution (1.5 mL) was added *tris*(hydroxymethyl)aminomethane (12.1 g, 100 mmol), followed by the dropwise addition with vigorous stirring of acrylonitrile (20 mL, 300 mmol). After 20 h, most of the dioxane was removed *in vacuo* and the product was extracted into DCM (3 x 40 mL), dried over potassium carbonate and the solvent removed *in vacuo*. The resultant oil was purified by gradient flash column chromatography (silica, 2% → 5% methanol in DCM) to yield a clear oil (11.04 g, 39 mmol, 39%).

ν_{max} (KBr)/cm^{-1} 3375, 3310 (NH_2), 2914, 2876 (CH), 2250 (CN), 1586 (NH), 1113 (COC); δ_H (300 MHz, $CDCl_3$) 2.34 (2H, s, NH_2), 2.64 (6H, t, ^3J 6.0, CH_2CN), 3.46 (6H, s, $C\underline{H}_2OCH_2CH_2CN$), 3.70 (6H, t, ^3J 6.0, $CH_2OC\underline{H}_2CH_2CN$); δ_C (75 MHz, $CDCl_3$) 19.01 ($\underline{C}H_2CN$), 56.35 ($H_2N\underline{C}$), 65.96 (OCH_2), 72.56 (OCH_2), 118.30 (CN); *m/z* (ES+, methanol) 281 ($[M+H]^+$,40%), 303 ($[M+Na]^+$, 100%), 561 ($[M_2+H]^+$, 10%).

CbzAminoTriester: *N*-Benzyloxycarbonyl-1,1,1-*tris*(methoxycarbonylethoxymethyl) aminomethane (64)

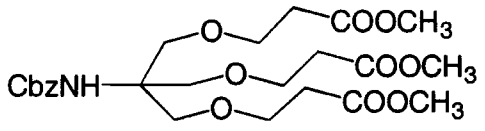

Dry hydrogen chloride gas was generated by dropping concentrated sulphuric acid (200 mL) onto sodium chloride (250 g) and passing through a calcium chloride drying tube. The gas was bubbled under positive pressure of argon into a stirred solution of 1,1,1-*tris*-(cyanoethoxymethyl)aminomethane, **62** (5.21 g, 13.7 mmol) in dry methanol (30 mL). After 20 h, water (50 mL) was added, and after a further hour, sodium hydrogencarbonate was added until pH≈7. The methanol was removed *in vacuo*, and the solution was made up to 30 mL with water. 1,4-Dioxane (10 mL) was added, followed by a 2M aqueous solution of sodium hydrogencarbonate (2.3 mL) with cooling to 0°C. Benzyl chloroformate (2.5 mL, 17.5 mmol) and a 2 M aqueous solution of sodium carbonate (2.5 mL,) were added in ten equal alternating portions over 90 min, maintaining the pH between ca. 8.5 and 9.5. After 20 h at ambient temperature, the product was extracted into DCM, dried over magnesium sulphate, filtered and solvent removed *in vacuo* to yield a crude liquid. The product was purified by removal of volatiles in a Kugelrohr to yield an oil (6.18 g, 11.7 mmol, 85%).

ν_{max} (KBr)/cm^{-1} 3423 (NH), 1741 (C=O), 1111 (COC); δ_H (500 MHz, $CDCl_3$) 2.52 (6H, t, ^3J 3.9, $C\underline{H}_2COOCH_3$), 3.63 (6H, s, $C\underline{H}_2OCH_2CH_2COOCH_3$), 3.65 (9H, s, $COOC\underline{H}_3$), 3.67 (6H, t, ^3J 3.9, $OC\underline{H}_2CH_2COOCH_3$), 4.90 (1H, s, NH), 5.03 (2H, s, $PhC\underline{H}_2$), 7.26-7.34 (5H, m, Ph); δ_C (126 MHz, $CDCl_3$) 34.66 ($\underline{C}H_2COOCH_3$), 51.57 ($COO\underline{C}H_3$), 58.60 (N-$\underline{C}(CH_2O)_3$), 66.07 ($Ph\underline{C}H_2$), 66.66 ($O\underline{C}H_2CH_2$), 69.23 ($C(\underline{C}H_2O)_3$), 127.88 (Ar), 128.35 (Ar), 136.60 (*ipso*-Ar); 154.96 (COONH), 171.89 ($\underline{C}OOCH_3$); *m/z* (ES+) $[M+NH_4]^+$, calc. 531.2554, meas. 531.2547.

CbzAminoTriacid: *N*-Benzyloxycarbonyl-1,1,1-*tris*(carboxyethoxymethyl) aminomethane (65)

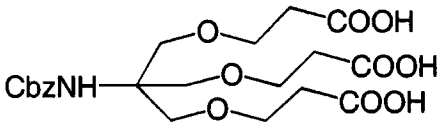

To a stirred saturated aqueous solution of lithium hydroxide (10 mL) and methanol (30 mL) was added *N*-benzyloxycarbonyl-1,1,1-*tris*(methoxycarbonylethoxymethyl) aminomethane, **64** (1.23 g, 2.4 mmol). After 20 h, the pH was carefully brought to 1.0 with hydrochloric acid and the product extracted into ethyl acetate (4 x 30 mL), dried over magnesium sulphate, filtered and the solvent removed in vacuo to yield a clear oil (1.15 g, 2.4 mmol, 99%).

ν_{max} (KBr)/cm^{-1} 3423 (NH), 3000 v br (CO<u>O</u>H), 1741 (C=O), 1111 (COC); δ_H (300 MHz, CD_3OD) 2.50 (6H, t, ^3J 6.3, C<u>H</u>$_2$COOH), 3.64 (6H, s, C<u>H</u>$_2$OCH$_2$CH$_2$COOH), 3.66 (6H, t, ^3J 6.3, OC<u>H</u>$_2$CH$_2$COCH), 4.93 (1H, br s, NH), 5.02 (2H, s, PhC<u>H</u>$_2$), 7.20-7.40 (5H, m, Ph); δ_C (75 MHz, CD_3OD) 34.56 (<u>C</u>H$_2$COOH), 59.12 (N-<u>C</u>(CH$_2$O)$_3$), 66.93 (Ph<u>C</u>H$_2$), 69.08 (C(<u>C</u>H$_2$O)$_3$),127.61 (Ar), 127.72 (Ar), 128.27 (*ipso*-Ar), 152.0 (COONH), 174.29 (<u>C</u>OOH); *m/z* (ES-, methanol) 470 ([M-H]$^-$, 65%).

CbzAminoTridendramide-2: *tris*-[2,2-*bis*-(2,2-Dibutyl-5-methyl-1,3-dioxan-5-ylmethoxymethyl)ethanamidoethoxymethyl] methanaminocarboxymethylbenzene (66)

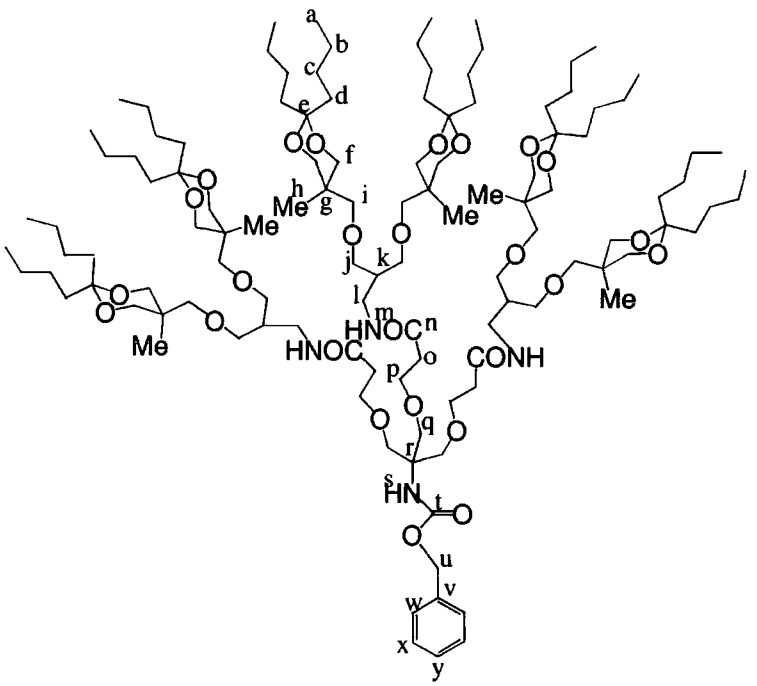

To a solution of *N*-benzyloxycarbonyl-1,1,1-*tris*(carboxyethoxymethyl)aminomethane, **65** (0.128 g, 0.27 mmol) in dry DMF (2.5 mL) at 0°C under argon was added 1-[3-(dimethylamino)propyl]-3-ethylcarbodiimide hydrochloride (0.19 g, 1.0 mmol) and 1-hydroxybenzotriazole monohydrate (0.135 g, 1.0 mmol). After 5 min, dendramine-2 (0.6 g, 1.0 mmol) was added as a solution in dry DMF (5.0 mL) and the reaction was stirred at ambient temperature. After 2 days, ESMS+ showed trisubstitution only. DMF was removed *in vacuo* and the dried product was extracted with diethyl ether. The ether was removed ether *in vacuo* and gradient flash column chromatography (silica, 50 → 75% ethyl acetate in hexane) yielded a clear, viscous oil (0.20 g, 96 μmol, 35%).

ν_{max} (KBr)/cm^{-1} 3300 (NH), 1651 (C=O), 1093 (COC); δ_H (400 MHz, CD_3OD); 0.87 (18H, s, C_aH_3), 0.90-0.96 (36H, m, C_hH_3), 1.25-1.40 (48H, m, $C_bH_2C_cH_2$), 1.58-1.65 (12H, m, $C_dH_{2(eq)}$), 1.70-1.78 (12H, m, $C_dH_{2(ax)}$), 2.10 (3H, septet, ^3J 5.6, C_kH), 2.41 (6H, t, ^3J 6.0, C_oH_2), 3.27 (6H, d, ^3J 6.8, C_lH_2), 3.39 (6H, s, C_qH_2), 3.46 (12H, d, ^3J 5.2, C_iH_2), 3.53 (12H, d , ^2J 11.6, $C_fH_{(ax)}$), 3.54-3.58 (12H, m, C_jH_2), 3.67 (12H, d, ^2J 11.6, $C_fH_{(eq)}$), 3.67 (6H, t, ^3J 6.0, C_pH_2), 5.03 (2H, s, C_uH_2), 7.27-7.37 (5H, m, ArH); δ_C (100 MHz,

$CDCl_3$) 14.57 ($C_{a(ax)}$), 14.66 ($C_{a(eq)}$), 18.89 (C_h), 24.07 ($C_{b(ax)}$), 24.13 ($C_{b(eq)}$), 26.38 ($C_{c(ax)}$), 26.84 ($C_{c(eq)}$), 32.19 ($C_{d(ax)}$), 34.12 (C_g), 36.63 ($C_{d(eq)}$), 37.68 (C_o), 39.94 (C_l), 41.26 (C_k), 66.84 (C_f), 67.64 (C_u), 68.72 (C_p), 70.46 (C_q), 71.27 (C_j), 75.26 (C_i), 100.68 (C_e), 128.89, 129.00, 129.53 (*tert*-Ar), 138.37 (*quat*-Ar), 173.82 (amide C=O), 174.31 (carbamate C=O); *m/z* (ES+, methanol) 2113 ($[M+Na]^+$, 100%).

AminoTridendramide-2: *tris*-[2,2-*bis*-(2,2-Dibutyl-5-methyl-1,3-dioxan-5-ylmethoxy methyl) ethanamidoethoxymethyl]methanamine (67)

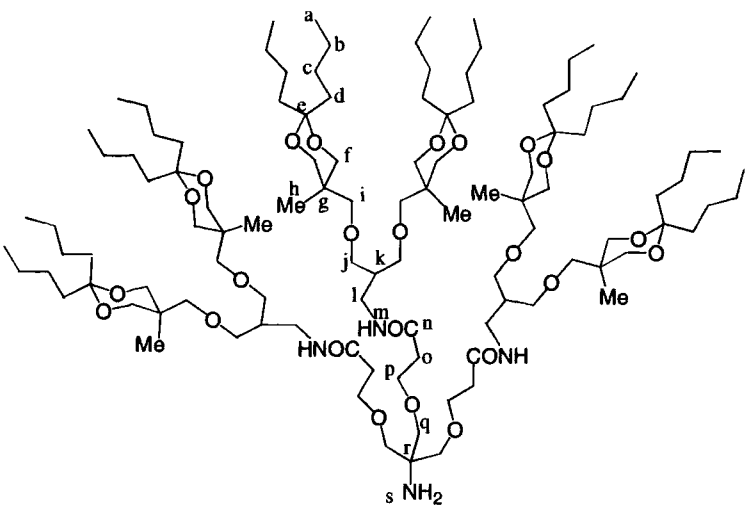

To a solution of *tris*-[2,2-*bis*-(2,2-dibutyl-5-methyl-1,3-dioxan-5-ylmethoxymethyl) ethanamidoethoxymethyl]methanaminocarboxymethylbenzene, **66** (0.20 g, 96 μmol) in methanol (1 mL) was added hydrazine hydrate (4 drops) and a catalytic amount of palladium hydroxide. The suspension was heated at reflux for 2 h, and at 60°C for a further 16 h. After cooling and filtration through Celite, the methanol was removed in vacuo and the product extracted into ethyl acetate from water (0.181 g, 92.5 μmol, 96%). ν_{max} (KBr)/cm^{-1} 3300 (NH), 1651 (C=O), 1093 (COC); δ_H (300 MHz, $CDCl_3$) 0.76-0.78 (18H, d, C_aH_3), 0.81-0.88 (36H, m, C_hH_3), 1.16-1.32 (48H, m, $C_bH_2C_cH_2$), 1.51-1.57 (12H, m, $C_dH_{2(eq)}$), 1.64-1.70 (12H, m, $C_dH_{2(ax)}$), 2.05 (3H, septet, ^3J 5.7, C_kH), 2.32 (6H, t, ^3J 5.7, C_oH_2), 3.25-3.28 (6H, m, C_lH_2), 3.30 (6H, s, C_qH_2), 3.34 (12H, m, C_iH_2), 3.39-3.42 (12H, m, C_jH_2), 3.46 (12H, d , ^2J 11.7, $C_fH_{(ax)}$), 3.59 (12H, d, ^2J 11.7, $C_fH_{(eq)}$), 3.63 (6H, t, ^3J 5.7, C_pH_2), 6.71 (3H, t, ^3J 5.3, CONH); δ_C (75 MHz, $CDCl_3$) 13.10 ($C_{a(ax)}$),

13.13 ($C_{a(eq)}$), 17.40 (C_h), 22.00 ($C_{b(ax)}$), 22.03 ($C_{b(eq)}$), 24.10 ($C_{c(ax)}$), 24.64 ($C_{c(eq)}$), 29.48 ($C_{d(ax)}$), 33.22 (C_g), 35.06 ($C_{d(eq)}$), 35.66 (C_o), 38.44 (C_k), 39.21 (C_l), 64.83 (C_f), 66.52 (C_p), 70.29 (C_j), 70.50 (C_q), 73.24 (C_i), 99.65 (C_e), 170.05 (C=O); *m/z* (ES+) 1642 (5%), 1957 (100%, $[M+H]^+$), 1980 (10%, $[M+Na]^+$), $[M+Na]^+$, calc. 1978.4917, meas. 1978.4919.

Dendrol-1: 2,2-Dibut-1-yl-5-hydroxymethyl-5-methyl-1,3-dioxane (72)

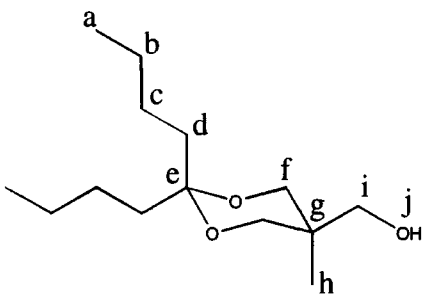

To a solution of 5-nonanone (51.6 mL, 300 mmol) in benzene (250 mL) was added 1,1,1-*tris*(hydroxymethyl)ethane (30.0 g, 250 mmol) and *p*-toluenesulphonic acid (0.30 g, 1.57 mmol). The mixture was heated under reflux with stirring in a Dean and Stark apparatus for 48 h. After cooling to ambient temperature, potassium carbonate (1.10 g, 8.0 mmol) was added with stirring for 1 h. The mixture was then filtered and the benzene removed *in vacuo*. The product was then dissolved in hexane (100 mL) and washed with aqueous potassium carbonate (2 x 50 mL) and water (1 x 50 mL). The hexane solution was then dried over potassium carbonate, filtered and the solvent removed *in vacuo*. The excess 5-nonanone was removed by vacuum distillation (70°C, 0.2 mbar) to yield a brown oil (47.0 g, 192 mmol, 77%). Gradient flash column chromatography (silica, 2.5% → 10% ethyl acetate in hexane) yielded a clear oil (43.2g, 176 mmol, 71%).

ν_{max} (KBr)/cm^{-1} 3421 s (OH), 2955 and 2870 vs (CH), 1093 and 1050 s (C-O-C); δ_H (300 MHz, $CDCl_3$) 0.81 (3H, s, C_hH_3), 0.90 (6H, m, C_aH_3), 1.20-1.40 (8H, m, $C_bH_2C_cH_2$), 1.56-1.64 (2H, m, $C_{d(eq)}H_2$), 1.72-1.80 (2H, m, $C_{d(ax)}H_2$), 1.86 (1H, t, ^3J 5.4, OH), 3.58 (2H, d, ^2J 11.7, C_fH_{ax}), 3.64 (2H, d, ^2J 11.7, C_fH_{eq}), 3.69 (2H, d, ^3J 5.4, C_iH_2); δ_C (75 MHz, $CDCl_3$) 14.28 (C_a), 17.85 (C_h), 23.22 (C_b), 25.86 (C_c), 30.10 ($C_{d(ax)}$), 34.75 (C_g), 36.78 ($C_{d(eq)}$), 65.80 (C_f), 65.84 (C_i), 100.92 (C_e); *m/z* (ES+, methanol) 245 ($[M+H]^+$, 40%), 267 ($[M+Na]^+$, 100%).

Dendrene-2: 2,2-*bis*(2,2-Dibut-1-yl-5-methyl-1,3-dioxan-5-ylmethoxymethyl)ethene (73)

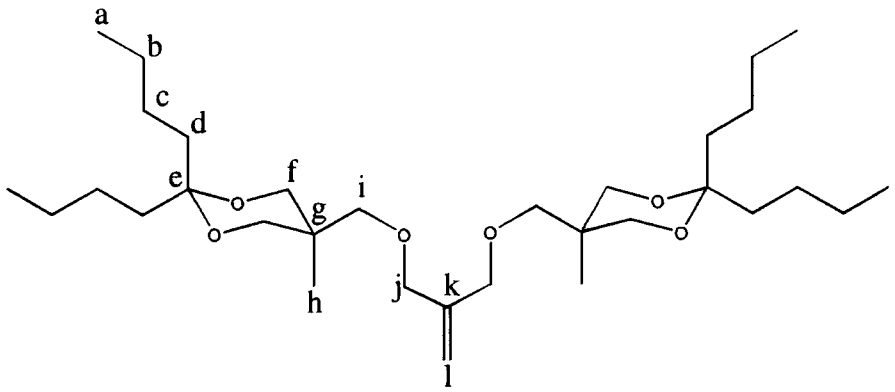

To a suspension of sodium hydride (2.73 g, 114 mmol) in dry THF (30 mL) was gradually added with stirring under argon a solution of 2,2-dibutyl-5-hydroxymethyl-5-methyl-1,3-dioxane, dendrol-1 **72** (13.9 g, 56.9 mmol) in dry THF (30 mL). After 1 h, potassium iodide (0.07 g, 0.40 mmol), 18-crown-6 (0.105 g, 0.40 mmol) and 3-chloro-2-chloromethyl-prop-1-ene (2.08 mL, 18.0 mmol) were added. The reaction was monitored by ^{1}H NMR and after 120 h, the reaction was quenched by slowly pouring into methanol (100 mL) and then adding water (50 mL). The methanol was removed *in vacuo* and the product was extracted into hexane (3 x 50 mL) from the aqueous solution. Removal of hexane *in vacuo* yielded a clear oil. Flash column chromatography (silica, 2% ethyl acetate in hexane) yielded a clear oil (8.86 g, 16.4 mmol, 91%).

ν_{max} (KBr)/cm^{-1} 2955 and 2863 vs (CH), 1094 vs (C-O-C); δ_H (300 MHz, $CDCl_3$) 0.87 (6H, s, C_hH_3), 0.89 (12H, m, C_aH_3), 1.20-1.40 (16H, m, $C_bH_2C_cH_2$), 1.58-1.64 (4H, m, $C_{d(eq)}H_2$), 1.66-1.70 (4H, m, $C_{d(ax)}H_2$), 3.41 (4H, s, C_iH_2), 3.52 (4H, d, ^2J 11.7, C_fH_{ax}), 3.68 (4H, d, ^2J 11.7, C_fH_{eq}), 3.99 (4H, s, C_jH_2), 5.15 (2H, s, C_lH_2); δ_C (75 MHz, $CDCl_3$) 14.33 (C_a), 18.03 (C_h), 23.26 (C_b), 25.32 ($C_{c(ax)}$) and 25.87 ($C_{c(eq)}$), 31.14 ($C_{d(ax)}$), 34.34 (C_g), 36.09 ($C_{d(eq)}$), 66.12 (C_f), 72.31 (C_j), 73.42 (C_i), 100.71 (C_e), 113.36 (C_l), 143.26 (C_k) ; *m/z* (ES+, TOF, methanol) 356 (5%), 563 ([M+Na]$^+$, 100%).

Dendrol-2: 2,2-*bis*(2,2-Dibut-1-yl-5-methyl-1,3-dioxan-5-ylmethoxymethyl)ethanol (74)

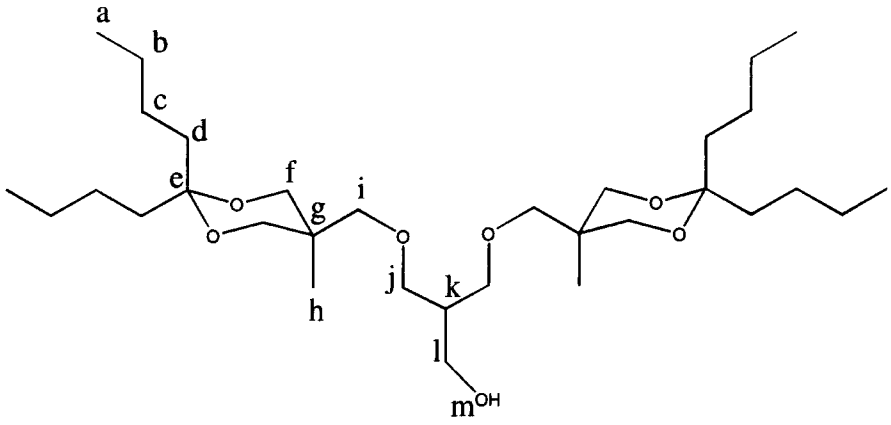

To a solution of dendrene-2, **73** (7.63 g, 14.1. mmol) in dry THF (50 mL) was added with stirring under argon 9-BBN (2.07 g, 17.0 mmol). After 20 h, a 30% w/v aqueous solution of hydrogen peroxide (7.5 mL) and a 6.0 M aqueous solution of sodium hydroxide (7.5 mL) were cautiously added, and the biphasic mixture stirred for 15 min. The THF was removed *in vacuo* and the product extracted into hexane (4 x 30 mL), then washed with water (1 x 30 mL), and then washed with a 2.5% v/v solution of water in methanol (3 x 30 mL). Gradient flash column chromatography (silica, 2.5% → 5.0% ethyl acetate in hexane) yielded a clear oil (5.42 g, 9.70 mmol, 69%).

δ_H (500 MHz, $CDCl_3$) 0.82 (6H, s, C_hH_3), 0.89 (12H, m, C_aH_3), 1.20-1.40 (16H, m, $C_bH_2C_cH_2$), 1.58-1.62 (4H, m, $C_{d(eq)}H_2$), 1.64-1.68 (4H, m, $C_{d(ax)}H_2$) 2.14 (1H, septet, ^3J 5.6, C_kH_2), 3.39 (2H, d, ^2J 9.0, C_iH_2), 3.43 (2H, d, ^2J 9.0, C_iH_2), 3.52 (4H, d, ^2J 12.0, C_fH_{ax}), 3.53 (4H, m, C_jH_2), 3.63 (4H, d, ^2J 12.0, C_fH_{eq}), 3.74 (2H, d, C_lH_2); δ_C (100 MHz, $CDCl_3$) 14.33 (C_a), 18.53 (C_h), 23.24 ($C_{b(ax)}$) and 23.27 ($C_{b(eq)}$), 25.30 ($C_{c(ax)}$), 25.87 ($C_{c(eq)}$), 31.74 ($C_{d(ax)}$), 34.43 (C_g), 36.27 ($C_{d(eq)}$), 41.59 (C_k), 64.43 (C_l), 66.07 (C_f), 71.70 (C_j), 74.62 (C_i), 100.88 (C_e); *m/z* (ES+) 101 (30%), 117 (20%), 581 ($[M+Na]^+$, 100%), $[M+NH_4]^+$, calc. 576.4839, meas. 576.4847.

Dendramine-2: 2,2-*bis*(2,2-Dibut-1-yl-5-methyl-1,3-dioxan-5-ylmethoxymethyl) ethanamine (75)

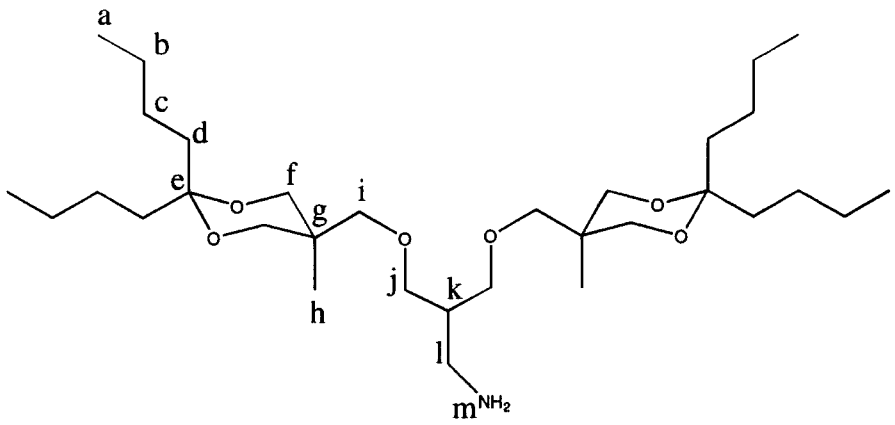

To a paste of sodium azide (6.0 g, 9.0 mmol) and water (6.0 mL) was added with vigorous stirring benzene (45 mL), followed by cooling to -10°C. Concentrated sulphuric acid (2.4 mL, 45 mmol) was gradually added, and the organic layer decanted, dried over sodium sulphate and filtered. This solution was then added to a solution of dendrol-2, **74** (3.33 g, 6.0 mmol) in dry THF (15 mL) with stirring, followed by a solution of diisopropyl azodicarboxylate (1.30 mL, 6.6 mmol) in dry THF (10 mL), and finally a solution of triphenylphosphine (3.46 g, 13.2 mmol) in dry THF (10 mL). After 1 h at ambient temperature, the reaction was heated at 60°C for 12 h. Water (50 mL) was then added and the temperature maintained at 60°C for 3 h. The volume was then reduced *in vacuo* and a saturated aqueous solution of sodium hydrogen carbonate (50 mL) was added and the products extracted into DCM and dried over potassium carbonate, filtered and the solvent removed *in vacuo*. The resultant solid was pulverised and extracted with warm hexane (5 x 50 mL), cooled to 0°C for 2 h and filtered. The hexane was removed to yield a yellow oil. Gradient flash column chromatography was carried out; 5% ethyl acetate in hexane to elute dendrazide-2, **79** (1.56 g, 2.67 mmol, 47%), 50% ethyl acetate in hexane to elute the dicarbamate by-product and unreacted dendrol-2, **74**, 10 % hexane in ethyl acetate to elute triphenylphosphine oxide by-product, and 100% ethyl acetate → 10% methanol in ethyl acetate to elute dendramine-2, **75** (0.40 g, 0.72 mmol, 12%).

Dendramine-2; ν_{max} (KBr)/cm^{-1} 3373 (NH), 2955 and 2865 (CH), 1094 (C-O-C); δ_H (500 MHz, $CDCl_3$) 0.78 (6H, s, C_hH_3), 0.85 (12H, m, C_aH_3), 1.18-1.31 (16H, m, $C_bH_2C_cH_2$), 1.52-1.58 (4H, m, $C_{d(eq)}H_2$), 1.62-1.68 (4H, m, $C_{d(ax)}H_2$), 1.91 (1H, septet, ^3J 6.0, C_kH_2), 2.73 (2H, d, ^3J 6.0 C_lH_2), 3.31 (2H, d, ^2J 9.0, C_iH_2), 3.34 (2H, d, ^2J 9.0, C_iH_2), 3.36-3.43

(4H, m, C_jH_2), 3.52 (4H, d, ^2J 11.5, C_fH_{ax}), 3.58 (4H, d, ^2J 11.5, C_fH_{eq}); δ_C (126 MHz, $CDCl_3$) 14.33 (C_a), 18.64 (C_h), 23.25 ($C_{b(ax)}$), 23.28 ($C_{b(eq)}$), 25.33 ($C_{c(ax)}$) and 25.90 ($C_{c(eq)}$), 31.11 ($C_{d(ax)}$), 34.45 (C_g), 35.99 ($C_{d(eq)}$), 42.28 (C_l), 42.48 (C_k), 66.13 (C_f), 71.37 (C_j), 74.43 (C_i), 100.80 (C_e); *m/z* (ES+) $[M+H]^+$, calc. 558.4734, meas. 558.4746.

Dendrene-3: 1,1-*bis*[2,2-*bis*(2,2-Dibut-1-yl-5-methyl-1,3-dioxan-5-ylmethoxymethyl) ethoxymethyl]ethene (76)

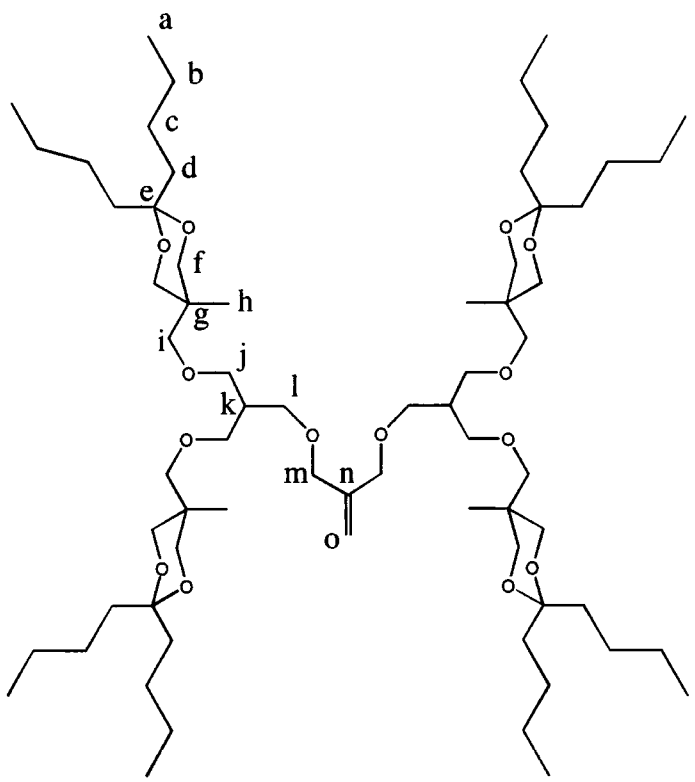

To a suspension of sodium hydride (0.24 g, 10.0 mmol) in dry THF (50 mL) was gradually added with stirring under argon a solution of 2,2-*bis*-(2,2-dibut-1-yl-5-methyl-1,3-dioxan-5-ylmethoxymethyl)ethanol, dendrol-2, **75** (3.66 g, 6.55 mmol) in dry THF (30 mL). After 30 min, potassium iodide (catalytic amount), 18-crown-6 (catalytic amount) and 3-chloro-2-chloromethyl-prop-1-ene (0.35 mL, 3.0 mmol) were added. The reaction was heated at 60°C and monitored by ^1H NMR. After 100 h, the reaction was quenched by slowly adding methanol (10 mL). The methanol was removed *in vacuo* and the product was extracted into hexane (3 x 50 mL) from an aqueous solution. Removal of hexane *in vacuo* following drying with potassium carbonate yielded a clear oil (3.70g).

Gradient flash column chromatography (silica, 5→10% ethyl acetate in hexane) eventually yielded the product, as a clear oil (1.38 g, 1.18 mmol, 39%).

ν_{max} (KBr)/cm^{-1} 2955, 2863 s (CH), 1654 vw (C=C), 1094 s (COC); δ_H (300 MHz, $CDCl_3$) 0.83 (12H, s, C_hH_3), 0.85-0.91 (24H, m, C_aH_3), 1.20-1.36 (32H, m, $C_bH_2C_cH_2$), 1.54-1.63 (8H, m, $C_dH_{2(eq)}$), 1.64-1.73 (8H, m, $C_dH_{2(ax)}$), 2.16 (2H, septet, ^3J 5.7, C_kH), 3.33 (8H, s, C_iH_2), 3.40 (4H, m, C_lH_2), 3.48 (8H, d , ^2J 11.7, $C_fH_{(ax)}$), 3.63 (8H, d, ^2J 11.7, $C_fH_{(eq)}$), 3.89 (4H, s, C_mH_2), 5.10 (2H, s, C_oH_2); δ_C (75 MHz, $CDCl_3$) 14.33 (C_a), 18.72 (C_h), 23.25 ($C_{b(ax)}$), 23.28 ($C_{b(eq)}$), 25.36 ($C_{c(ax)}$), 25.81 ($C_{c(eq)}$), 31.50 ($C_{d(ax)}$), 34.45 (C_g), 35.61 ($C_{d(eq)}$), 40.56 (C_k), 66.14 (C_f), 68.96 (C_l), 69.99 (C_j), 71.96 (C_m), 74.31 (C_i), 100.70 (C_e), 113.44 (C_o), 143.17 (C_n); *m/z* (ES+) 1170 ([M+H$^+$], [M+H]$^+$, calc. 1169.9381, meas. 1169.9379.

Dendrol-3: 2,2-*bis*[2,2-*bis*(2,2-Dibut-1-yl-5-methyl-1,3-dioxan-5-ylmethoxymethyl) ethoxymethyl]ethanol (77)

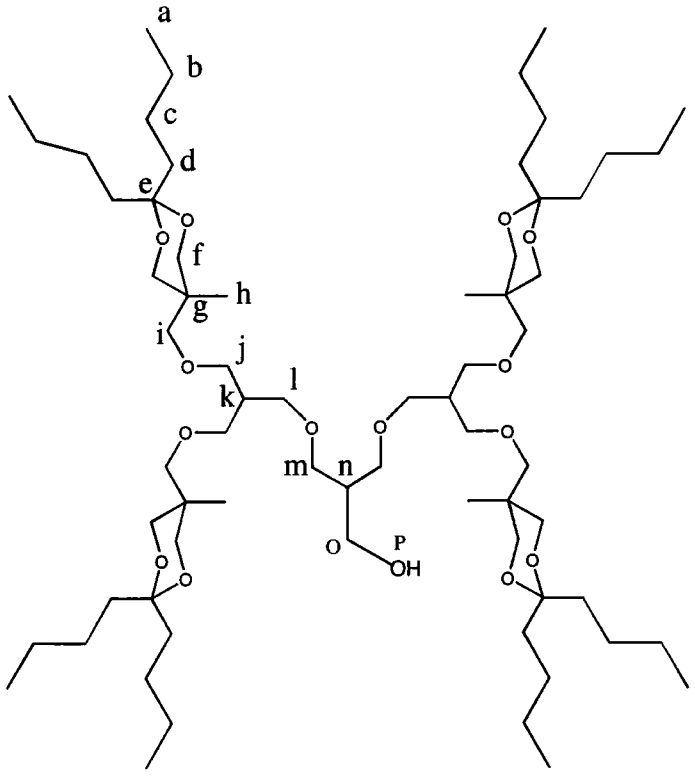

To a solution of dendrene-3, **76** (1.38 g, 1.18 mmol) in dry THF (20 mL) was added with stirring under argon 9-BBN (0.26 g, 2.15 mmol). After 20 h, a 30% w/v aqueous solution of hydrogen peroxide (1.0 mL) and a 6.0 M aqueous solution of sodium hydroxide (1.0

mL) were cautiously added, and the biphasic mixture stirred for 15 min. The THF was removed *in vacuo* and the product extracted into hexane (4 x 30 mL), then washed with water (1 x 30 mL), and then washed with a 2.5% v/v solution of water in methanol (3 x 30 mL). The product was extracted into diethyl ether (3 x 30 mL), dried over potassium carbonate, filtered and the solvent removed *in vacuo*. The octan-1,5-diol by-product was removed by vacuum distillation (100°C, 0.1 mbar) to yield a clear oil (1.121g, 80%).

ν_{max} (KBr)/cm^{-1} 3400 (OH), 2950 and 2863 (CH), 1093 (COC); δ_H (300 MHz, $CDCl_3$) 0.85 (12H, s, C_hH_3), 0.87-0.94 (24H, m, C_aH_3), 1.23-1.37 (32H, m, $C_bH_2C_cH_2$), 1.59-1.65 (8H, m, $C_dH_{2(eq)}$), 1.69-1.74 (8H, m, $C_dH_{2(ax)}$), 2.10 (1H, m, C_nH) 2.15 (2H, septet, ^3J 5.7, C_kH), 3.33 (8H, s, C_iH_2), 3.70 (2H, d, C_oH_2), 3.50 (4H, s, C_mH_2), 3.45 (4H, m, C_lH_2), 3.50 (8H, d , ^2J 11.7, $C_fH_{(ax)}$), 3.65 (8H, d, ^2J 11.7, $C_fH_{(eq)}$); δ_C (75 MHz, $CDCl_3$) 14.30 (C_a), 18.70 (C_h), 23.25 ($C_{b(ax)}$), 23.30 ($C_{b(eq)}$), 25.37 ($C_{c(ax)}$), 25.78 ($C_{c(eq)}$), 31.55 ($C_{d(ax)}$), 34.50 (C_g), 35.67 ($C_{d(eq)}$), 40.50 (C_k), 41.60 (C_n), 66.14 (C_f), 64.90 (C_l), 70.01 (C_j), 71.71 (C_m), 74.36 (C_i), 100.72 (C_e), 64.44 (C_o); *m/z* (ES+) 1188 ([M+H^+], 100%, $[M+H]^+$, calc. 1187.9487, meas. 1187.9482.

Dendramine-3: 2,2[2,2-*bis*-(2,2-Dibut-1-yl-5-methyl-1,3-dioxan-5-ylmethoxymethyl) ethoxymethyl]ethanamine (78)

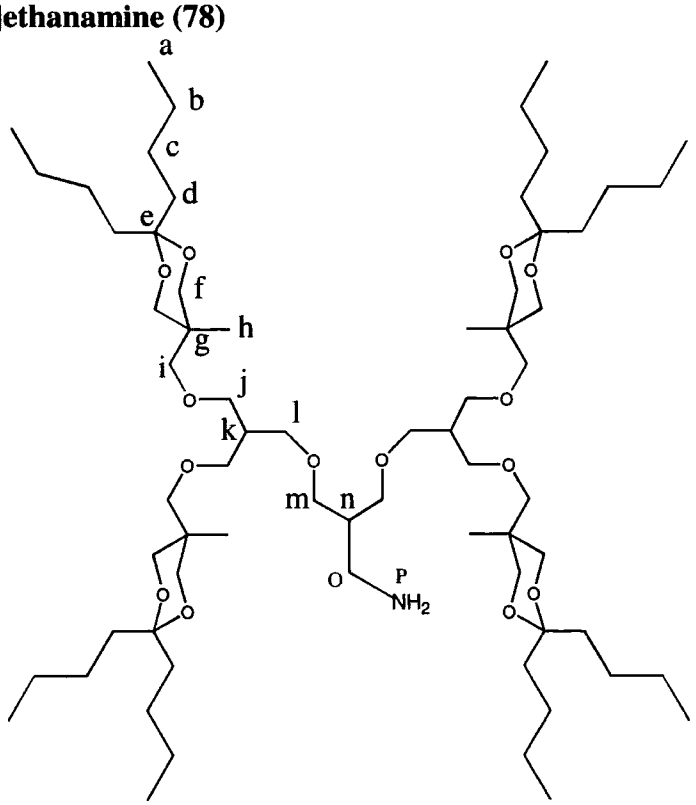

To a solution of dendrol-3, **77** (1.121 g, 0.94 mmol) in THF (10 mL) was added an approximately 1 M solution of hydrazoic acid in benzene (7.5 mL), followed by a solution of diisopropyl azodicarboxylate (0.22 mL, 1.11 mmol) in THF (5 mL). To the reaulting mixture was added a solution of triphenylphosphine (0.57 g, 2.2 mmol) in THF (5 mL) with stirring. After 1 h at ambient temperature, the reaction mixture was heated at 60°C for 16 h. Water (50 mL) was added and the temperature maintained at 50°C for 3 h. After removal of most of the THF *in vacuo* the product was extracted into DCM from a potassium carbonate saturated aqueous solution. The organic layer was dried over potassium carbonate, filtered and the solvent removed *in vacuo*. Warm hexane (3 x 50 mL) was added to the product mixture and after vigorous agitation, the supernatant was decanted, filtered, combined and reduced to *ca.* 25 mL. The solution was allowed to stand for 12 h at 4-5°C, whereupon more triphenylphosphine oxide and diisopropyl dicarbamate precipitated out. The supernatant was filtered off and the solvent removed *in vacuo* to yield the impure amine and azide, which were then treated directly with hydrazine hydrate (0.073 mL, 1.5 mmol) and palladium (II) hydroxide in methanol (20 mL) at reflux for 15 h. After cooling, filtration, extraction into DCM and solvent removal a yellow oil (0.72 g, 64%) was isolated in reasonably pure form by gradient flash column chromatography (100% ethyl acetate → 10% methanol in ethyl acetate).

ν_{max} (KBr)/cm^{-1} 3381 (NH), 2954 and 2864 (CH), 1094 s (COC); δ_H (300 MHz, $CDCl_3$) 0.85 (12H, s, C_hH_3), 0.87-0.93 (24H, m, C_aH_3), 1.24-1.36 (32H, m, $C_bH_2C_cH_2$), 1.59-1.64 (8H, m, $C_dH_{2(eq)}$), 1.69-1.74 (8H, m, $C_dH_{2(ax)}$), 1.90 (1H, m, C_nH) 2.16 (2H, septet, ^3J 5.7, C_kH), 2.76 (2H, d , NH_2) 3.35 (8H, s, C_iH_2), 3.38 (2H, d, C_oH_2), 3.43 (4H, s, C_mH_2), 3.45 (4H, m, C_lH_2), 3.49 (8H, d , ^2J 11.7, $C_fH_{(ax)}$), 3.66 (8H, d, ^2J 11.7, $C_fH_{(eq)}$); δ_C (75 MHz, $CDCl_3$) 14.33 (C_a), 18.72 (C_h), 23.25 ($C_{b(ax)}$), 23.28 ($C_{b(eq)}$), 25.36 ($C_{c(ax)}$), 25.81 ($C_{c(eq)}$), 31.50 ($C_{d(ax)}$), 34.45 (C_g), 35.61 ($C_{d(eq)}$), 40.56 (C_k), 66.14 (C_f), 68.96 (C_l), 69.99 (C_j), 71.96 (C_m), 74.31 (C_i), 100.70 (C_e), 113.44 (C_o), 143.17 (C_n); *m/z* (ES+) 1186 (100%, $[M+H]^+$), 1208 (20%, $[M+Na]^+$, $[M+H]^+$, calc. 1186.9648, meas. 1186.9634.

Dendrazide-2: 2,2-*bis*(2,2-Dibut-1-yl-5-methyl-1,3-dioxan-5-ylmethoxymethyl)ethyl azide (79)

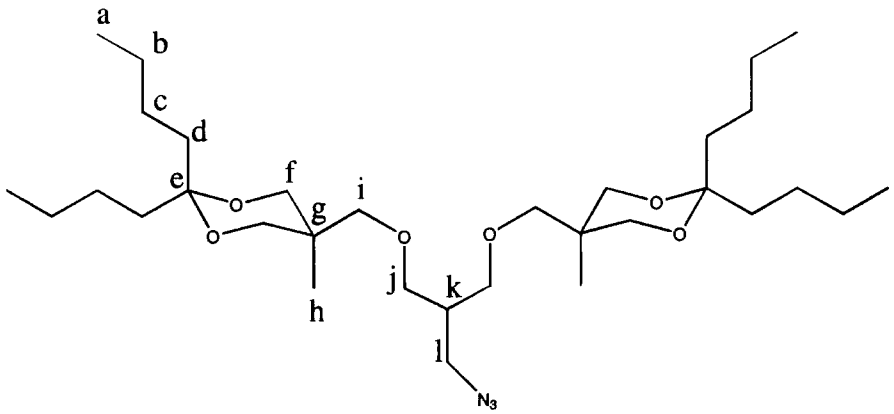

Dendrazide-1; ν_{max} (KBr)/cm^{-1} 2955 and 2863 (CH), 2098 (N_3), 1094 (C-O-C); δ_H (300 MHz, $CDCl_3$) 0.86 (6H, s, C_hH_3), 0.91 (12H, m, C_a), 1.25-1.41 (16H, m, $C_bH_2C_cH_2$), 1.59-1.65 (4H, m, $C_{d(eq)}H_2$), 1.70-1.77 (4H, m, $C_{d(ax)}H_2$) 1.98 (1H, septet, ^3J 6.0, C_kH), 3.40-3.43 (2H, m, C_lH_2), 3.37-3.42 (4H, m, C_iH_2), 3.41-3.51 (4H, m, C_jH_2), 3.59 (4H, d, ^2J 11.5, C_fH_{ax}), 3.58 (4H, d, ^2J 11.5, C_fH_{eq}); δ_C (75 MHz, $CDCl_3$) 14.36 (C_a), 18.62 (C_h), 23.27 ($C_{b(ax)}$), 23.31 ($C_{b(eq)}$), 25.34 ($C_{c(ax)}$), 25.88 ($C_{c(eq)}$), 31.06 ($C_{d(ax)}$), 34.48 (C_g), 36.09 ($C_{d(eq)}$), 40.26 (C_k), 50.68 (C_l), 66.10 (C_f), 69.91 (C_j), 74.34 (C_i), 100.82 (C_e); *m/z* (ES+) 281 (5%), 303 (5%), 606 ([M+Na]$^+$, 100%).

***N*-(*tert*-Butyloxycarbonyl)-*tris*-(hydroxymethyl)aminomethane (81)**[184]

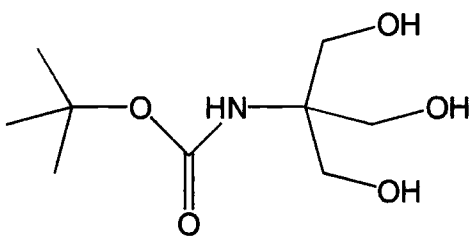

A solution of *tris*-(hydroxymethyl)aminomethane (3.75 g, 30 mmol), 2-[(*tert*-butyloxycarbonyloxy)imino]-2-phenylacetonitrile (Boc-ON), (7.5 g, 30 mmol) and triethylamine (4.12 mL, 30 mmol) in dry DMF (100 mL) was heated at 50°C under argon for 3 h. After cooling, the majority of the solvent was removed *in vacuo* and the oil was crystallised from ethyl acetate to yield a white solid (5.11 g, 77%).

δ_H (300 MHz, $CDCl_3$) 1.38 (9H, s, CH_3), 3.52 (6H, d, ^3J 7.5, CH_2), 4.46 (3H, t, ^3J 7.5, OH), 5.69 (1H, s, NH); δ_C (75 MHz, $CDCl_3$) 32.00, 64.15, 67.10, 81.60, 158.81; *m/z* (ES+, methanol) 222 ($[M+H]^+$, 100%) m.p. 148-152°C.

_N_-(*tert*-Butyloxycarbonyl)-*tris*-(hydroxymethyl)aminomethane (82)

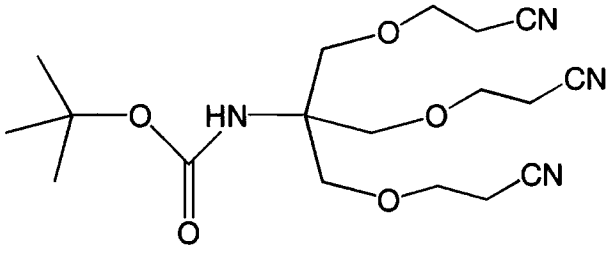

To a stirred suspension of Boc-TRIS, **81** (3.40 g, 15.4 mmol) in dioxane (5 mL) and water (1 mL) containing sodium hydroxide (0.11 g, 2.8 mmol) was added acrylonitrile (3.29 mL, 50 mmol). After stirring for 18 h, at ambient temperature, the product was extracted into chloroform:ethanol 3:1 (3 x 30 mL) from brine. The organic layer was washed with water, dried over potassium carbonate, filtered and the solvent removed *in vacuo* to yield an oil. Purification by flash column chromatography (silica, 100% DCM) yielded a clear oil (1.77 g, 4.65 mmol, 30%).

δ_H (300 MHz, $CDCl_3$) 1.42 (9H, s, CH_3), 2.60 (6H, t, ^3J 6.0, CH_2CN), 3.68 (6H, t, ^3J 6.0, OCH_2), 3.76 (6H, s, CH_2O), 4.86 (1H, s, NH); δ_C (75 MHz, $CDCl_3$) 18.76 ($\underline{C}H_2CN$), 28.27 (($\underline{C}H_3)_3C$), 58.42 ($NH\underline{C}(CH_2)_2$), 65.69 (OCH_2), 69.31 (CH_2O), 79.58 (($CH_3)_3\underline{C}$), 117.86 (CN), 154.73 (C=O) ; *m/z* (ES+, methanol) 381 ($[M+H]^+$, 100%).

Generation-2 Gd(gDOTA) Dendrimer (85)

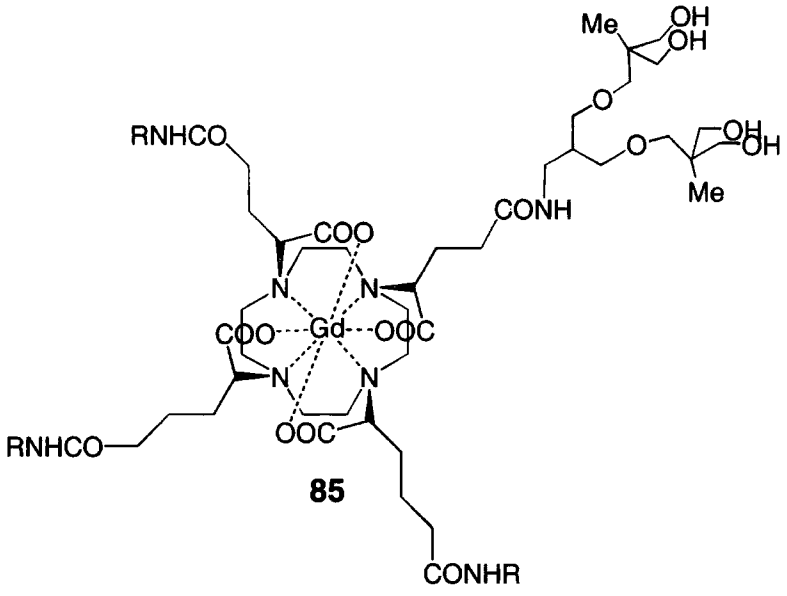

85

Complexation: A solution of gDOTA (50 mg, 72 μmol) and $GdCl_3.6H_2O$ (27 mg, 72 μmol) was brought to pH=3 with dilute hydrochloric acid and heated at reflux for 72 h. The pH was brought to 7 and the water removed *in vacuo* to yield 90 mg (72 μmol, 100%).

Coupling: To a solution of the Gd(gDOTA)$^-$ in DMSO (0.5 mL) was added NHS (16 mg, 138 μmol) and NaCl (4 mg, 70 μmol), and the solution heated with stirring at 55°C for 2 h. Diisopropylethylamine (2 drops) and EDC (26.5 mg, 138 μmol) were then added to the solid solution at -78°C and allowed to come to ambient temperature with stirring. After 20 h, negative ESMS showed tetraactivation of the carboxylates as the NHS ester, and dendramine-2 **75** (77 mg, μmol) was added as a solution in DMSO (0.5 mL). After 4 h, negative ESMS showed full tetrasubstitution. A small amount (5%) of the (generation-2)$_3$(generation-1) mixed product was observed. The product was extracted into warm hexane, and dried over potassium carbonate. The solvent was removed *in vacuo* to yield 70 mg (23 μmol, 46%). *m/z* (ES+) 1003 (35%), 1246 (30%), 1317 (25%), 1390 (20%), 2687 (10%), 3001 ([M+H$^+$], 100%).

Deprotection: The ketal groups were removed by a weak solution of hydrochloric acid in chloroform at ambient temperature. After 2 h, the solution was neutralised with sodium hydrogencarbonate, filtered and the volatiles removed *in vacuo* to yield a brown glassy

solid (40 mg). No further purification was attempted. *m/z* (ES+) 1100 (100%), 1113 (90%),1516 (45%), 2010 ([M-H]$^-$, 25%).

Generation-3 Gd(gDOTA) Dendrimer (86)

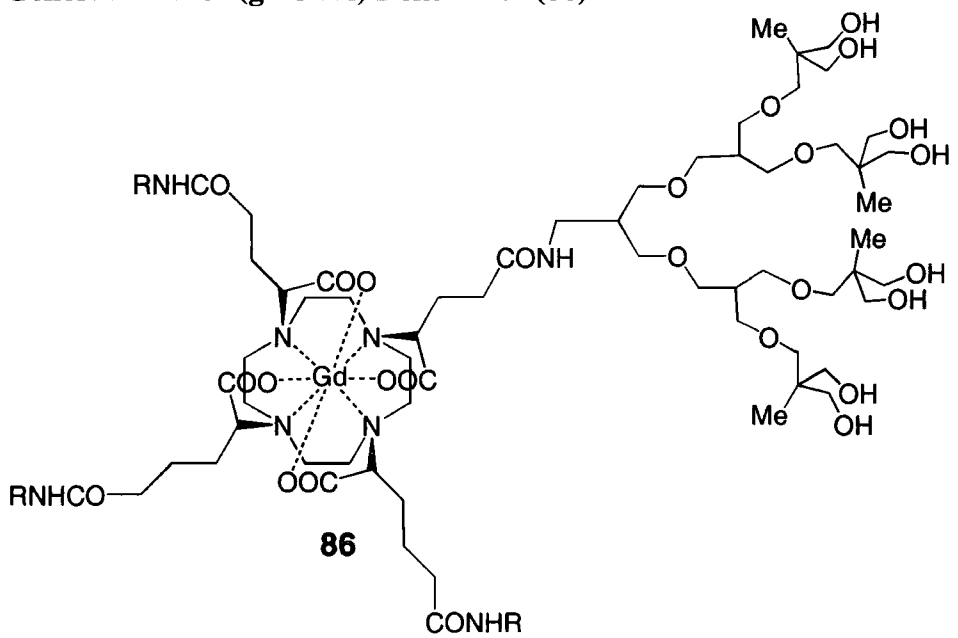

86

Deprotection: The ketal groups were removed from dendramine-3, **78** (0.32g) using a 2M solution of hydrochloric acid in dioxane at ambient temperature (40 mg). ^{1}H NMR confirmed deprotection. No further purification was attempted and the product was used directly in the amide coupling reaction.

Coupling: To a solution of Gd(gDOTA)$^-$ (25 mg, 3 μmol) in water/dioxane (1.0 mL) was added HOBt (5.0 mg), dendramine-3 (0.16 g, 0.24 mmol) and EDC (34 mg). The solution was stirred at ambient temperature and the pH adjusted to ~ 6.5 using dilute aqueous NaOH solution. After 20h, the solution was diluted with water and the resultant white solid filtered off. No attempts were made at purification. *m/z* (ES+) 3150 (30%), 3533 ([M+H$^+$], 100%).

List of References

(1) Koenig, S. H. In *Encyclopedia of Nuclear Magnetic Resonance*; Grant, D. M., Harris, R. K., Eds.; Wiley: New York, 1996; Vol. 1.
(2) Rabi, I. I.; Zacharias, J. R.; Millman, S.; Kusch, P. *Phys. Rev.* **1938**, *53*, 318.
(3) Rabi, I. I.; Zacharias, J. R.; Millman, S.; Kusch, P. *Phys. Rev.* **1939**, *55*, 526.
(4) Bloch, F.; Hansen, W. W.; Packard, M. *Phys. Rev.* **1946**, *69*, 127.
(5) Bloch, F.; Hansen, W. W.; Packard, M. *Phys. Rev.* **1946**, *70*, 474.
(6) Purcell, E. M.; Torrey, H. C.; Pound, R. V. *Phys. Rev.* **1946**, *69*, 37.
(7) Bertini, I.; Luchinat, C. *NMR of Paramagnetic Molecules in Biological Systems*; Benjamin-Cummings: Boston, 1986.
(8) Stark, D.; Bradley, W. G. *Magnetic Resonance Imaging*; C. V. Mosby Ed.: New York, 1988.
(9) Diem, K.; Leutner, C. *Documenta Geigy Scientific Tables*; Gregory Ed.: Basel, 1970.
(10) Lauterbur, P. C. *Nature* **1973**, *242*, 190.
(11) Mansfield, P.; Morris, P. G. *NMR Imaging in Biomedicine*; Academic: New York, 1982.
(12) Damadian, R. US Patent 3798832, 1974.
(13) Kormano, M.; Dean, P. B. *Radiology* **1976**, *121*, 379.
(14) Damadian, R. *Proc. Natl. Acad. Sci. USA* **1974**, *71*, 1471.
(15) Lauterbur, P. C.; Mendoca-Dias, M. H.; Rudin, A. M. ; Dutton, P. L., Leigh, L. S., Scarpa, A., Eds.; Academic Press: New York, 1978.
(16) Young, I. R.; Clarke, G. J.; Gailes, D. R. *Computed Tomography* **1981**, *5*, 534.
(17) Carr, D. H.; Brown, J.; Bydder, G. M.; Weinmann, H. J.; Speck, U.; Thomas, D. J.; Young, I. R. *Lancet* **1984**, 484.
(18) Block, F. *Phys. Rev.* **1955**, *99*, 559.
(19) Bloch, F.; Hansen, W. W.; Packard, M. *Phys. Rev.* **1948**, *70*, 474.
(20) Solomon, I. *Phys. Rev.* **1955**, *99*, 559.
(21) Lauffer, R. B. *Chem. Rev.* **1987**, *87*, 901.
(22) Aime, S.; Botta, M.; Fasano, M.; Terreno, E. *Chem. Soc. Rev.* **1998**, *27*, 19.
(23) Kumar, K.; Tweedle, M. F. *Pure Appl. Chem.* **1993**, *65*, 515.
(24) Schwarzenbach, G. *Helv. Chim. Acta.* **1952**, *35*, 2344.
(25) Hancock, R. D.; Martell, A. E. *Chem. Rev.* **1989**, *89*, 1875.
(26) Cabbiness, D. K.; Margerum, D. W. *J. Am. Chem. Soc.* **1969**, *91*, 6540.
(27) Parker, D.; Williams, J. A. G. *J. Chem. Soc. Dalton Trans.* **1996**, 3613.
(28) Parker, D.; Pulukkody, K.; Norman, T. J.; Royle, L.; Broan, C. Y. *J. Chem. Soc., Perkin Trans. 2* **1993**, 605.
(29) Wedeking, P. W.; Kumar, K.; Tweedle, M. F. *Magn. Reson. Imaging* **1992**, *10*, 641.
(30) Tweedle, M. F.; Hagen, J. J.; Kumar, K.; Chang, C. A. *Magn. Reson. Imaging* **1991**, *9*, 409.
(31) Parker, D. *Chem. Soc. Rev.* **1990**, *19*, 271.
(32) Paul-Roth, C.; Raymond, K. N. *Inorg. Chem.* **1995**, *34*, 1408.
(33) Desreux, J. F. *Inorg. Chem.* **1980**, *19*, 1319.
(34) Wang, X.; Jin, T.; Comblin, V.; Lopez-Mut, A.; Merciny, E.; Desreux, J. F. *Inorg. Chem.* **1992**, *31*, 1095.

(35) Spirlet, M.; Rebizant, J.; Desreux, J. F. *Inorg. Chem.* **1984**, *23*, 359.
(36) Dubost, J. P.; Leger, J. M.; Langlois, M. H.; Meyer, D.; Schaefer, M. *C. R. Acad. Sci., Ser. 2* **1991**, *312*, 349.
(37) Parker, D. In *Comprehensive Supramolecular Chemistry*; Reinhoudt, D. N., Atwood, J. E., Vogtle, F., MacNicol, D. D., Lehn, J.-M., Eds.; Pergamon: Oxford, 1996; Vol. 10.
(38) Tweedle, M. F. In *Lanthanide Probes in Life, Chemical and Earth Sciences*; Bunzli, J.-C. G., Choppin, G. R., Eds.; Elsevier: Amsterdam, 1989.
(39) Chang, C. A. *Inorg. Chem.* **1993**, *32*, 3501.
(40) Stetter, F. *Angew. Chem.* **1976**, *88*, 760.
(41) Hoeft, S. *Chem. Ber.* **1993**, *126*, 869.
(42) Jacques, V. *Inorg. Chem.* **1994**, *33*, 4048.
(43) Howard, J. A. K.; Kenwright, A. M.; Moloney, J. M.; Parker, D.; Port, M.; Navet, M.; Rousseau, O.; Woods, M. *Chem. Commun.* **1998**, 1381.
(44) Aime, S.; Botta, M.; Ermondi, G. *Inorg. Chem.* **1992**, *31*, 4291.
(45) Aime, S.; Barge, A.; Botta, M.; Fasano, M.; Ayala, J. D.; Bombieri, G. *Inorg. Chim. Acta* **1996**, *246*, 423.
(46) Corey, E. J.; Bailar, J. C. *J. Am. Chem. Soc.* **1959**, *81*, 2620.
(47) Parker, D.; Pulukkody, K.; Smith, F. C.; Batsanov, A.; Howard, J. A. K. *J. Chem. Soc., Dalton Trans.* **1994**, 689.
(48) Corey, E. J.; Bailar, J. C. Jr. *J. Am. Chem. Soc.* **1978**, *100*, 7166.
(49) Woods, M.; Aime, S.; Barge, A.; Bruce, J. I.; Botta, M.; Howard, J. A. K.; Moloney, J. M.; Parker, D.; Sousa, A. S. D. *J. Am. Chem. Soc.* **1999**, *121*, 5762.
(50) Aime, S.; Botta, M.; Fasano, M.; Paoletti, S.; Anelli, P. L.; Uggeri, F.; Virtuani, M. *Inorg. Chem.* **1994**, *33*, 4707.
(51) Gonzalez, G.; Powell, D. H.; Tissiéres, V.; Merbach, A. E. *J. Phys. Chem.* **1994**, *1994*, 53.
(52) Powell, D. H.; Dhubhghaill, O. M. N.; Pubanz, D.; Helm, L.; Lebedev, Y. S.; Schlaepfer, W.; Merbach, A. E. *J. Am. Chem. Soc.* **1996**, *118*, 9333.
(53) Aime, S.; Barge, A.; Botta, M.; Sousa, A. S. D.; Parker, D. *Angew. Chem. Int. Ed. Engl.* **1998**, *37*, 2673.
(54) Dunand, A. F.; Aime, S.; Merbach, A. E. *J. Am . Chem. Soc.* **2000**, *122*, 1506.
(55) Pubanz, D.; Gonzalez, G.; Powell, D. H.; Merbach, A. E. *Inorg. Chem.* **1995**, *34*, 4447.
(56) Koenig, S. H.; Brown, R. D. *Relaxometry of Tissue in NMR Spectroscopy of Cells and Organisms*; C.R.C. Press: Boca Raton, 1987.
(57) Aime, S.; Botta, M.; Ermondi, G.; Fedeli, F.; Uggeri, F. *Inorg. Chem.* **1992**, *31*, 1100.
(58) Sherry, A. D.; Brown, R. D.; Geraldes, C. F. G. C.; Koenig, S. H.; Kuan, K.-T.; Spiller, M. *Inorg. Chem.* **1989**, *28*, 620.
(59) Swift, T. J.; Connick, R. E. *J. Chem. Phys.* **1962**, *37*, 307.
(60) Bénazeth, S.; Purans, J.; Chalbot, M.-C.; Mguyen-van-Duong, M. K.; Nicolas, L.; Keller, F.; Gaudemer, A. *Inorg. Chem.* **1998**, *37*, 3667.
(61) Koenig, S. H.; Epstein, M. *J. Chem. Phys.* **1975**, *63*, 2279.
(62) Chen, J. W.; Belford, R. L.; Clarkson, R. B. *J. Phys. Chem.* **1998**, *102*, 2117.
(63) Micskei, K.; Helm, L.; Brücher, E.; Merbach, A. E. *Inorg. Chem.* **1993**, *32*, 3844.

(64) André, J. P.; Maecke, H. R.; Tóth, E.; Merbach, A. E. *J. Biol. Inorg. Chem.* **1999**, *4*, 341.
(65) Szilágyi, E.; Tóth, E.; Brücher, E.; Merbach, A. E. *J. Chem. Soc. Dalton Trans.* **1999**, 2481.
(66) Lammers, H.; Maton, F.; Pubanz, D.; Laren, M. W. V.; Bekkum, H. V.; Marbach, A. E.; Muller, R. N.; Peters, J. A. *Inorg. Chem.* **1997**, *36*, 2527.
(67) Tóth, E.; Connac, F.; Helm, L.; Adzamli, K.; Merbach, A. E. *Eur. J. Inorg. Chem.* **1998**, 2017.
(68) Tóth, E.; Uffelen, I. v.; Helm, L.; Merbach, A. E.; Ladd, D.; Briley-Saebo, K.; Kellar, K. E. *Magn. Res. Chem.* **1998**, *36*, S125.
(69) Aime, S.; Crich, S. G.; Gianolio, E.; Terreno, E.; Beltrami, A.; Uggeri, F. *Eur. J. Inorg. Chem.* **1998**, 1283.
(70) Aime, S.; Botta, M.; Fasano, M.; Terreno, E. *Acc. Chem. Res.* **1999**, *32*, 941.
(71) Aime, S.; Botta, M.; Fasano, M.; Marques, M. P. M.; Geraldes, C. F. G. C.; Pubanz, D.; Merbach, A. E. *Inorg. Chem.* **1997**, *36*, 2059.
(72) Tóth, E.; Pubanz, D.; Vauthey, S.; Helm, L.; Merbach, A. E. *Chem. Eur. J.* **1996**, *2*, 1607.
(73) Tóth, E.; Helm, L.; Kellar, K. E.; Merbach, A. E. *Chem. Eur. J.* **1999**, *5*, 1202.
(74) Kanno, H.; Hiraishi, J. *J. Phys. Chem.* **1982**, *86*, 1488.
(75) Johnson, G.; Wakita, H. *Inorg. Chem.* **1985**, *24*, 3047.
(76) Cossy, C.; Merbach, A. E. *Pure Appl. Chem.* **1988**, *60*, 1785.
(77) Alpoim, M. C.; Urbano, A. M.; Geraldes, C. F. G. C.; Peters, J. A. *J. Chem. Soc. Dalton Trans.* **1992**, 463.
(78) Horrocks, W. D.; Sudnick, D. R. *J. Am. Chem. Soc.* **1979**, *101*, 334.
(79) Kropp, J. L.; Windsor, M. W. *J. Chem. Phys.* **1963**, *39*, 2769.
(80) Kropp, J. L.; Windsor, M. W. *J. Chem. Phys.* **1965**, *42*, 1599.
(81) Kropp, J. L.; Windsor, M. W. *J. Chem. Phys.* **1966**, *45*, 761.
(82) Beeby, A.; Clarkson, I. M.; Dickins, R. S.; Faulkner, S.; Parker, D.; Royle, L.; Sousa, A. S. d.; Williams, J. A. G.; Woods, M. *J. Chem. Soc., Perkin Trans 2* **1999**, 493.
(83) Albin, M.; Farber, G. K.; Horrocks, W. D. *Inorg. Chem.* **1984**, *23*, 1648.
(84) Geier, G.; Jorgensen, C. K. *Chem. Phys. Lett.* **1971**, *9*, 263.
(85) Graeppi, N.; Powell, D. H.; Laurenczy, G.; Zékány, L.; Merbach, A. E. *Inorg. Chim. Acta* **1994**, *235*, 311.
(86) Tóth, E.; Dhubhghaill, O. M. N.; Besson, G.; Helm, L.; Merbach, A. E. *Magn. Res. Chem.* **1999**, *37*, 701.
(87) Yerly, F.; Dunand, F. A.; Tóth, E.; Figueirinha, A.; Kovács, Z.; Sherry, A. D.; Geraldes, C. F. G. C.; Merbach, A. E. *Eur. J. Inorg. Chem* **2000**, 1001.
(88) Frey, S. T.; Horrocks, W. D. J. *Inorg. Chim. Acta* **1995**, *229*, 383.
(89) Bloembergen, N.; Purcell, E. M.; Pound, R. V. *Phys. Rev.* **1948**, *73*, 678.
(90) Bloembergen, N.; Morgan, L. O. *J. Chem. Phys.* **1961**, *34*, 842.
(91) McLachlan, A. D. *Proc. R. Soc. London* **1964**, *A280*, 271.
(92) Koenig, S. H.; Brown, R. D. *Prog. NMR Spectrosc.* **1996**, *22*, 487.
(93) Koenig, S. H.; Brown, R. D. *Prog. Nucl. Magn. Reson. Spectrosc.* **1990**, *22*, 487.
(94) Caravan, P.; Ellison, J. J.; McMurray, T. J.; Lauffer, R. B. *Chem. Rev.* **1999**, *99*, 2293.
(95) Lauffer, R. B. *Magn. Reson. Imaging* **1985**, *3*, 11.

(96) Lauffer, R. B.; Brady, T. J.; Brown, R. D.; Baglin, C.; Koenig, S. H. *Magn. Reson. Med.* **1986**, *3*, 541.
(97) Dunham, S. U.; Tyeklar, Z.; Midlefort, K. S.; McDermid, S. A.; McMurray, T. J.; Lauffer, R. B. COST D1 Meeting, The Hague, 1996.
(98) Woods, M. , University of Durham, 1998.
(99) Bosman, A. W.; Janssen, H. M.; Meijer, E. W. *Chem. Rev.* **1999**, *99*, 1665.
(100) Buhleier, E.; Wehner, W.; Vogtle, F. *Synthesis* **1978**, 155.
(101) Tomalia, D. A.; Baker, H.; Dewald, J. R.; Hall, M.; Kallos, G.; Martin, S.; Roeck, J.; Ryder, J.; Smith, P. *Polym. J. (Tokyo)* **1985**, *17*, 117.
(102) Tomalia, D. A.; Baker, H.; Dewald, J. R.; Hall, M.; Kallos, G.; Martin, S.; Roeck, J.; Ryder, J.; Smith, P. *Macromolecules* **1986**, *19*, 2566.
(103) Newkome, G. R.; Yao, Z.-q.; Baker, G. R.; Gupta, K. *J. Org. Chem.* **1985**, *50*, 2003.
(104) Hawker, C. J.; Frechet, J. M. J. *J. Am. Chem. Soc.* **1990**, *112*, 7638.
(105) Hawker, C. J.; Frechet, J. M. J. *J. Chem. Soc., Chem. Commun.* **1990**, 1010.
(106) Mourey, T. H.; Turner, S. R.; Rubinstein, M.; Frechet, J. M. J.; Hawker, C. J.; Woolley, K. L. *Macromolecules* **1992**, *25*, 2401.
(107) Mansfield, M. L.; Klushin, L. I. *Macromolecules* **1993**, *26*, 4262.
(108) Gorman, C. B.; Hager, M. W.; Parkhurst, B. L.; Smith, J. C. *Macromolecules* **1998**, *31*, 815.
(109) Inoue, K. *Progr. Polym. Sci.* **2000**, *25*, 453.
(110) Wiener, E. C.; Auteri, F. P.; Chen, J. W.; Brechbiel, M. W.; Gansow, O. A.; Schneider, D. S.; Clarkson, R. B.; Lauterbur, P. C. *J. Am. Chem. Soc.* **1996**, *118*, 7774.
(111) Wiener, E. C.; Brechbiel, M. W.; Brothers, H.; Magin, R. L.; Gansow, O. A.; Tomalia, D. A.; Lauterbur, P. C. *Magn. Reson. Imaging* **1994**, *31*, 1.
(112) Chen, J. W.; Clarkson, R. B.; Belford, R. L. *J. Phys. Chem.* **1996**, *100*, 8093.
(113) Allerhand, A.; Hailstone, R. K. *J. Chem. Phys.* **1972**, *56*, 3718.
(114) Bullock, A. T.; Cameron, G. G.; Krajewski, V. *J. Chem. Phys.* **1976**, *80*, 1792.
(115) Meltzer, A. D.; Tirrell, D. A.; Jones, A. A.; Inglefield, P. T.; Hedstrand, D. M.; Tomalia, D. A. *Macromolecules* **1992**, *25*, 4541.
(116) Berthezene, Y.; Vexler, V.; Price, D. C.; Wisner-Dupon, J.; Moseley, M. E.; K, P. A.; Brasch, R. C. *Invest. Radiol.* **1992**, *27*, 346.
(117) Berthezene, Y.; Vexler, V.; Kuwatsurn, R.; Rosenau, W.; Muhler, A.; Clement, O.; Price, D. C.; Brasch, R. C. *Radiology* **1992**, *185*, 97.
(118) Tomalia, D. A.; Hedstrand, D. M.; Wilson, L. R. In *Encyclopaedia of Polymer Science and Engineering*; Mark, H. F., Bikales, N. M., Overberger, C. G., Menges, G., Eds.; Wiley Interscience: New York, 1990.
(119) de Brabander, E. M. M.; Meijer, E. W. *Angew. Chem. Int. Ed. Engl.* **1993**, *32*, 1308.
(120) Mourey, T. H.; Turner, S. R.; Rubinstein, M.; Frechet, J. M. J.; Hawker, C. J.; Wooley, K. L. *Macromolecules* **1992**, *25*, 2401.
(121) Zalipsky, S.; Gilon, C.; Zilkha, A. *Eur. Polym. J.* **1983**, *19*, 1177.
(122) Brittain, H. G.; Desreux, J. F. *Inorg. Chem.* **1984**, *23*, 4459.
(123) Dischino, D. D.; Delaney, E. J.; Emswiler, J. E.; Gaughan, G. T.; Prasad, J. S.; Srivastava, S. K.; Tweedle, M. F. *Inorg. Chem.* **1991**, *30*, 1265.
(124) Kumar, K.; Tweedle, M. F. *Inorg. Chem.* **1993**, *32*, 4193.

(125) Gacek, M.; Undheim, K. *Tetrahedron* **1973**, *29*, 863.
(126) Kang, S. I.; Ranganathan, R. S.; Emswiler, J. E.; Kumar, K.; Gougoutas, J. Z.; Malley, M. F.; Tweedle, M. *Inorg. Chem.* **1993**, *32*, 2912.
(127) Effenberger, F.; Burkard, U.; Willfahrt, J. *Angew. Chem. Int. Ed. Engl.* **1983**, *22*, 65.
(128) Meyer, J. H.; Bartlett, P. A. *J. Am. Chem. Soc.* **1998**, *120*, 4600.
(129) Hoffman, R. V.; Tao, J. *Tetrahedron* **1997**, *53*, 7119.
(130) Hoffman, R. V.; Kim, H.-O. *Tetrahedron* **1993**, *34*, 2051.
(131) March, J. *Advanced Organic Chemistry*; 4th ed.; Wiley-Interscience: New York, 1992.
(132) Kolasa, T. *Can. J. Chem.* **1985**, *63*, 2139.
(133) Dickins, R. S.; PhD. Thesis *Chiral Lanthanide Complexes*, Durham, 1997.
(134) Dickins, R. S.; Parker, D.; Sousa, A. S. d.; Williams, J. A. G. *J. Chem. Soc., Chem. Commun.* **1996**, *36*, 697.
(135) Koga, K.; Wu, C. C.; Yamada, S. *Tetrahedron Lett.* **1971**, 2287.
(136) Barton, D. H. R.; Narang, S. C. *J. Chem. Soc., Perkin Trans. I* **1977**, 1114.
(137) Howells, R. D.; McCown, J. D. *Chem. Rev.* **1977**, *77*, 69.
(138) Gramstad, T.; Haszeldine, R. N. *J. Chem. Soc.* **1957**, 4069.
(139) Stang, P. J.; Hanack, M.; Subramanian, L. R. *Synthesis* **1982**, 85.
(140) Ponnusamy, E.; Fotadar, U.; Spisni, A.; Fiat, D. *Synthesis* **1986**, 48.
(141) Greene, T. W.; Wuts, P. G. M. *Protective Groups in Organic Synthesis*; 2nd ed.; Wiley: New York, 1991.
(142) Johnstone, R. A. W.; Rose, M. E. *Tetrahedron* **1979**, *35*, 2169.
(143) Olah, G. A. In *Friedel Crafts and Related Reactions*; Wiley-Interscience: New York, 1963-1965.
(144) Ahmad, M. S.; Baddeley, G. *J. Chem. Soc.* **1961**, 2520.
(145) Staunton, J.; Eisenbraun, E. J. *Org. Syn. Coll.*; Wiley: New York, 1973.
(146) Menicagli, R.; Piccolo, O. *J. Org. Chem.* **1980**, 2581.
(147) Grant, H. N.; Prelog, V.; Sneeden, R. P. A. *Helv. Chim. Acta* **1963**, *46*, 415.
(148) Takanashi, S.; Takagi, M.; Takikawa, H.; Mori, K. *J. Chem. Soc., Perkin Trans. I* **1998**, *10*, 1603.
(149) Vyas, G. N.; Shah, N. M. *Org. Synth., Coll. Vol. IV* **1963**, 836.
(150) Mackenzie, A. R.; Moody, C. J.; Rees, C. W. *Tetrahedron* **1986**, *42*, 3259.
(151) Kende, A. S.; Rizzi, J. P. *Tetrahedron Lett.* **1981**, *22*, 1779.
(152) Adam, W.; Lazarus, M.; Saha-Moller, C. R.; Schreier, P. *Tetrahedron Asymmetry* **1998**, *9*, 351.
(153) Wang, Z.; La, B.; Fortunak, J. M.; Meng, X.-J.; Kabalka, G. W. *Tetrahedron Lett.* **1998**, *39*, 5501.
(154) Uchida, R.; Shiomi, K.; Sunazuka, T.; Inokoshi, J.; Nishizawa, A. *J. Antibiot.* **1996**, *49*, 886.
(155) Chattopadhyay, S. K.; Pattenden, G. *J. Chem. Soc., Perkin Trans. I* **2000**, *15*, 2429.
(156) Feenstra, R. W.; Stokkingreef, E. H. M.; Nivard, R. J. F.; Ottenheijm, H. C. J. *Tetrahedron* **1988**, *44*, 5583.
(157) Saito, S.; Yabuki, T. *Bull. Chem. Soc. Jpn.* **1978**, *51*, 529.
(158) Kruizinga, W. H.; Strijveen, B.; Kellogg, R. M. *J. Org. Chem.* **1981**, *46*, 4321.
(159) Frechet, J. M. J. *Science* **1994**, 263.

(160) Newkome, G. R.; Lin, X. *Macromolecules* **1991**, *24*, 1443.
(161) Young, J. K.; Baker, G. R.; Newkome, G. R.; Morris, K. F.; Johnson, C. S. Jr. *Macromolecules* **1994**, *27*, 3464.
(162) Senter, P. D.; Svensson, H. P.; Schreiber, G. J.; Rodriguez, J. L.; Vrudhula, V. M. *Bioconjugate Chem.* **1995**, *6*, 389.
(163) Greenwald, R. B.; Pendri, A.; Bolikal, D. *J. Org. Chem.* **1995**, *60*, 331.
(164) Grayson, S. M.; Jayaraman, M.; Frechet, J. M. J. *Chem. Commun.* **1999**, 1329.
(165) Dandliker, P. J.; Diederich, F.; Zingg, A. *Helv. Chim. Acta* **1997**, *80*, 1773.
(166) Newkome, G. R.; Lin, X.; Young, K. *Synlett* **1992**, 53.
(167) Nierengarten, J. F.; Habicher, T.; Kessinger, R.; Cardullo, F.; Diederich, F.; Gramlich, V.; Gisselbrecht, J.-P.; Boudon, C.; Gross, M. *Helv. Chim. Acta* **1997**, *80*, 2238.
(168) Newkome, G. R.; He, E.; Godinez, L. A.; Baker, G. R. *Chem. Commun.* **1999**, 27.
(169) Perhnutter, P. *Conjugate Addition Reactions in Organic Synthesis*; Pergamon: Oxford, 1992.
(170) Simonot, B.; Rousseau, G. *J. Org. Chem.* **1994**, *59*, 5912.
(171) Schanzer, A.; Libman, J.; Dayan, J.; Felder, C. E.; Lifson, S. *J. Am. Chem. Soc.* **1991**, *113*, 3431.
(172) Dupraz, A.; Guy, P.; Dupuy, C. *Tetrahedron Lett.* **1996**, *37*, 1237.
(173) Grayson, S. M.; Frechet, J. M. J. *J. Am. Chem. Soc.* **2000**, *122*, 10335.
(174) David Parker, Personal Communication
(175) Grosu, I.; Ple, G.; Mager, S.; Martinez, R.; Mesaros, C.; Camacho, B. d. C. *Tetrahedron* **1997**, *53*, 6215.
(176) Knight, E. F.; Brown, H. C. *J. Am. Chem. Soc.* **1968**, *90*, 5280.
(177) Staudinger; Meyer *Helv. Chim. Acta* **1919**, *2*, 635.
(178) Malik, A. A.; Preston, S. B.; Archibald, T. G.; Cohen, M. P.; Baum, K. *Synthesis* **1989**, 450.
(179) Newkome, G. R.; Moorefield, C. N.; Baker, G. R. *Aldrichim. Acta* **1992**, *25*, 31.
(180) Newkome, G. R.; Weis, C. D.; Childs, B. J. *Designed Monomers and Polymers* **1998**, *1*, 3.
(181) Fedrizzi, G.; Bernardi, L.; Marazzi, G.; Melloni, P.; Frigerio, M. *J. Chem. Soc., Perkin Trans. I* **1995**, *13*, 1755.
(182) Seto, C. T.; Mathias, J. P.; Whitesides, G. M. *J. Am. Chem. Soc.* **1993**, *115*, 1321.
(183) Itoh, M.; Hagiware, D.; Kamiya, T. *Tetrahedron Lett.* **1975**, 4393.
(184) Itoh, M.; Hagiware, D.; Kamiya, T. *Bull. Chem. Soc. Jpn.* **1977**, *50*, 718.
(185) Seto, C. T.; Mathias, J. P.; Whitesides, G. M. *J. Am. Chem. Soc.* **1993**, *115*, 1321.
(186) Knoelker, H.-J.; Braxmeier, T.; Schlechtingen, G. *Angew. Chem., Int. Ed. Engl.* **1995**, *34*, 2497.
(187) Herranz, R.; Castro-Pichel, J.; Garcia-Lopez, T. *Synlett* **1992**, 45.
(188) Stahl, G. L.; Walter, R.; Smith, C. W. *J. Org. Chem.* **1978**, *43*, 2285.
(189) Bergmann, M.; Zervas, L. *Ber.* **1932**, *65*, 1192.
(190) Atwell, G. J.; Denny, W. A. *Synthesis* **1984**, 1032.
(191) Bodanzsky; Bodanzsky *The Practice of Peptide Synthesis*; 2nd ed.; Springer: Berlin, 1994.
(192) Vogel, P. *Carbocation Chemistry*; Elsevier: Amsterdam, 1985.
(193) O'Hagan, D.; Robins, R. J.; Wilson, M.; Wong, C. W.; Berry, M.; Zabetakis, I. *J. Chem. Soc., Perkin Trans. 1* **1999**, 2117.

(194) J. Koch *Acc. Chem. Res.* **1984**, *17*, 137.
(195) Fabiano, E.; Golding, B. T.; Sadeghi, M. M. *Synthesis* **1987**, 190.
(196) Mitsunobu, O. *Synthesis* **1981**, 1.
(197) Wolff, H. *Org. React.* **1947**, *3*, 327.
(198) Gololobov, Y. G.; Zhmurora, I. N.; Kasukhin, L. F. *Tetrahedron* **1981**, *37*, 437.
(199) Doble, D. M. J.; Botta, M.; Wang, J.; Aime, S.; Barge, A.; Raymond, K. N. *J. Am. Chem. Soc.* **2001**, *123*, 10758.
(200) Senanayake, K. Personal Communication.
(201) Toth, E.; Uffelen, I. v.; Helm, L.; Merbach, A. E.; Ladd, D.; Briley-Saebo, K. K.; Kellar, K. E. *Magn. Reson. Chem.* **1998**, *36*, S125.
(202) Lowe, M. *Unpublished Work* **1999**.
(203) Gorbatschewa, M. *Zh. Obshch. Khim., engl. Ausg. S.* **1957**, *27*, 2336.
(204) S. Chui; L. Bunting *Can. J. Chem.* **1978**, *56*, 2188.
(205) Kano, S.; Yuasa, Y.;Yokomatsu, T.; Shibuya, S. *J. Org. Chem.* **1988**, *53*, 3865.
(206) Quagliato, D. A.; Andrae, P. M.; Matelan, E. M.; *J. Org. Chem.* **2000**, *65*, 5037.